Supercapacitor Technologies for Renewable Energy Application

A thesis

submitted in partial fulfilment

of the requirements for the degree

of

Master of Engineering

at

The University of Waikato

Hamilton, New Zealand

by

OKEKE AMALACHUKWU. A

THE UNIVERSITY OF
WAIKATO
Te Whare Wānanga o Waikato

Year of submission

2019

Abstract

Supercapacitors are increasingly gaining popularity since the advent of “world campaign” for clean energy generation. They are characteristically high power-dense energy storage devices with very low ESR. They are known to have more cycle life and less prone to explosion than the conventional lithium ion batteries. With Research activities on the rise, supercapacitors could be potential alternatives for the less durable battery energy storage systems.

This paper explores the behaviour of different supercapacitor technologies as energy storage devices. Three different technologies are analysed, they include; The Electrochemical double layer capacitor, the hybrid supercapacitor and the battery-type supercapacitor. More emphasis was laid on the battery type supercapacitor as the latest supercapacitor technology with a capacitance of 40,000F. Empirical tests were conducted on the devices with the charge and discharge characteristic curves obtained to further analyse their behaviours. To investigate the supercapacitor’s storage capability, a boost converter was designed. The converter enables the 2.7V supercapacitor power a 12V LED. A 150W push-pull converter was also designed to enable a bank of supercapacitors power a 120V LED flood light. This was done to demonstrate the commercial applicability of the battery type supercapacitor for street lighting system. Detailed design procedures of the two converters are described, including the Printed circuit board and the push-pull transformer.

Acknowledgements

I am grateful to almighty God, for his grace and protection all through this period.

I am extremely grateful to the government of New Zealand for awarding me a scholarship to complete this master's program and also for making my stay in New Zealand a wonderful one.

I wish to express my gratitude to my amiable supervisor, A.D.V. Nihal Kularatna, for his motivation, his patience with me throughout the learning period, and most importantly, his guidance, without which this work might not have been completed.

I thank my senior research colleagues and PhD students, Thilanga Ariyarathna, Dilini Jayananda, and Nimesha Wijesooriya who were always there to answer any technical questions I had.

A special thanks to my family for their prayers and moral support throughout the period of preparing this thesis.

Finally, I wish to thank my wonderful friends and the Nigerian community in New Zealand for all their support.

Table of Contents

List of Figures

List of Tables

Chapter One

1.1 Introduction

In today's world, the demand for energy is consistently on the increase. The reason for this increase can be attributed to an overall growth in the world population and a steady increase in technological inventions which mostly need energy to function. The US Energy Information Administration (E.I.A) has projected a 28% increase in the world energy demand by the year 2040; This would take the total world energy consumption to about (2.39×10^{14}) kWh[1]. While the need for more energy is evident, the environmental implication of increasing the use of conventional energy sources may be counterproductive. This counter-productivity is demonstrated in [2], where the author analysed the economic impacts of carbon emissions. In a bid to reduce carbon emissions; International conferences, sensitizations, and treaties have aimed to limit the overall usage of fossils fuels as a source of energy.

The adoption of renewable energy technologies to meet the world's growing energy demand is therefore seen as a remedy in salvaging the situation. This has caused a steady growth in the popularity of renewable energy. According to the International Renewable Energy Agency, 25% of the world energy consumption in 2017 was supplied from renewable energy sources. It is also projected that by the year 2050, about 85% of world energy supply would be from renewable sources[3]. This popularity has equally led to increased research activities in the area of renewable energy. While renewable energy is seen as a worthy alternative and solution, it also presents new challenges. The sources which are mostly sun and wind are erratic in

nature and dependent on climatic factors for availability. Meanwhile, the energy demand is nearly steady, hence energy storage is required.

Scientists have struggled to justify the economic gain of using energy storage devices in conventional energy generating systems. The reason for this, as explained in [4] is the availability of large amount of the energy which can be varied whenever necessary to match demand.

In renewable energy systems, the availability of energy has an irregular pattern. For instance, in solar energy systems, the availability of energy from the solar panels depends on the intensity of the sunlight, which in itself varies. In this scenario, it is necessary to store the energy when an excess is produced and be made available to the consumers when the energy production is below demand. This makes energy storage devices very important components in renewable energy systems.

Basically, the properties that an ideal energy storage system should possess can be summarised thus:

- The ideal energy storage system should have the capacity to store infinite amount of energy.
- The ideal energy storage system should be able to return the same amount of energy it received during storage.
- The ideal energy storage system should be able to receive or supply energy at any desired rate.
- The ideal energy storage system should be durable.

In real situations however, the available energy storage devices fall short of the above properties at different levels. Different technological concepts have been applied in the development of energy storage devices, with the most widely used

being the Lithium-ion batteries. Lithium-ion batteries have high energy density; therefore, they can store large amount of energy compared to other energy storage devices of similar volume. The draw backs of lithium-ion batteries include; higher Equivalent Series resistance (ESR), Low Power density, high propensity to explosion, shorter cycle life and high weight to volume ratio.

Another less popular energy storage device is the supercapacitor: The supercapacitor technology improves greatly on the weaknesses of the lithium-ion batteries. They have characteristically very low ESR, their weight to volume ratio is relatively low, they have high power density, longer cycle life and are not prone to explosion. The major concern of the supercapacitor had been its low energy density compared to the batteries and other energy storage devices. However, with the recently manufactured battery-type hybrid supercapacitor of 40,000 Farad capacity, the potentials of supercapacitor technologies in renewable energy application has become evident.

This thesis examines the available supercapacitor technologies. Experimental analysis of the different properties is made, and converter circuits are designed to demonstrate its usability in renewable energy systems.

1.2 Objectives

In this project, the technologies inherent in supercapacitor devices are explained in detail while exploring the latest research activities and progress in the supercapacitor industry. Various laboratory tests were conducted on three different types of supercapacitors. The tests were done to study the implications of the different technological approaches employed in the development of the three

supercapacitors. The supercapacitors were used to power 12Volts LED bulbs to examine their performances as energy storage devices. A boost converter was designed to achieve this. The boost converter was necessary to enable the 2.7V, 40,000 F supercapacitor to power a 12V LED bulb. A push-pull converter was also designed to enable the supercapacitor power a 100V LED flood light suitable for street lighting system.

The objectives of the project are summarised as follows:

- To study and explore the supercapacitor technological concept.
- To study the properties and performance of the new 40,000 Farad supercapacitor in comparison to previous supercapacitor technologies.
- To analyse the performance of the 40,000 Farad supercapacitor as an energy storage device for LED lighting system.

1.3 Outline

This work is divided into seven chapters:

Chapter One gives a brief introduction that highlights the necessity of the project. The main objectives of the work is also contained in this chapter and descriptions of the other chapters of the thesis are discussed.

Chapter Two gives a background review of the three major topics of the thesis which are; renewable energy, energy storage, and power converters. This chapter discusses the different sources of renewable energy and their limitations. Various energy storage devices including the available supercapacitor technologies are discussed. Different power converter topologies are also discussed.

Chapter Three gives a detailed exploration of the available technologies employed in supercapacitor production. These include details on the electrochemistry, electrode materials, and the electrolytes.

Chapter Four contains the performance characteristics of the three supercapacitor technologies as obtained from laboratory measurements. These characteristics include the discharge curves under different conditions, and the equivalent series resistance. Finally, a comparison of the supercapacitors is made.

Chapter Five contains detailed design procedure and analysis of the low input voltage boost converter. The chapter comprises of two broad sections: the boost converter power stage design which covers the relevant parameter calculations and components selection. The second section is the implementation of the control circuit using the MAX669 current mode controller. A brief discussion of the available modes of control is also done in this chapter. The PCB design considerations are discussed and finally the performance analysis of the circuit is discussed, this include the load and line regulations, efficiency variations with input voltage and the LED illuminance variation.

Chapter Six deals with the design procedures of a boost push-pull converter as is suitable for a supercapacitor-based street lighting system. The converter was designed to power a 120Volts LED flood light. Detailed transformer design procedures is discussed, and a simulation to confirm the design is also done.

Chapter Seven is the conclusion to the thesis and a brief discussion on the future development in the supercapacitor technologies and suitable power converters.

Chapter Two

Background

2.1 Renewable Energy Technologies

Different renewable energy technologies are applied in power generation today. The most popular being wind, hydro, solar and geothermal energy. Less popular technologies include; wave energy, tidal and bioenergy technologies.

2.1.1. Wind renewable energy system

Wind energy is regarded as one of the fastest growing renewable energy sources. European countries like Denmark, Portugal, Ireland and Germany have over 15% of their power supply generated from wind, with Denmark at 37% and Ireland at 27% [5]. While similar levels is not seen in New Zealand, the potentials remain huge. As at the year 2018, wind farms in New Zealand have a combined installed capacity of 690MW, this represents 6% of the country's total annual electricity generation [6]. Electricity is produced from wind using wind turbines. The turbine blades capture the kinetic energy of the wind, which rotates the blade system and further converted into electricity using a generator. This forms the basic operating principle of the wind powers systems today. The performance and effectiveness of a wind turbine depends largely on the availability and speed of wind. Offshore wind farms have been constructed in different countries to harness the enormous wind energy produced by the ocean breezes. Due to cost and a few technical constraints, offshore wind farms is still less popular than the onshore wind farms. Figure *2.1* shows a typical offshore wind turbine located in Scotland, United Kingdom. While Figure *2.2* is the more popular onshore wind farm.

Figure 2.1. Offshore wind turbine (5-MW, 126m tall, 45m depth) Scotland.[7]

Figure 2.2. Onshore wind turbine.[5]

2.1.2 Solar renewable energy system

This renewable energy system harnesses the energy from the sun to produce electricity. This is achieved using solar modules which contain arrays of solar cells. The solar cells convert energy from the sun into electrical energy through photovoltaic effect. Individual cells produce minute voltage levels; a silicon solar cell produces a maximum open circuit voltage of about 0.5 to 0.6V. Therefore, cells

are connected in series and parallel to achieve higher voltage and current levels. One of the major drawbacks of solar energy system is the relatively low efficiency of the solar cells. Silicon based solar cells which dominate the solar cell technology market operate in the efficiency of 24.7%[8]. However, researches are ongoing to improve the efficiency of solar cells; Multijunction solar cells based on gallium indium phosphide (GaInP), gallium arsenide (GaAs), Gallium Indium Arsenide (GaInAs) and Gallium Indium Arsenide Phosphide (GaInAsP) have been developed in recent times, with test results suggesting a promising 46% efficiency under concentrated sunlight[9]. Despite the low efficiency of solar cells, the popularity and usage continues to experience tremendous growth. China, the world's largest solar market have an installed capacity of 154.1GW as at August 2018[10]. Figure 2.3 shows installed solar modules in commercial capacity.

Figure 2.3. Installed solar modules.[10]

2.1.3 Hydro renewable energy system

This is one of the oldest forms of renewable energy system, with its first usage dating back to the late 19th century. Today, hydropower accounts for over 80% of global renewable electricity production with China having the largest installed

capacity[11]. A hydropower system works basically by using the force of moving water current to turn turbines. These rotating turbines rotate the shaft of an electric generator to produce useful electricity. Years of research and innovation have given rise to various forms of hydro energy systems both in the small scale and in the large scale. Micro-hydro power produce about 5 to 100KW of electricity to power small homes in the rural areas. While the operation of a hydropower plant does not emit significant greenhouse gases, concerns have been raised on the negative impacts of hydropower dams on the aquatic environment. However, they remain the major source of energy for most Oceania countries and countries with access to water bodies. An estimated 55 to 60% of power generation in New Zealand comes from Hydro energy[12].

2.1.4 Geothermal energy

Geothermal energy is heat energy from inside the earth. The temperature of the earth gets higher towards the earth core. This steady supply of heat is harnessed for power generation. A conventional geothermal system is made up of three major components: the heat source, the reservoir and the fluid, which is mostly meteoric water[13]. The Steam from the high temperature is used to turn a turbine for electricity generation. The temperature of the heat determines its suitability for power generation. Most geothermal power systems require temperatures above 150 ^{o}C for operation, while lower temperatures are employed for direct-use applications, for example heating buildings[14]. Unlike other renewable energy sources like wind and solar, geothermal energy does not depend on weather, therefore it can provide reliable power supply. In the year 2017, 12.9 GW of geothermal power station had been installed worldwide[15]. Geothermal energy also accounts for over 13% of New Zealand Electricity Production[16].

Figure 2.4. Ngatamariki Geothermal Power Station, New Zealand.[16]

2.2 Energy Storage Devices

One of the challenges of most renewable energy systems is the erratic nature of the sources. The amount of wind and solar energy available at any time depends on the weather and climatic conditions of the area. Energy storage devices are necessary to store excess energy from these systems and supply back to the system when needed. Various technologies are used in energy storage devices.

2.2.1 Flywheel energy storage

Flywheel, as the name implies, is a wheel which is designed to store rotational kinetic energy as it rotates about its axis. It employs rotors of high moment of inertia to ensure sustained rotation after the rotational force is taken out. To clearly describe the working principle, consider a flywheel attached to the moving wheels of a car, the flywheel system has a mechanism that enables it to be engaged or disengaged from the car wheels as desired. The flywheel rotates along with the wheel of the vehicle as it moves. Due to the nature of the flywheel's moment of inertia, it sustains rotation after the car has stopped moving. The kinetic energy of

the car tyre has been transferred to the flywheel. This kinetic energy can be used to move the car when engaged back to the tyre.

In practice, the rotor is built in such a way that the mass is kept low while the moment of inertia is made high[17], this makes it easier to rotate. The amount of energy stored in a flywheel is limited by the tensile strength of the material used for the rotor, therefore the stress in the flywheel is not expected to exceed the tensile strength of the material[18]. Flywheels can be charged and discharged at high speeds, when connected to a machine. The flywheel charges when the machine accelerates it and it discharges when it is being slowed down by the machine as energy is being extracted. Power electronic interface is used to control the amplitude and frequency of the output voltage when used to provide electrical energy. While the energy density of a flywheel energy storage system is limited by its mechanical properties, the power density is limited by the capacity of the power electronic interface[18]. Flywheel energy storage system finds application in various systems. It is used in railway systems to store regenerative braking energy, it is used in wind energy systems to store the fluctuating wind energy, other applications are found in voltage compensation networks, space satellite systems, and marine ship systems.[19]

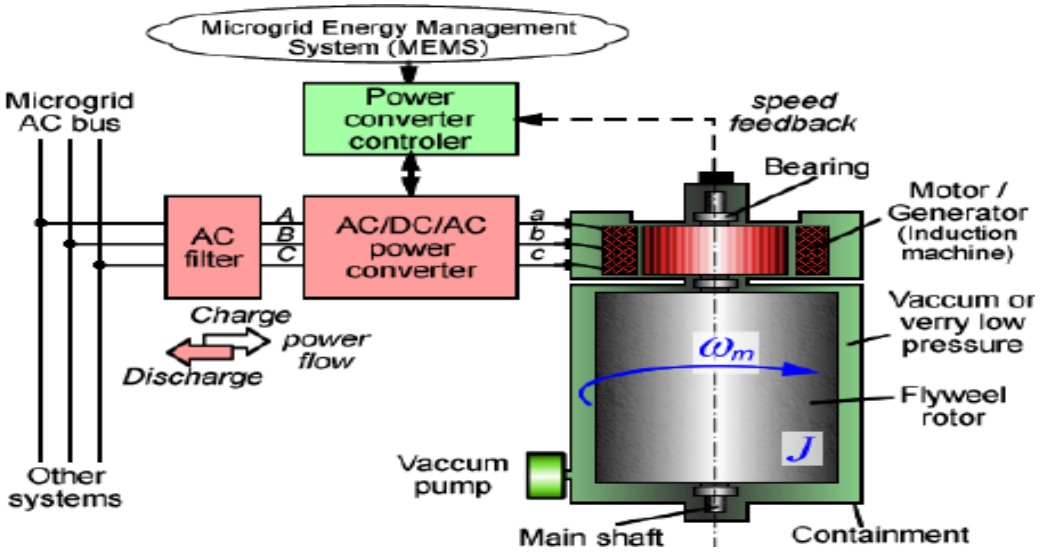

Figure 2.5. Flywheel energy storage structure.[20]

2.2.2 Superconducting magnetic energy storage

A superconductor is a material that can conduct electricity with little or no resistance at very low temperatures. During this conduction state, the material does not obey ohms law and the material retains its current flow even when the voltage source is removed. This superconductive property is adopted in the superconducting magnetic energy storage. Energy is stored in the magnetic field of a coil when energized. This energy is quantified by equation 2.1, where L is the inductance of the coil and I is the current flowing through the coil. Part of this energy can be lost as heat through the resistance of the coils as given by equation 2.2.

$$E = \frac{1}{2} LI^2 \qquad 2.1$$

$$H = I^2 Rt \qquad 2.2$$

However, with zero resistance, no energy is lost and the stored energy in the coil is retained for a long period. This concept is the principle behind the SMES system.

It basically consists of a coil of superconductive material which has been cryogenically cooled, a refrigeration system and a voltage source. When the conductor is cooled below a critical temperature known as the critical superconductive temperature, it allows dc current flow with zero resistance, magnetic field is created in the process, due to the superconductive nature of the material, the magnetic field does not collapse after the voltage source has been disconnected. Therefore, the energy is stored in persistent mode, until required[21]. This method of energy storage offers minimized delay in release of energy and has a very high efficiency. The temperature below which a material becomes superconductive is called the superconductive critical temperature. Different materials have different superconductive critical temperatures. Therefore, SMES is classified into High temperature systems (HTS) and low temperature systems (LTS) according to their superconductive critical temperatures.

SMES can be applied in micro grid systems due to its fast response in release of energy. It acts as a constant current source and a back up to inject power into the grid during periods of interruption[22]. A 10kv HTS power substation has been constructed in China to investigate its application in power systems [23]. The figure below shows the different components of an SMES.

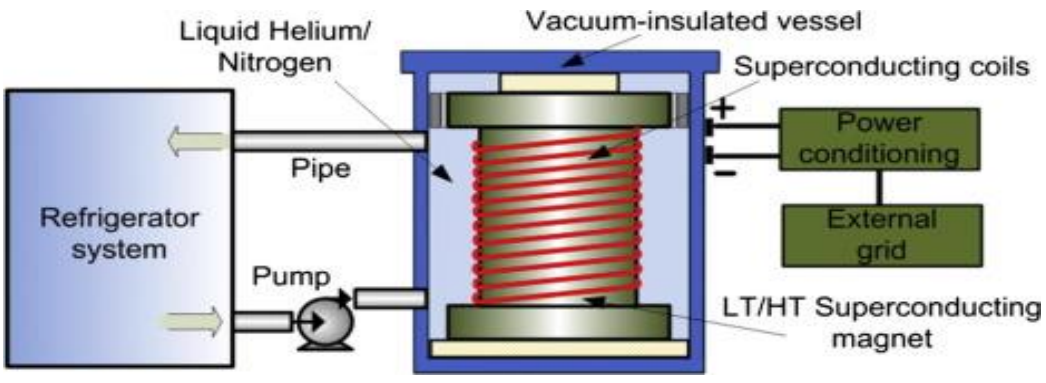

Figure 2.6. General components of SMES.[20]

2.2.3 Batteries

Battery is the most popularly used energy storage device. They operate by converting chemical energy in electrolyte to Electrical energy through faradaic process. A battery consists of one or more cells, each cell containing an anode, a cathode, a separator and an electrolyte. The electrolyte undergoes redox reaction with the electrodes, releasing ions and electrons in the process, these electrons are responsible for electricity conduction through an external circuit. Figure *2.7* is a visual representation of the working principle of a battery.

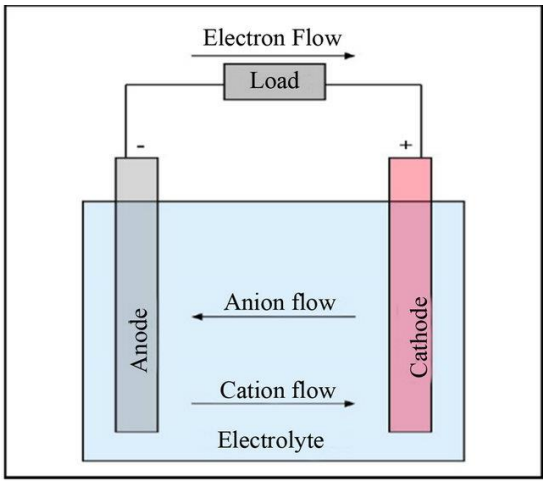

Figure 2.7. How a battery works.[24]

There are two types of cells: The Primary cells and the secondary cells. The primary cells are not rechargeable and must be replaced when the reactants are depleted. However, secondary cells are rechargeable and require a DC charging source to restore reactants to their fully charged state. The rechargeable batteries generally have lower energy storage capabilities than the primary cells[25]. The lead acid batteries and Lithium-ion batteries dominate the rechargeable battery market. Table

2.1 shows some of the common electrolytes used in battery technology and their characteristics.

Table 2.1: *Rechargeable Battery Electrolyte and Their Characteristics*[26]

Parameter	Units/conditions	Sealed lead acid	NiCd	NiMH	Li-Ion	Li-polymer	Li-iron phosphate	Rechargeable alkaline
Average cell voltage	V	2.0	1.2	1.2	3.6	1.8-3.0	3.2-3.3	1.5
Relative cost	NiCd=1	0.6	1	1.5-2.0				0.5
Internal resistance		Low	Very low	Moderate	High	High	High	
Self-discharge	%/month	2-4%	15-25%	20-25%	6-10%	18-20%		0.3%
Cycle life	Cycles to reach 80% of rated capacity	500-2000	500-1000	500-800	1000-1200		1500-2000	<25
Overcharge tolerance		High	Med	Low	Very low			Med
Internal resistance		Low	Very low	Moderate	High (coke electrode) Highest (graphite electrode)			
Energy by volume (volumetric energy density)	watt-hour/liter	70-110	100-150	200-350	200-330	230-410	200	220
Energy by weight (gravimetric energy density)	watt-hour/kg	30-45	40-60	60-80	120-160	120-210	100	80

2.2.4 Capacitors

Capacitors are electronic components which function as charge storage devices. They are the second part of the reactive components in electronic circuits, the first part being the inductor. Capacitors were first invented by Pieter van Musschenbroek a Dutch scientist from the university of Leyden in the year 1746[27]. Almost every electronic circuit makes use of a capacitor for different purposes. These purposes include: DC blocking, RF tuning, ripple smoothing application, timing, energy storage and many more. Capacitors have also found applications in various voltage regulator techniques and electric vehicles. Wherever it is used and whatever function it serves, the working principle of a capacitor remains the same. Basically, the capacitor comprises of two parallel conducting plates separated by an insulator which is called a dielectric. When the plates are connected to a dc voltage source, an electric field is created between the plates. The positive charges collect on one plate while the negative charges collect on the other plate, the capacitor stores its energy in the electric field created by the charges between the plates. The ability of a capacitor to store charges is measured as its capacitance. Like the batteries,

Capacitors can be connected in series or parallel to achieve higher or lower capacitance values as desired in a circuit. Capacitors are classified according their dielectric materials. The different types of capacitors available today include: Paper capacitor, Mica- Capacitor, Ceramic Capacitors, Film Capacitors, Electrolytic Capacitors. Owing to the developments over the years, capacitance has been associated with the physical properties of a capacitor. Equation 2.3 describes the relationship of some physical features of a parallel plate capacitor to its capacitance.

$$C = \frac{\varepsilon o A}{d} \qquad 2.3$$

Where, A is the effective area of the plates

d is the distance between the plates and εo is the permittivity of the dielectric between the plates.

From the above formulae, the capacitance of a capacitor is directly proportional to the area of the plates and inversely proportional to the distance between the plates. Consequently, higher capacitances is achieved by increasing the area of the conducting plates and reducing the distance between the plates.

2.2.5 Supercapacitors

Supercapacitors are capacitors which have the capacity to store more charges than the conventional capacitors. They store as much as ten to one hundred times more charges than the ordinary capacitors. From the previous section, it was explained that the capacitance of a capacitor is directly proportional to the area of the plates and inversely proportional to the distance apart between the plates. The supercapacitor employs these two features in ensuring larger capacitance values.

The plate's area is effectively large and made of porous material, the porous nature of the materials increase the total surface area, hence they are able to retain more charges. The supercapacitor also has thin insulator between its plates as a dielectric. The charges on the plates polarise the dielectric, making opposite charges appear on each side of the dielectric. This phenomenon makes the supercapacitor appear like a double layer capacitor. Supercapacitors are commercially available up to 40,000 farads. Supercapacitors have a high power density, therefore energy can be stored and released at very high rates, this feature has been employed in surge protector designs[17].

2.3 DC-DC Converter Topologies

The circuit boards of electronic appliances contain DC voltage rails of different voltage levels, this is necessary to meet the voltage requirements of the various components of the board. DC-DC converters are used to convert available voltages to the required voltage levels. In energy storage systems, converters are used to change the voltage level of the storage system to the voltage acceptable by the load. Years of research and innovation has seen various converter topologies proposed and patented, while researches are still ongoing to improve the efficiency and performance of the available DC-DC converter topologies.

2.3.1 Buck converter

The buck converter is a non-transformer isolated converter used basically to step down dc voltages from higher level to lower level. The power stage of the topology consists of a switch, a diode, a capacitor and an inductor arranged as shown in

Figure *2.8*. A controller is used on the feedback network to control the duty cycle of the switch gate signal and maintain a constant output voltage.

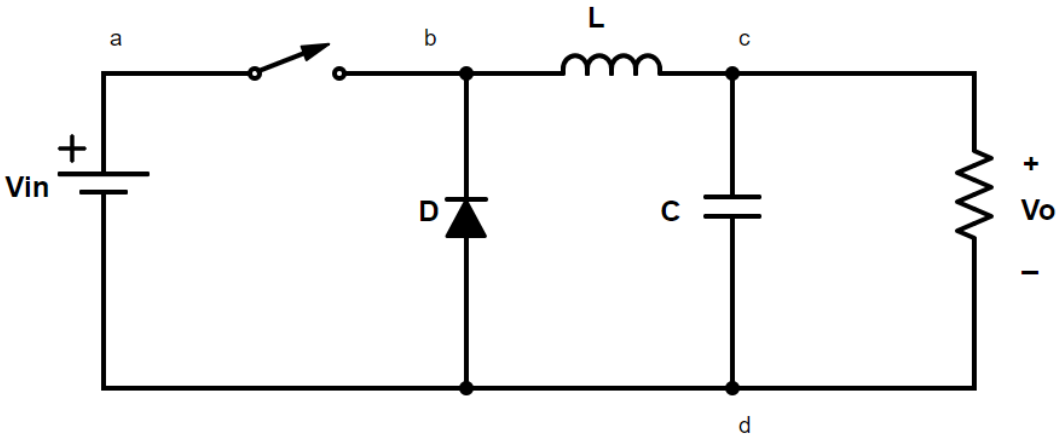

Figure 2.8. Buck converter circuit.

When the switch is closed, the diode is reverse biased and branch b-d becomes an open circuit. The current therefore flows through the inductor round the a-b-c-d loop. During this period, the current in the inductor rises steadily while energy is stored in its magnetic field. When switch is opened, the polarity of the inductor changes to bias the diode and create a current path. The energy stored in the inductor is discharged, hence the inductor current falls steadily. The output capacitor is used to minimise the output voltage ripple. The voltage transfer function of a buck converter is given by equation 2.4.

$$\frac{V_o}{V_{in}} = \frac{t_{on}}{T_s} = D \qquad 2.4$$

Where, V_o = Output Voltage

V_{in} = Input Voltage

t_{on} = On time of the switch

T_s = Total switching time

D = Duty Cycle

2.3.2 Boost converter

The boost converter is a step-up dc-dc converter. It changes the input voltage level to a higher voltage level at the output. The power stage consists of the same components as in the buck converter with a different arrangement. The topology layout is as shown in

Figure 2.9

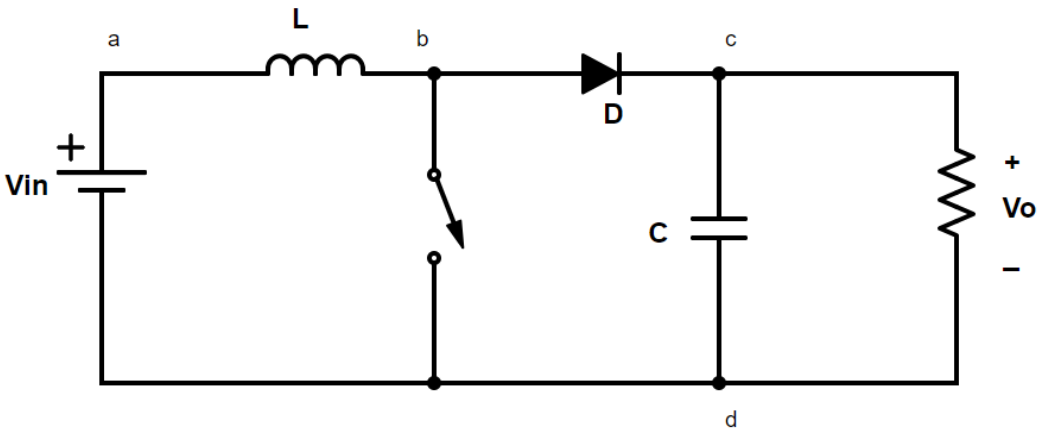

Figure 2.9 Boost converter circuit.

When the switch is on, the diode is revers biased, therefore current flows through the inductor round the loop a-b-d. During this time, the inductor stores energy and its current rises steadily. When the switch is turned off, the inductor voltage polarity reverses to bias the diode. The voltage across the inductor appears in series with the input voltage source to apply a higher voltage across the output capacitor. The inductor current also decrease steadily during t_{off}. During the operation of a boost converter, the output section of the circuit is separated from the input voltage during $t_{on.}$ Hence, the boost converter output generates higher voltage ripple at the output, however, this is reduced by a well-sized output capacitor. The voltage transfer function of a boost converter is given by Equation 2.5.

$$\frac{V_o}{V_{in}} = \frac{T_s}{t_{off}} = \frac{1}{1-D} \qquad 2.5$$

2.3.3 Buck-boost converter

As the name implies, this topology can be used for either buck or boost action. The power stage consists of the same set of components as in the buck and boost topologies,

Figure *2.10* shows the arrangement of these components in the buck-boost topology. In this topology, the output voltage has a reverse polarity in comparison to the input voltage; consequently, it is sometimes referred to as "inverting configuration"[26].

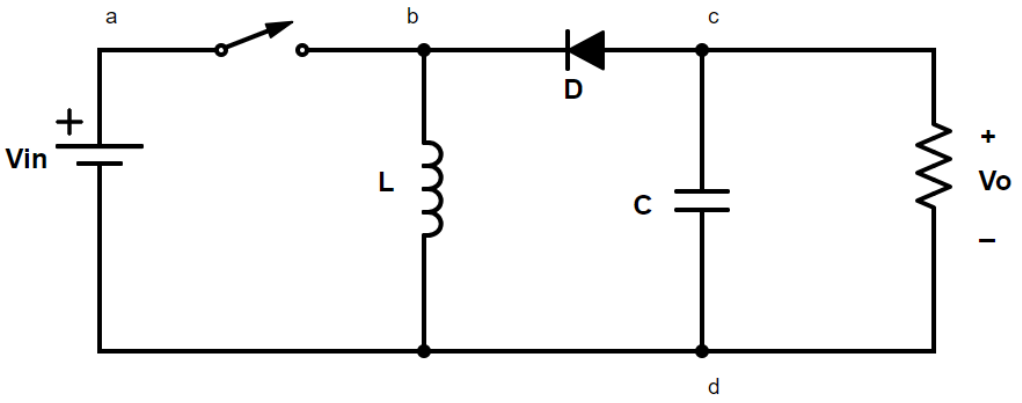

Figure 2.10. Buck-boost converter circuit.

When the switch is On, the diode (D) is reverse-biased and all the current flows through the inductor. This inductor current increases steadily while energy is stored in its magnetic field. During this time, the output capacitor (C) supplies the load current. When the switch is turned off, the inductor changes polarity to forward-bias the diode. The energy stored in the inductor during the on-time is expended during the off-time, thereby supplying current to the capacitor and output load. The duty cycle of this converter can be adjusted to change the output voltage level either

above or below the input voltage. The voltage transfer function is given by equation 2.6.

$$\frac{V_o}{V_{in}} = \frac{D}{1-D} \qquad 2.6$$

2.3.4 Ćuk converter

The Ćuk converter, pronounced as (*chook converter*) is named after the inventor, Slobodan Ćuk, of the California Institute of Technology after he first presented the design in 1976[28]. As obtained in the buck-boost converter of section 0, this topology can achieve both buck and boost actions. Its power stage contains the same components as in the other converters discussed so far with different configuration. The output voltage is also reversed as compared to the input voltage. Figure 2.11 shows the basic circuit of a Ćuk converter.

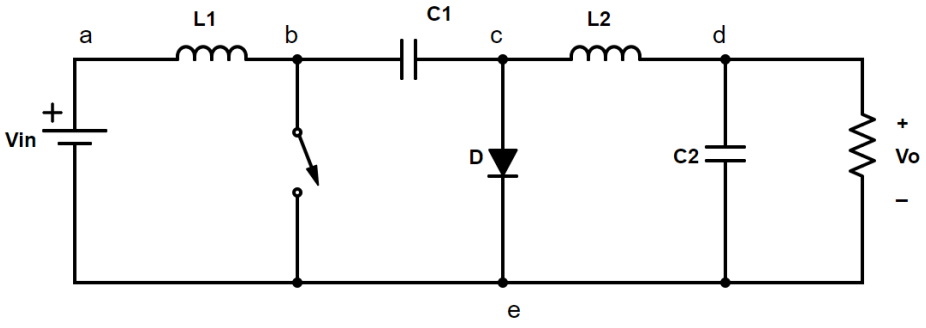

Figure 2.11. Ćuk converter circuit.

Unlike the other switch-mode converters discussed so far, Ćuk converter uses a capacitor as the main energy storage device. When the switch is on, the inductor (L1) is connected across the input voltage source, while the current through it rises steadily storing energy in the process. When the switch is off, the diode (D) forward-biases and the stored energy in the inductor is discharged to capacitor (C1)

charging it in the process. When the switch turns on again, the charged capacitor (C1) supplies the output filter and load. The major advantage of the Ćuk converter over the buck-boost converter is its continuous nature of the input and output current which gives a very low input and output ripple. The duty cycle is also adjusted to change the output voltage level. Equation 2.7 shows the voltage transfer function of the converter.

$$\frac{V_o}{V_{in}} = \frac{-D}{1-D} \qquad 2.7$$

2.3.5 Flyback converter

The converters described so far are more suited for low power applications. When Higher power and galvanic isolation is desired, transformer-isolated converters become the right class of converters. The Flyback converter is a transformer isolated converter derived from the buck-boost topology. Compared to other transformer isolated converters, it simpler and cheaper. Multiple outputs of different voltage levels is easily achieved using the Flyback converter. The circuit configuration is shown in Figure *2.12*.

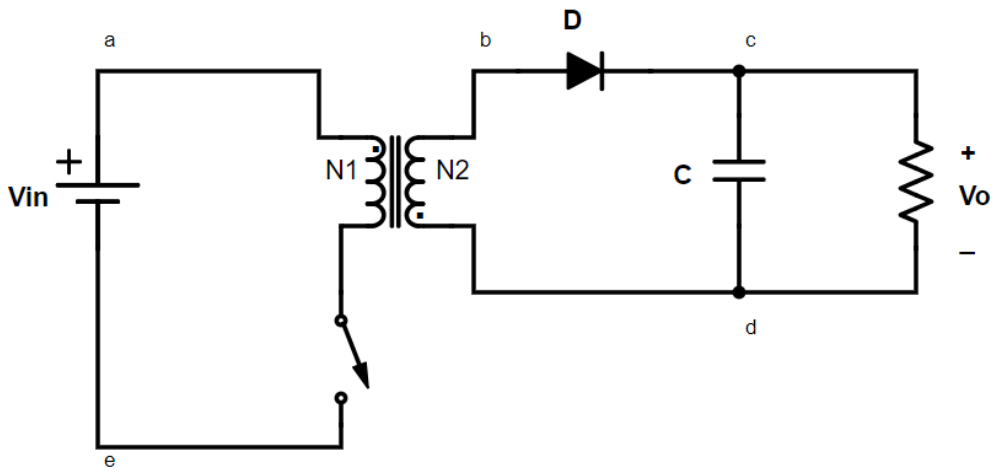

Figure 2.12. Flyback converter circuit.

The transformer in this converter uses a gapped core. The gap is used for energy storage during operation. To better understand the operation of the flyback transformer, it can be analogised with an energy reservoir, which is filled and emptied alternately. It fills when the switch is on and empties into the secondary side when the switch is off. During the switch on-time, current flows through the primary winding and energy is stored in the core air gap. At this time, the induced voltage at the secondary winding is negative, thereby reverse-biasing the diode (D), while the output capacitor supplies the output current. At the switch off-time, the stored energy is transferred to the secondary winding whose polarity changes to forward-bias the diode and supply the output current. The output voltage level is determined by the duty cycle and the transformer windings. The voltage transfer function is shown by Equation 2.8.

$$\frac{V_o}{V_{in}} = \frac{N_2}{N_1}\frac{D}{1-D} \qquad 2.8$$

2.3.6 Forward mode converter

The forward mode converter is a transformer-isolated converter derived from the buck topology. It uses a single low side switch for operation. While the buck topology is used for step down conversion only, the forward mode converter can be designed to achieve either a step up or a step-down voltage conversion. Figure *2.13* shows the circuit configuration of a forward mode converter.

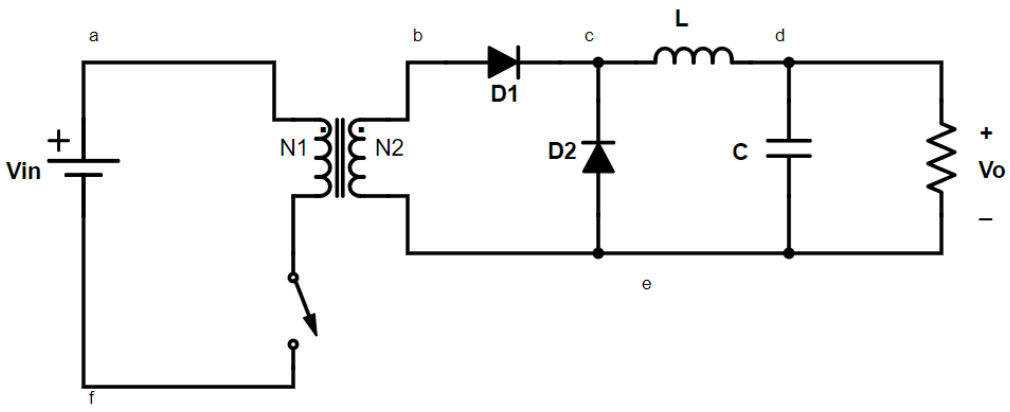

Figure 2.13. Forward mode converter circuit.

When the switch is closed, diode (D1) is forward-biased while diode (D2) is reverse-biased. The current through the inductor rises steadily while storing energy in its magnetic field. When the switch is opened, diode (D1) is reverse-biased while D2 conducts, the inductor current drops steadily through the output capacitor and load. The working principle is similar to the buck converter except for the transformer turns, this is also shown in the voltage transfer function of Equation 2.9.

$$\frac{V_o}{V_{in}} = \frac{N_2}{N_1} D \qquad 2.9$$

In practice, the core of the transformer tends to saturate due to repeated application of voltage of the same polarity on the primary winding. A third winding is incorporated to reset the core when the switch opens. Winding, N3 and diode, D3 of Figure *2.14* are used to achieve the core reset.

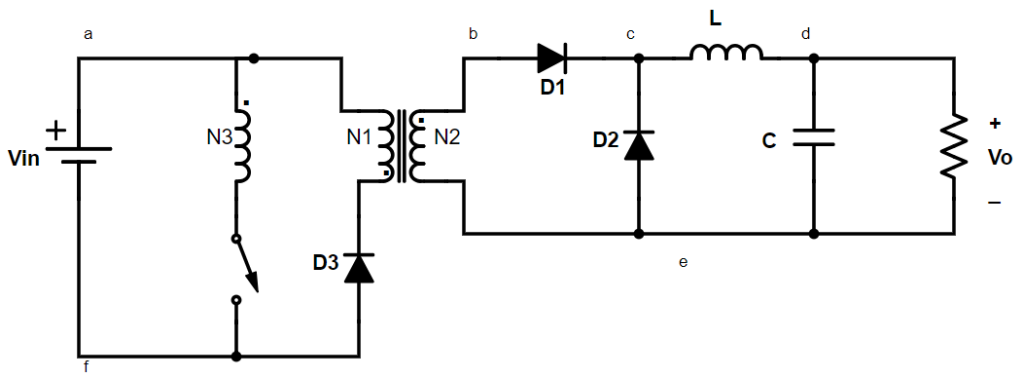

Figure 2.14. Forward mode converter with core reset winding.

2.3.7 Push-pull converter

This is a more complex transformer-isolated topology than the flyback and forward mode. As the name implies, the primary current is made to flow alternately in two directions, 180 degrees out of phase. This opposing directions of the primary currents and flux resets the transformer core and ensures that it does not saturate. Therefore, a demagnetising winding is not needed. Two power switches are used to achieve the push-pull operation, Figure *2.15* shows the circuit arrangement.

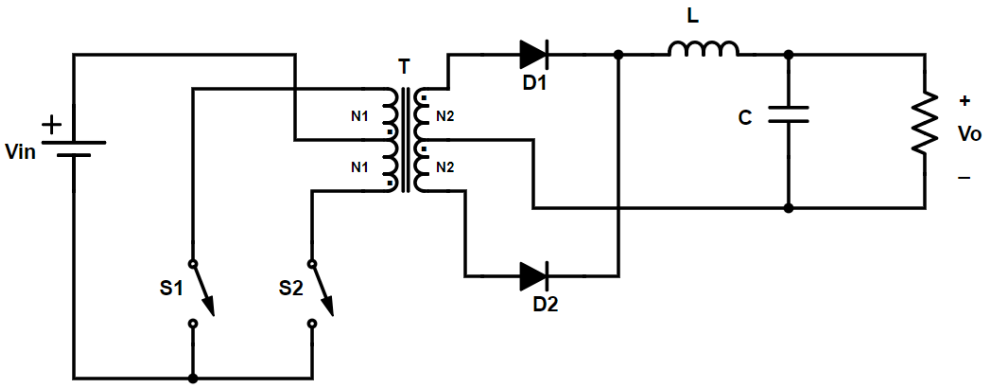

Figure 2.15. Push-pull converter circuit.

When switch (S1) is closed, diode (D1) is forward biased while diode (D2) is reverse biased. The inductor current rises steadily, flowing through to the load while storing energy in the process. In practise, a dead time is implemented on the switching cycle. This is to ensure that the first switch completely turns off before

the second switch turns on. During the dead time when the two switches are off, the inductor energy discharges through the two diodes to the output capacitor and load. When switch (S2) is closed, diode (D2) conducts while diode (D1) is reverse biased. The polarity of the voltage at this time is such the flux is in opposite direction to the flux created by the first switch action. This ensures that the transformer core does not saturate. Equation 2.10 shows the voltage transfer function of the push-pull converter.

$$\frac{V_o}{V_{in}} = 2\frac{N_2}{N_1}D \qquad 2.10$$

2.3.8 Half-bridge converter

One of the technical challenges of the push-pull converter is the possibility of flux imbalance in the transformer core. This happens when the flux created by one half of the primary winding is not completely cancelled by the flux created by the second half of the primary winding. The resultant flux gradually builds up and walks the transformer into saturation. This problem is eliminated in a half-bridge converter. A half-bridge converter does not use centre-tapping on its primary. The working principle is similar to that of the push-pull converter. As shown in Figure *2.16*, the circuitry consists of a high side switch and a low side switch, with two similar bulk capacitors at the input side. The capacitors alternately supply half of the input voltage to the primary winding as the switching alternates.

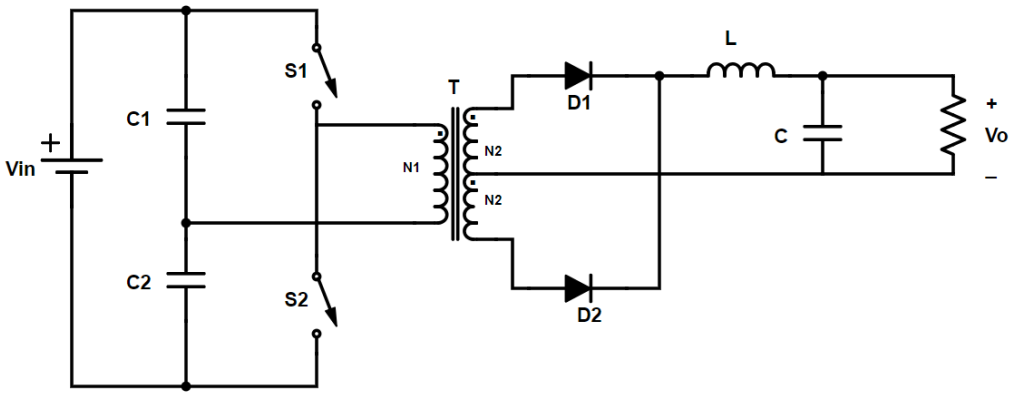

Figure 2.16. Half bridge converter circuit.

When switch (S1) is closed, the voltage of the input capacitor (C1) is applied to the primary winding. Diode (D2) is reverse biased, while Diode (D1) is forward biased and conducts current to the output load through the inductor. When switch (S2) is closed, the voltage of capacitor (C2) is applied to the primary winding. This time, the diode (D2) is forward biased and conducts current to the output load. In both phases, the inductor current rises steadily while storing energy, and reduces steadily during the deadtime to discharge into the output capacitor and load. Equation 2.11 shows the voltage transfer function of the half-bridge converter.

$$\frac{V_o}{V_{in}} = \frac{N_2}{N_1} D \qquad 2.11$$

2.3.9 Full-bridge converter

This is one of the most expensive and most complex DC-DC converters. With two additional switches for operation it has more component count that other converter types. However, higher power capabilities and efficiencies can be achieved with proper design. Figure *2.17* shows the circuit configuration of a full bridge converter.

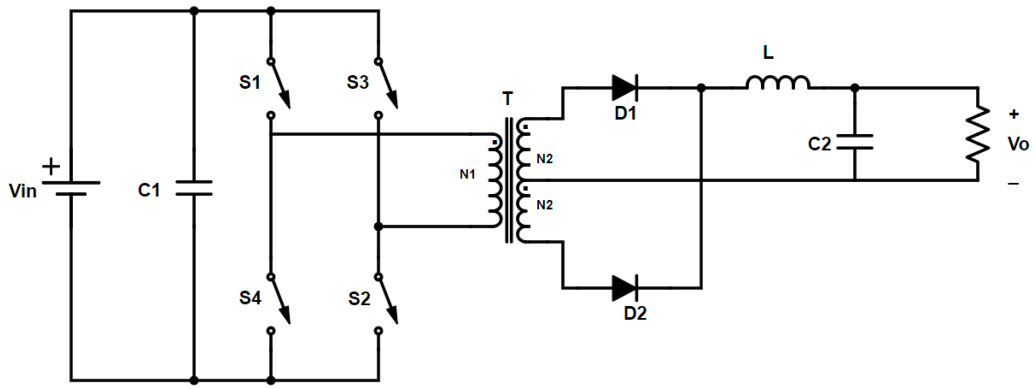

Figure 2.17. Full bridge converter circuit.

Switches (S1 & S2) close at the same time to apply the input voltage across the primary winding. Diode (D1) is forward biased to conduct current to the output. The second switching phase involves the switches (S3 & S4), they both close to apply the input voltage to the winding, this time in reverse polarity. Therefore, diode (D2) is forward biased to conduct current to the output. Since the full input voltage is applied to the primary winding at each switching phase, the full bridge converter is more suited for high input voltage application than the half-bridge converter. This also makes it suitable for higher power applications. In practise, full bridge converters are mostly used for power ratings above 1KW for a cost-effective solution. As is the case in other transformer-isolated converters, full bridge converter can be used to achieve both step-up and step-down function. Equation 2.12 shows the voltage transfer function of the converter.

$$\frac{V_o}{V_{in}} = 2\frac{N_2}{N_1}D \qquad 2.12$$

2.3.10 Single ended primary inductance converter (SEPIC)

This converter is derived from the buck-boost topology with the ability to execute both step-up and step-down function. It maintains a constant output voltage even

when the input voltage fluctuates above or below the initial value. It contains the same components as the other switch-mode converters arranged as shown in *Figure 2.18*.

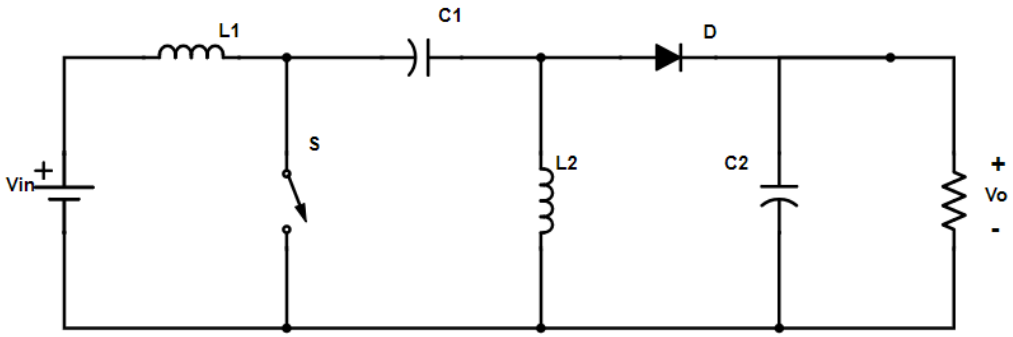

Figure 2.18. SEPIC circuit.

Since an inductor appears as a mere conductor to a dc signal, when the input voltage is connected, before the start of the switching process, the capacitor (C_1) first gets charged by the input voltage source. When the switch(S) is closed, diode (D) is reverse biased, the inductor (L_1) gets charged from the input voltage source while the inductor (L_2) gets charged from the capacitor (C_1). At this time, the two inductors and capacitor (C_1) are both disconnected from the load and the output capacitor (C_2) supplies the load current. When the switch is opened, the diode (D) is forward biased, inductor (L_1) recharges the capacitor (C_1) and at the same time supplies the load current. The inductor (L_2) also supplies the load current at this time. A PWM control circuit adjusts the duty cycle of the switch to maintain a constant output voltage. The output current is not continuous; hence the converter has the tendency for high output current ripples. The input current is however continuous. SEPIC converter is mostly used in battery powered devices where a constant voltage is required on load circuit even when the battery voltage discharges or is being charged. The voltage transfer function of the converter is shown in equation 2.13.

$$\frac{V_o}{V_{in}} = \frac{D}{1-D} \qquad 2.13$$

Chapter Three

Supercapacitor Technologies

3.1 An Overview

Supercapacitors generally are capacitors of high capacitance values, 10 to 100 times the value of a conventional electrolytic capacitor. They store more charges than the conventional capacitors. However, most commercially available Supercapacitors have low voltage ratings. While the supercapacitor and the electrolytic capacitors serve the same core purpose of storing charges, the technologies inherent are different. From the relationship between the capacitance of a capacitor and its physical properties as stated in Equation 2.1, capacitance is directly proportional to the area of the plates and inversely proportional to the distance apart between the plates. The supercapacitor employs these two principles to ensure larger capacitance values. The plate area is effectively large and made of porous material, the porous nature of the materials increase the total surface area. The supercapacitor also has thin insulator between its plates as a dielectric. The charges on the plates polarise the dielectric, making opposite charges appear on each side of the dielectric. This phenomenon makes the supercapacitor appear like a double layer capacitor, forming the basis for the first type of supercapacitor known as the Electrochemical Double layer capacitor.

Before a detailed overview of the different technologies inherent in commercially available supercapacitors is made, it is necessary to understand the existing charge storage processes in energy storage devices.

Generally, the known charge storage processes are classified under two major groups:

I. Faradaic process

II. Non-faradaic process

Faradaic process – In this process of charge storage, charge accumulation is achieved by an electron transfer that produces chemical or oxidation state changes in the electroactive materials according to Faraday's Law[29]. Popularly known processes that are of the faradaic nature include; under-potential deposition, reversible electrochemical doping (intercalation), and redox reaction of transition metal oxides [30, 31].

Non-Faradaic process – In this process, charge storage is achieved electrostatically by positive and negative charges residing on two interfaces separated by a dielectric or a vacuum[29].

3.2 Supercapacitor Electrochemistry

The unique feature of a supercapacitor is its ability to store higher amount of charges than the conventional electrolytic capacitor. While the energy density of a supercapacitor is much higher than that of an electrolytic capacitor, it is low when compared with other energy storage devices. Therefore, the improvement of the supercapacitor energy density has become an area of intensive research activity in recent years. A popular way of achieving this is by the development of highly porous electrode material with varying properties. A porous electrode provides an effectively large electrode surface area for charge storage. Another common way of improving the energy density of supercapacitors is through the implementation

of electrodes with highly effective charge storage processes. The electrochemistry of a supercapacitor involves the electronic interaction or behaviour of the different supercapacitor constituents (electrode, separator and electrolyte) to achieve charge storage. The electrochemistry behaviour of different electrode materials and electrolyte determine the charge storage processes and consequently the capacitance level of the supercapacitor device. Therefore, a study of the supercapacitor electrochemistry provides a good foundation knowledge for innovative research in supercapacitor technology. Basically, supercapacitor energy storage processes involve either the accumulation of charges or reversible redox reactions[32]. These mechanisms are achieved through different means, some of which are explored in the subsequent sections of this paper.

3.2.1 Electrosorption

This electrochemistry process involves the reversible movement of charged ions in an electrolyte to the surface of oppositely charged electrode due to an electric field formed by the potential difference between the electrode and electrolyte[33, 34]. It is a non-faradaic process; therefore, in the ideal situation, the charged ions do not react with the electrode or combine chemically with the electrode, rather they stay on the surface of the electrode to form a layer of charges. However, in real-world application, some ions combine with the electrode materials as undesirable effects. The attraction between oppositely charged ions form the adhesive force keeping the charges on the electrode surface. The movement of the charged ions unto the electrode from the electrolyte is termed *adsorption*, while *desorption* is the movement in the opposite direction. Underpotential deposition (UPD) is an example of an adsorption process.

3.2.2 Intercalation

The dictionary meaning of intercalation is “to insert”. In electrochemistry, intercalation refers to the reversible insertion of ions into vacant spaces in compounds with layered structures. For example, Li-ion intercalation into tunnel-structured iron sulphide[35]. Since intercalation involves a chemical combination of ions, it is regarded as a faradaic process. Intercalation is basically a form of redox reaction. It exhibits pseudocapacitance and therefore commonly applied in Pseudocapacitors. The opposite of intercalation is *detercalation*.

3.3 Supercapacitor Electrode Material

The overall performance of supercapacitor devices is closely related to the materials employed for the electrodes. The structure of the electrode materials and some intrinsic properties of the materials are keys to its performance[36]. As the capacitance of a supercapacitor varies linearly with the surface area of the electrodes, the major feature of a supercapacitor electrode has become its porosity. Porous materials have larger surface area than non-porous materials of similar volume, hence the use of porous materials in supercapacitor electrodes ensures higher capacitance. Other desirable properties of a supercapacitor electrode material include; high electronic conductivity, low electrical resistance, low cost, adequate mechanical strength and good thermal stability. Carbon is a very popular material used in supercapacitor electrodes, its superior electronic/ion conductivity, low electrical resistance, availability, thermal stability, corrosion resistance and low cost contribute to its popularity in supercapacitor technology[37, 38]. Advanced studies to increase the accessible pores of porous carbon has given rise to different forms of carbon-based electrodes, some of which are discussed in the next sections

of this thesis. Metal oxides and conducting polymers are also common electrode materials with unique features of higher specific capacitance than the carbon counterparts.

3.3.1 Activated carbon

Activated carbon is the most widely used electrode material in supercapacitors[37]. They are basically carbon processed to have small pores for larger surface area. They are produced from carbonaceous source materials such as wood and coal, through different activation processes. The physical activation process involves the heating of the carbon materials at high temperature (700 ^{o}C - 1200 ^{o}C) and treatment in the presence of oxidizing gases like steam and CO_2[39]. The chemical activation process is simply the treatment of the carbon precursor at much lower temperature in the presence of chemicals like alkalis and alkaline earth metals. Activated carbon electrodes have wide range of pore sizes, from micropores (<2 nm), mesopores (2nm-50nm) to macropores (> 50nm)[37, 38]. Charges are stored electrostatically on activated carbon, making them exhibit double layer capacitance.

3.3.2 Carbon nanotubes (CNT)

While electrode surface area is an important factor in capacitance sizes, it has been shown from research results that the pore size distribution is also a factor that plays an important role in the performance of a material as supercapacitor electrode[40]. Pores whose sizes are less than the electrolyte ion sizes do not participate in the electrochemical process. With the wide range of pore sizes in activated carbon, many of the pores are not involved in the charge storage process. However, the pore sizes in carbon nanotubes are predominantly mesoporous and interconnected, therefore allowing easier access to electrolyte ions, this makes for more efficient use of the electrode surface area. Supercapacitors with carbon nanotubes tend to

have lower ESR than the those with activated carbon, this is due to easier diffusion of the electrolyte ions into the mesoporous network[41]. The discovery of carbon nanotubes with the unique pore structure has posed to be a great improvement in the carbon-based supercapacitor electrodes. They have better electrical conductivity, mechanical and chemical stabilities than activated carbon. They are produced by controlled decomposition of certain hydrocarbons, for example a carbon nanotube is made by the catalytic decomposition of acetylene[42]. The control enables adjustment of different parameters to achieve a nanostructure. While carbon nanotubes theoretically have more specific capacitance than activated carbon, actual supercapacitors based on carbon nanotubes only show slightly better or sometimes poorer specific capacitances[43]. The specific capacitance is however improved through better production processes. CNTs are categorised according to their structures into single walled and multi-walled carbon nanotubes. As carbon nanotubes do not always show higher specific capacitances despite their unique structures, they are usually combined in composite electrodes with materials that possess much higher specific capacitances. This is an area of current research focus in the supercapacitor technology, and electrode materials superior to activated carbon have been developed through this process. Some of these composites include; CNTs/polypyrrole[44], CNTs/MNO_2[45] , CNTs/RUO_2.

3.3.3 Carbon aerogels

Aerogels are gel substances where the liquid part of the gel has been dried out and replaced with air. Carbon aerogels are prepared by the pyrolysis or carbonisation of organic aerogels, example resorcinol-formaldehyde aerogels, in the presence of inert gases at temperatures above 600 ^oC[46]. They are highly porous with mostly mesoporous sizes, and the production can be controlled to vary the pore size distribution. They are exceptionally light in weight and possess a monolithic

structure. The monolithic structure enables them to be fabricated as electrodes without binders, hence giving the advantage of lower ESR. Their low density, high surface area, mesoporous and monolithic structure and conductivity make them a good choice for supercapacitor electrode material. They have shown good specific capacitance in lab reports. The cost of the supercritical drying of the gel is high and the commonly used precursors (resorcinol and phenol) are toxic to the environment, these have therefore, slowed down the application of carbon aerogels in commercially available supercapacitors. Other nanostructured forms of carbon that have showed good potentials include carbon nanofoams and carbon nanocoils. Due to factors ranging from cost of production and low conductivity, they are mostly used in electrodes as composites with metal oxides.

3.3.4 Graphene

This is an allotrope of carbon that exists as a single layer of graphite. Recent studies have shown huge potentials in the use of graphene as electrode material. They have high specific surface area, good electrical conductivity, chemical and thermal stability. The surface area of a single sheet of graphene measured to be 2630 m^2/g is higher than the activated carbons used in most supercapacitors[47]. Experiments have shown that the high surface area when properly utilised gave and energy density of 136 Wh/kg at 80 °C[48]. Due to their mechanical strength, they can also be used as substrate for metal oxides and conducting polymers in composite electrodes. Significant amount of research is being conducted on graphene electrode material for supercapacitors, and it offers huge potential for the future of supercapacitor electrodes.[49].

3.3.5 Metal oxides

Electrode materials from metal oxides exhibit pseudocapacitance through faradaic charge storage process. They have much higher specific capacitance than the carbon electrodes therefore making them suitable for high energy dense supercapacitors. One of the most popular metal oxides used in supercapacitors is ruthenium oxide. Experiments have shown specific capacitance as high as 788 F g^{-1} for ruthenium oxide[50]. It is a common practise to combine metal oxides and carbon-based electrodes in order to achieve superior electrode material. The combined material enjoys the high specific capacitance of metal oxides and the high electrical conductivity of carbon. Other commonly used metal oxides include manganese oxide (MnO_2), Nickel oxide (NiO_2), iridium oxide (IrO_2).

3.3.6 Conducting polymer

Conducting polymers are simply organic polymers that conduct electricity. They have been found to possess pseudocapacitive properties. Therefore, when used as supercapacitor electrodes they undergo fast redox reactions during charge and discharge cycles. Like in metal oxides, they have high specific capacitance, high conductivity and low ESR. Two forms of conducting polymers are usually used; the n-doped conducting polymer used for negative electrodes and the p-doped conducting polymer used for positive electrodes. One of the draw backs have been the lack of n-doped conducting polymers, and the resulting mechanical stress after several cycles[51]. These have limited the progress as electrode materials. Due to the mechanical weakness of conducting polymers, numerous composites with the mechanically stronger carbon materials have been proposed by researchers and produced in labs. Some examples of conducting polymers include; Polypyrrole (PPy), Polyaniline (PANI), poly-(3,4-ethylenedioxythiophene) (PEDOT).

Table 3.1 is a summary of different electrode materials and their respective specific capacitances in specified electrolytes.

Table 3.1: *Supercapacitor Electrode Materials and Specific Capacitances*[32]

Electrode materials	**Electrolyte**	**Specific Capacitance (Fg^{-1})**
Activated Carbon	Aqueous (NaOH/KOH)	200-400
Carbon nanotubes	Aqueous (NaOH/KOH)	20-180
Carbon Aerogels	Aqueous (NaOH/KOH)	40-200
Graphite and reduced Graphene oxide (RGO)	Tetraethylammonium tetrafluoroborate (Et_4NBF_4)	10-150
Manganese oxide (MnO_2)	K_2SO_4	261
Ruthenium oxide (RuO_2)	H_2SO_4	650-735
Polypyrrole (PPy)	Aqueous Electrolyte	40-588
Polyanaline (PANI)	Aqueous Electrolyte	120-1530

3.4 Supercapacitor Electrolyte

The electrolyte used in supercapacitors also play a role in the device performance. They determine key parameters such as the ESR, operating temperature range and voltage capability[40]. The maximum voltage capacity of the supercapacitor depends on the decomposition potential of the electrolyte used[52]. Researches and experiments have shown that non-aqueous electrolytes tend to have higher

decomposition potential than aqueous electrolytes[53, 54]. Electrolyte decomposition is an undesirable phenomenon in a supercapacitor, because of this, better supercapacitor performance is achieved when the temperature rise is kept minimal as possibilities of decomposition increases with temperature[55]. Table 3.2 shows some of the common electrolytes used in supercapacitor technologies and their respective voltage capabilities. Electrolytes with smaller ion sizes have better chances of accessing smaller pores of the electrode to participate in electrochemical action. Therefore, such electrolytes give rise to higher capacitances.

Table 3.2: *Common Electrolytes Used for Supercapacitor Application*[56]

Properties of various electrolytes.			
Electrolyte	**Density (gm/ cm^3)**	**Resistivity (Ohm-cm)**	**Cell Voltage**
KOH	1.29	1.9	1.0
Sulfuric acid	1.2	1.35	1.0
Propylene carbonate	1.2	52	2.5-3.0
acetonitrile	.78	18	2.5-3.0
Ionic liquid	1.3-1.5	125 (25°C) 28 (100°C)	4.0 3.25

3.5 Supercapacitor Model and Equivalent Circuit

A capacitor is modelled as a capacitance in series with a resistor which represents the equivalent series resistance. Due to the porous nature of the electrodes, the equivalent circuit model of a supercapacitor is more complex. The pores contribute to the Supercapacitor's internal resistance; therefore, the non-uniformity of the pores makes the modelling more complex.

Several models have been proposed by researchers in the industry. One of the common models is an array of pores arranged in parallel. Each pore is represented by a set of repeated two-port components as shown in *Figure 3.1* [57] this model assumes that the pores are uniform. However, in the case of activated carbon electrode where the pores are non-uniform, this model fails. Subsequent equivalent circuits have been developed, where the non-uniformity of the pores is taken into consideration. The universal equivalent circuit for a symmetric carbon-based Supercapacitors consists of a vertical ladder network connected in series with a parallel RC network[57]. The circuit contains parallel branches with unique time constants (RC), the model is based on the knowledge that the network of pores in the activated carbon electrode behaves like a group of smaller capacitances connected in parallel, where each connecting wire has its own resistance, hence the unique time constant of each branch[58]. The equivalent circuit explains some of the characteristic of a supercapacitor, which are the open circuit voltage decay, loss of capacitance at high frequency and voltammetric distortion at high scan rate. More information about this model can be found in [57]. The approximate equivalent circuit is used for analysis in this project.

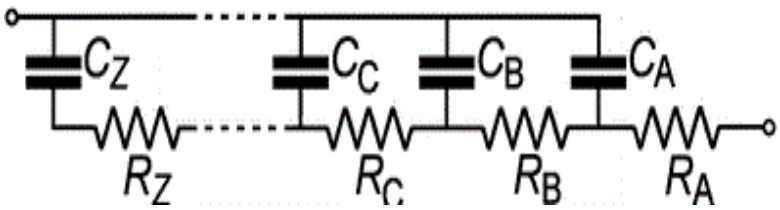

Figure 3.1. Horizontal ladder network.[57]

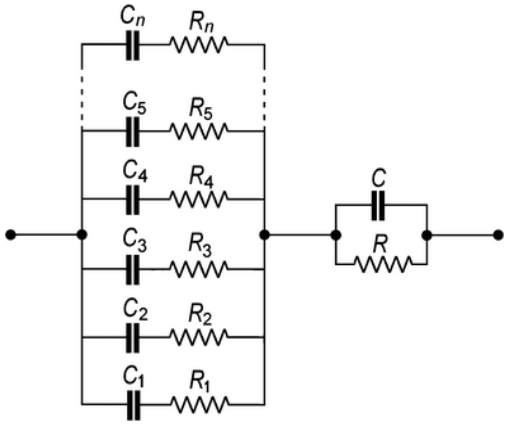

Figure 3.2. Vertical ladder network.[57]

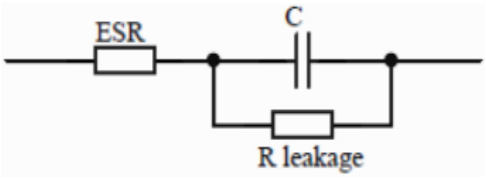

Figure 3.3. Equivalent circuit of a symmetric carbon based supercapacitor.[57]

3.6 Supercapacitor Types

There are different mechanisms of charge storage in supercapacitor electrochemistry, these mechanisms as described above belong to either of two processes namely the faradaic process and the non-faradaic process. These storage mechanisms are utilised in Supercapacitors either separately or in combination to give rise to the different supercapacitor technologies available today. The types of Supercapacitors based on these storage mechanisms include:

I. Electrochemical double-layer capacitor
II. Pseudo-capacitor
III. Hybrid capacitor

3.6.1. Electrochemical double layer capacitor (EDLC). The non-faradaic process is the dominant charge storage process in this type of supercapacitor. Charges are stored electrostatically without any chemical reaction at the electrode - electrolyte interface. They consist of two blocks of activated electrode materials, a thin separator and a high conductivity electrolyte. When voltage is applied to the terminals, opposite charges accumulate on the electrodes, each electrode attracts unlike charges from the electrolyte. The result is that each electrode has two layers

of charges, the positive and the negative charges. Due to the nature and design of the electrodes employed, the ions do not recombine. The layers of positive and negative charges on the electrodes constitute capacitances, and in addition to the capacitance produced across the separator, the EDLC has much higher energy densities than the conventional capacitors. Also, since the ions do not recombine, it can sustain high number of charge-discharge cycles making it more durable than batteries. An electrolyte provides the ions which form the double layers with the electrodes. The separator in the supercapacitor functions to maintain a barrier between the two electrodes, it is made as thin as possible to reduce the capacitor's equivalent series resistance. The electrodes are made to have very large true surface to geometric volume, this means that more effective surface is achieved in a small volume of space, this large surface area is achieved by expanding the pores in the carbon[59]. Figure *3.4* shows the effective surface area of ordinary electrode and the surface area of the activated carbon. The curvature of the pore makes available larger area than the flat ordinary electrode. Note that a continuous increase in the activated carbon electrode surface area does not always represent increased capacitance. This can be as a result of smaller sized pores of the electrode not being accessible to the electrolyte ions[32, 33, 60]. Hence the pores sizes are optimised for better energy density[54]. The electrodes of the Electrochemical Double layer capacitor are usually made of carbon of different forms, the popular carbon electrodes include: Activated carbon electrodes, Carbon aerogel electrodes, Carbon nanotubes electrodes. The EDLC is the most commercially available supercapacitor type. Examples include; 3,000F SC by SAMWHA capacitor group, 2,000F SC by Ioxus. Inc. etc

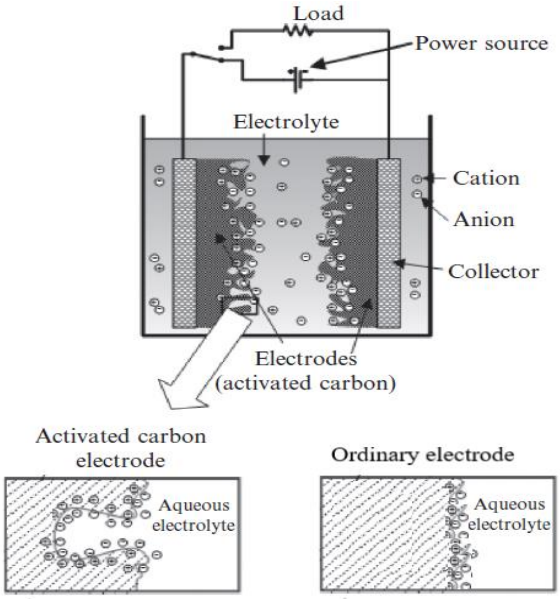

Figure 3.4. Working principle of the EDLC with activated carbon electrodes.[61]

3.6.2 Pseudocapacitor

While the EDLC does not involve any chemical changes in the electrolyte, the reverse is the case in pseudo-capacitors. The chemicals of the electrolyte break down through the Faradaic process to release ions that get attracted to the electrodes. This is accomplished majorly through either electro-sorption, reduction-oxidation reactions, or intercalation processes[31, 62]. These faradaic processes that lead to charge transfer take place at the electrode-electrolyte interface and are highly reversible[31]. Usually, the Faradaic reaction gives rise to a capacitance much higher than that of the typical ultracapacitor which develops only charge Separation-based double layer capacitance[53]. While the capacitance tends to be higher, the power capability of the pseudo-capacitor is lower than that of EDLC, and they suffer lack of stability during cycling [63]. This is due to the slow rate of the faradaic processes when compared to the non-faradaic ones. Unlike the EDLC whose electrodes are inert to the electrolyte used, it is expected that the electrodes of the pseudo-capacitor be reactive with the electrolyte. The electrode materials

used in this type of supercapacitor are mostly conducting polymers and some oxides of metal. The pseudocapacitive processes are sometimes easily confused with the faradaic reactions at the battery electrodes. While similarities exist, the pseudocapacitive process exhibit more constant capacitance over the operating voltage while the capacitance varies over the voltage window when a battery electrode is used[64]. Nesscap 300F, 2.3V Pseudocapacitor as shown in Figure *3.5* is an example of a commercially available Pseudocapacitor with 19ml volume and 24g weight.

Figure 3.5. Commercially available pseudocapacitor.[65]

3.6.3 Hybrid supercapacitor

Hybrid Supercapacitors combine the advantages of both the EDLC and pseudo-capacitor to achieve a better performing capacitor. It has a higher energy density than the EDLC and more current capability and charge-discharge cycles than the pseudo-capacitor. The electrodes of the EDLC and pseudo-capacitor are both used in a hybrid capacitor. Hybrid capacitors can be grouped according to how these electrodes are combined.

3.6.3.1 Composite-electrode hybrid

In this type of electrode, each electrode is a composite of materials from EDLC and pseudo-capacitor or battery electrodes. This type of electrode combines the good conductivity of carbon materials with the high specific capacitance of pseudocapacitive materials to achieve a superior electrode material[66]. A composite of carbon nanotubes and polypyrrole (a conducting polymer) has proven to be a success in the past[67], lithium-ion capacitors employ anodes which are mostly composites of carbon based material doped with lithium[68]. Other examples of composite electrodes include graphene/MnO composite[69, 70], MnO/carbon nanotubes composite[71, 72].

3.6.3.2 Asymmetric-electrode hybrid

Asymmetric electrodes have one electrode made from either the EDLC electrode materials and the other electrode made from the pseudo-capacitor electrode material. For instance, a positively charged electrode from active carbon together with a negatively charged electrode from metal oxide which has pseudocapacitive property can be combined to have asymmetric electrodes. However, the overall capacitance of this technology is usually limited by the lower capacitance electrode[73, 74]. Figure *3.6* is a commercially available hybrid supercapacitor produced by *VARTA microbattery* with EDLC-Pseudocapacitor asymmetric electrodes.

Figure 3.6. 90F, 4.2V hybrid supercapacitor.

3.6.3.3 Battery-type hybrid supercapacitor

This method adopts a battery electrode. One electrode uses the capacitor electrode, mostly activated carbon, while the other electrode is a battery electrode. This feature enables the supercapacitor to have more energy density than the conventional supercapacitor while also possessing the power density higher than a battery. A battery type hybrid supercapacitor based on Cobalt-phosphate positive electrode and activated carbon negative electrode has been reported to deliver energy density of 3.53 mWh cm^{-3} [75]. Figure *3.7* is a prototype 40,000F battery-type hybrid supercapacitor produced by SAMWHA capacitor group.

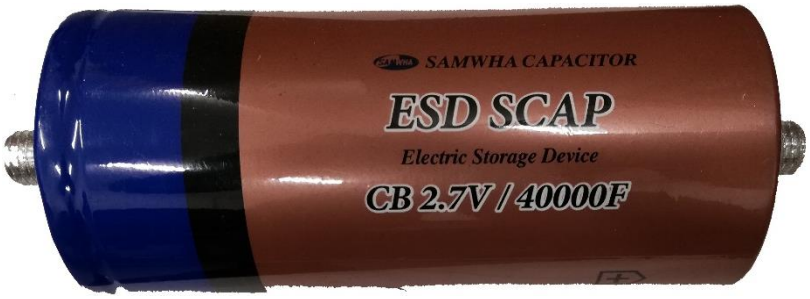

Figure 3.7. 40,000F, 2.7V battery-type hybrid supercapacitor.

Figure *3.8* is a ragone plot showing the positions of energy storage devices and the different types of supercapacitor in terms of energy and power density.

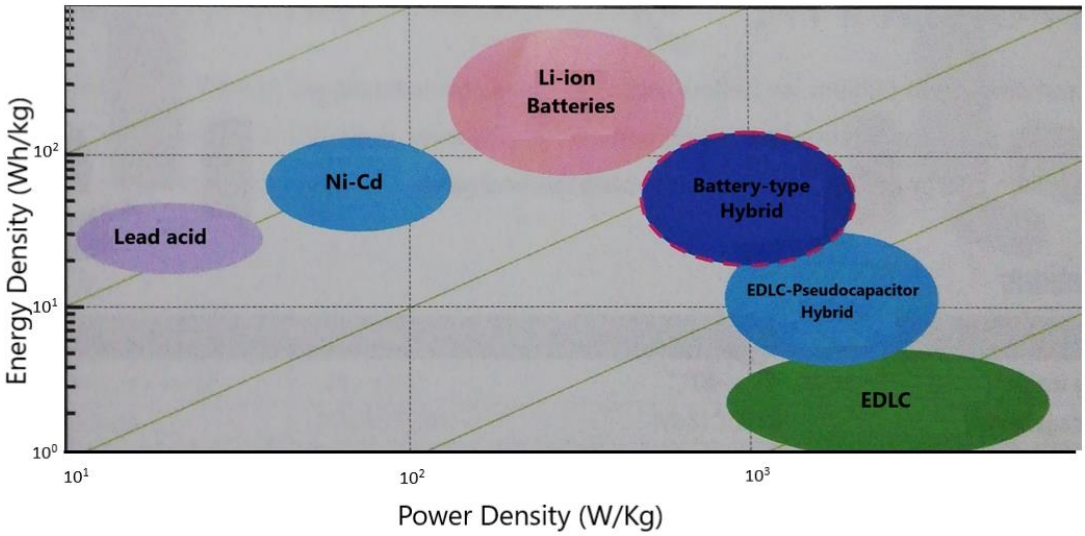

Figure 3.8. Ragone plot.

3.7 Traditional Applications of Supercapacitor

Traditional applications are the more popular and common applications of supercapacitors. Supercapacitors find usage as power back up in the memory function of various electronic products such as: mobile phones and personal computers, their usage ensures retention of data while the main power source is unavailable. They provide peak power assistance to systems with pulsed load, for instance, the bright flash light of a digital camera takes up high current when used. Therefore, a combination with batteries reduces high current stress on them and improves the battery life. In electric vehicles, supercapacitors are used as temporary energy storage devices for the brake regenerative system, this is due to their fast rate of taking in and giving out energy.

3.8 Non-traditional Supercapacitor Applications

Asides the commonly known applications of the supercapacitor devices, the research team at the university of Waikato has developed various innovative applications of supercapacitors, these applications are termed “non-traditional” a brief summary is given in subsequent sections of this thesis. Further details on the these applications is found in the book, Energy storage devices for Electronic systems, Nihal Kularatna (2015)[61]

3.8.1 Supercapacitor-assisted low dropout regulator (SCALDO)

A low dropout regulator is a type of linear voltage regulator which can maintain regulation even at low voltage difference between the input and the output, or more precisely, between the series pass element. The voltage difference across the series pass element, below which the linear regulator stops regulation is termed the “dropout voltage”. Figure *3.9* is the basic circuit of a low dropout voltage regulator.

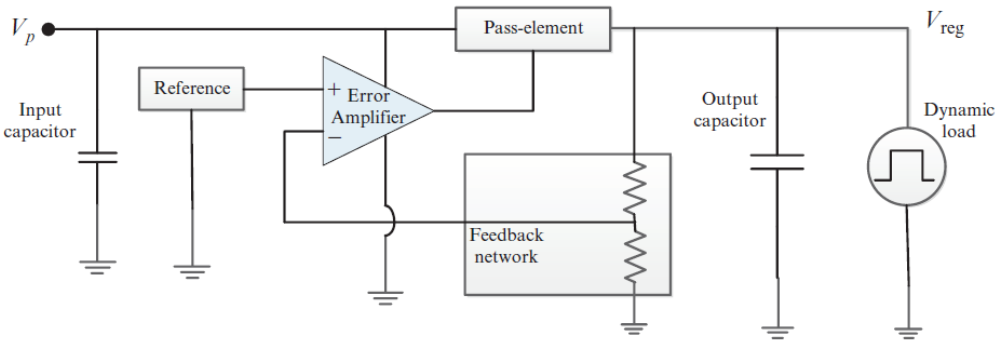

Figure 3.9. Basic circuit of an LDO.

During the operation of an LDO, power is lost majorly in the form of heat across the series pass element. This power loss depends on the resistance of the series pass element and the voltage across it. The resistance is constant, therefore the efficiency of the LDO depends largely on the voltage across the series pass element. Technically, if the voltage across the series pass element can be made to reduce, the overall efficiency of the LDO would be increased accordingly. To achieve this voltage reduction, a resistor may be connected in series to the series pass element. However, this solution would not be viable as the resistor in itself dissipates heat. Hence, a voltage dropper which would not dissipate heat becomes the best possible solution. At this point, a supercapacitor is used as the lossless voltage dropper. When a finite current flow through a capacitor, the voltage changes according to equation 3.1

$$\Delta V = \frac{I_c \Delta t}{C} \qquad 3.1$$

Supercapacitors have large capacitances and low ESR, hence when current flows through them in a circuit, they take longer time for blocking voltage to be developed

across. This is the basic concept of the SCALDO technique. Figure *3.10* shows the first stage of the SCALDO operation.

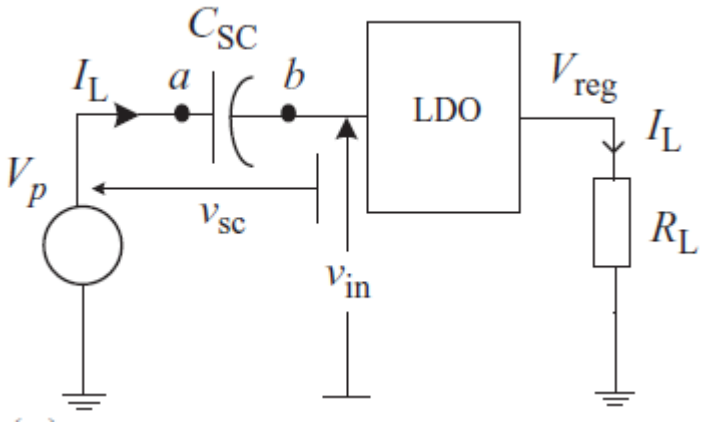

Figure 3.10. SCALDO technique (first stage).

In this stage the supercapacitor charges as current is passed through it, the voltage reaching the series pass element reduces in the process to improve efficiency. Before the SC is charged to a blocking voltage, the second stage is started. At this stage, the charged SC is made to act as the input voltage source to the LDO while the original input is disconnected. The energy stored during charging phase is discharged back into the circuit. Figure *3.11* shows the second stage of the operation.

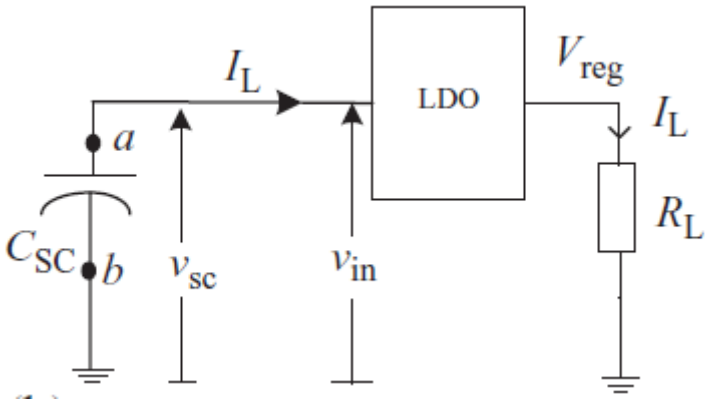

Figure 3.11. SCALDO technique (second stage).

The SCALDO technique has shown a practical efficiency of 70-80% for 12V to 5V regulator, compared to the maximum theoretical efficiency of 42% for a linear regulator of same voltage range.

3.8.2 Supercapacitor-assisted temperature modification apparatus (SCATMA)

It is a common experience with a bathroom hot water tap that cold water flows out for a while before the hot water begins to flow. This cold water are water left in the buried pipes from previous usage which has cooled over time and need to make way for the hot water. The quantity of cold water that flows out depends on the length of the pipe from the central heating system to the faucet. While this may be little amount of water for each usage instance, it is a massive volume of wasted water when the number of homes in the country is taken into consideration. To solve this problem, a heating system which can be rapid enough to heat the cold water at a point close to the faucet is required. With the SC's low ESR which gives it high power capability, a heating system based on supercapacitors have been developed. The SCATMA technique uses supercapacitors as energy storage devices to provide the required amount of current to increase the temperature of water within a very short time at a point close to the water faucet. Figure *3.12* is a block diagram of the SCATMA technique.

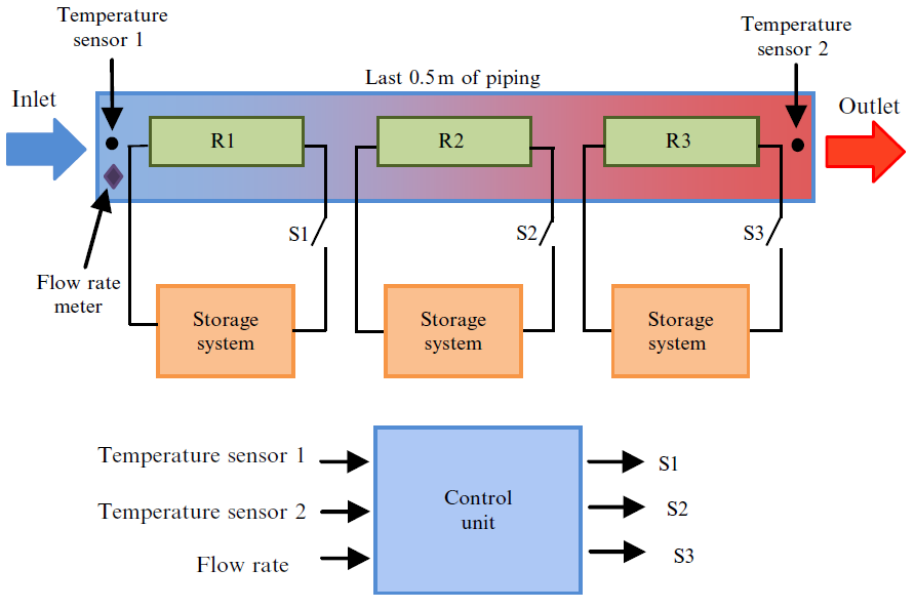

Figure 3.12. Block diagram of SCATMA technique.

3.8.3 Supercapacitor-assisted surge absorber (SCASA)

Most commercial surge absorbers use the metal oxide varistor to shunt out transient voltages away from the sensitive loads. Despite the popularity of these types of surge absorbers, they still suffer some challenges. When a transient voltage spike occurs, energy is dissipated in the form of heat on the varistors. Sometimes, energy from the transient voltages exceeds the threshold of the varistor and leads to permanent damage of the varistor. Additionally, the transient-load voltage of the surge cannot be reduced below the clamping voltage of the surge absorber. SCASA technique uses the supercapacitor to absorb part of the transient energy in the superimposed surge[76]. A coupled inductor is also used to transfer part of the transient energy into the supercapacitor in such a way that the transient load voltage is lowered. Figure *3.13* is the schematic of a SCASA circuit.

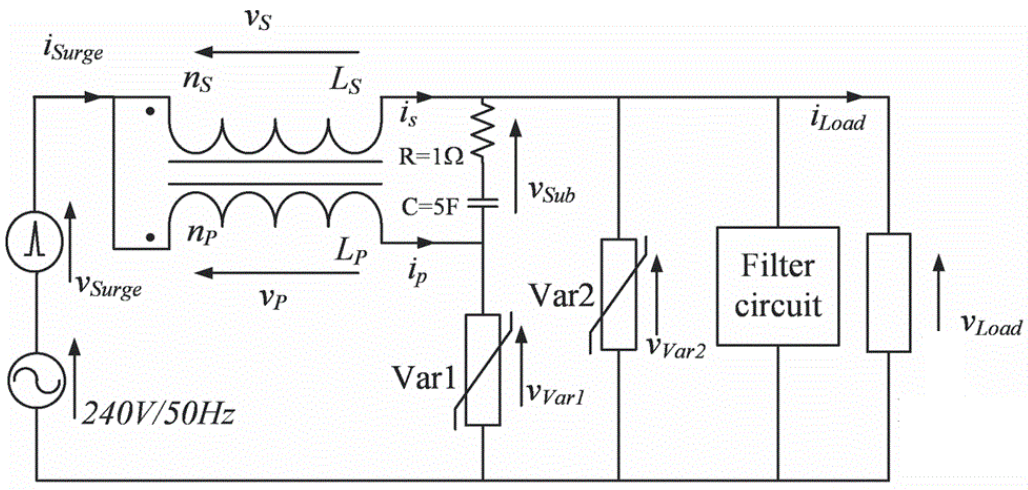

Figure 3.13. Circuit of the SCASA technique.

3.8.4 Surge resistant uninterruptible power supply (SRUPS)

This is a UPS connection technique where the supercapacitor functions as both the energy storage device and a surge absorber. Supercapacitors have the ability to absorb high voltage transients without any damage. This feature is harnessed in the SRUPS concept. It is made of an online UPS system, with three separate banks of supercapacitors. The three banks supply the load alternately. At a given time, one SC bank powers the load, one is being charged by the input while one is fully charged and is idling. When there is a transient voltage spike from the mains input, it is safely absorbed by the supercapacitor bank while keeping the load safe. SRUPS also achieves galvanic isolation as the mains input has no direct connection to the load. Figure *3.14* is a block diagram of the SRUPS technique.

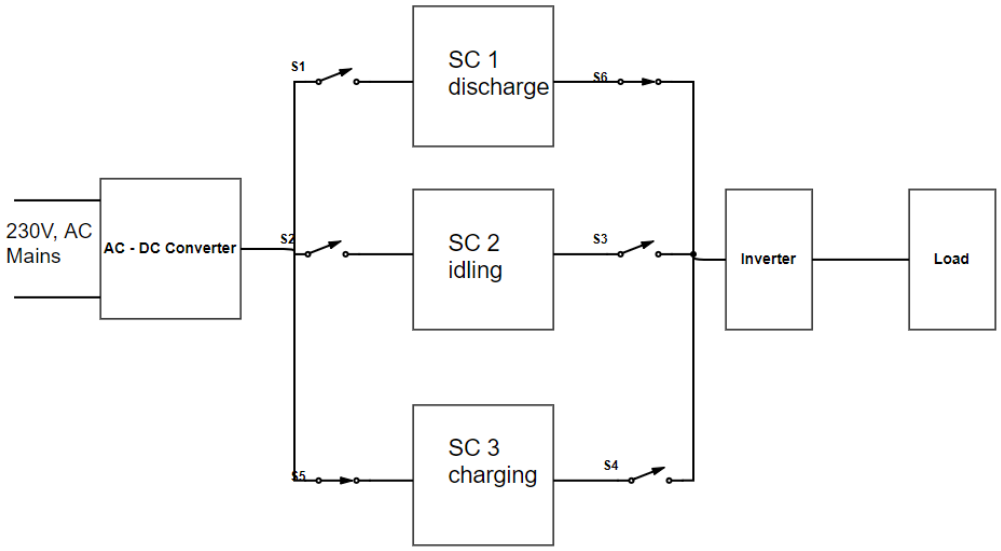

Figure 3.14. Block diagram of SRUPS technique.

3.8.5 Supercapacitor-assisted high-density inverter (SCAHDI)

The aim of this concept is to reduce the volume of inverter systems and also to increase their efficiencies. The volume of an inverter is largely determined by the transformer and electrolytic capacitors. Planar transformers have been used to achieve inverters of higher density in the past. To further reduce the size, the electrolytic capacitors can be replaced with supercapacitors. The supercapacitors also contribute in efficiency improvement. In the RC charging of a capacitor, the energy stored in the capacitor is equivalent to ($0.5CV^2$), this same amount of energy is also dissipated in the loop resistance. If an inverter system is seen as a resistive load connected in series to the supercapacitor of an RC charging circuit, then part of the energy which was wasted in the loop resistance is fed into the inverter as part of the circuit resistance, this is termed ‘loss circumvention’. This concept improves the efficiency of the inverter. Figure *3.15* shows the basic schematics.

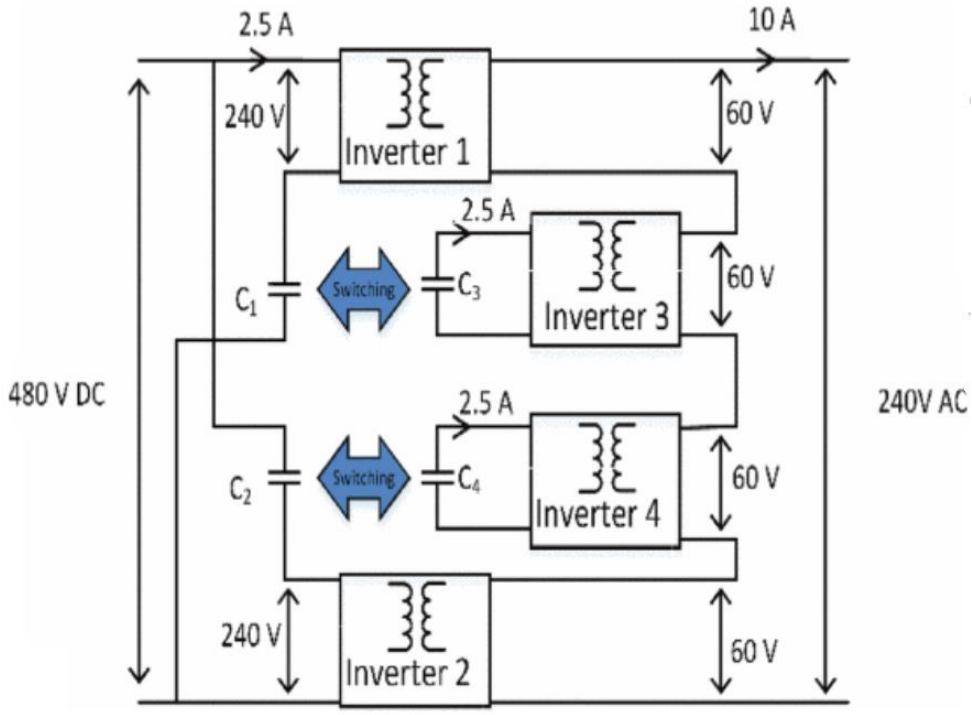

Figure 3.15. Schematic of SCAHDI.

3.8.6 Supercapacitor-assisted light emitting diode (SCALED)

The same loss circumvention applied in SCALDO and SCAHDI is also adopted in the SCALED technique[77]. In this case, LED lamps are used as the resistive component of the circuit. During the charging of the supercapacitor, the dissipated energy in the circuit loop resistance is consumed by the LED lamp for useful lighting. An LED lamp can be powered separately from its own power source, but the SCALED technique powers the LED lamp with what could have been wasted energy in the SC charging loop. The SCALED technique has two major stages; the charging phase and the discharging phase. During the discharging phase, the LED lamp is powered from the supercapacitor(s). Figure *3.16* shows the circuit topology of the SCALED technique.

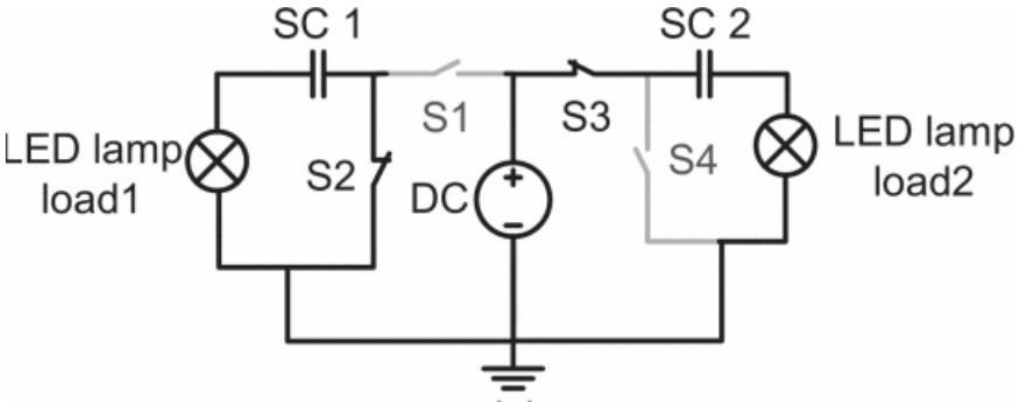

Figure 3.16. Schematic of SCALED.

Chapter Four

Laboratory Result Comparison of Supercapacitor Types

The performance characteristics of three different technologies of supercapacitor were studied in the lab. The samples include:

- A 3,000 F, 2.7V supercapacitor of EDLC technology,
- A 7,500 F, 2.8V supercapacitor of the pseudocapacitive hybrid technology
- A 40,000 F, 2.7V supercapacitor of the battery-type hybrid technology.

The following performance was evaluated:

- Constant Resistance discharge
- Constant Current discharge
- ESR Measurement

4.1 Constant Resistance Discharge

Figure *4.1* shows the circuit set up used to measure the supercapacitor's discharge characteristics

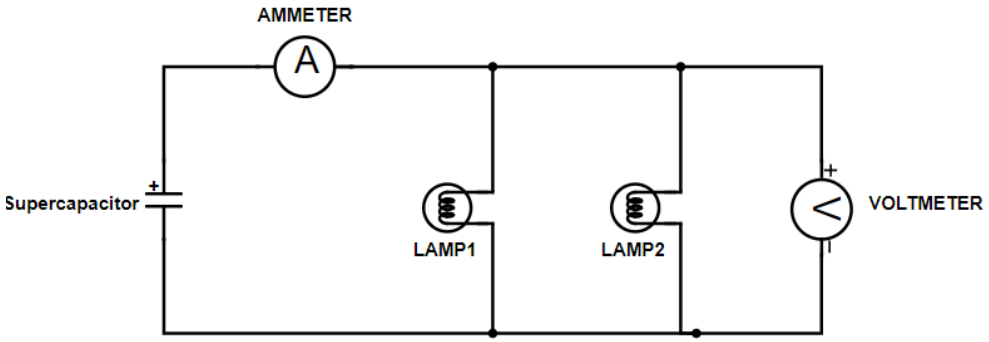

Figure 4.1. Constant resistance discharge circuit.

Two 12V, 21Watt bulbs were used as the load, this offers a relatively constant resistance load ignoring the filament change in resistance with temperature.

$$R = \frac{V^2}{P} \qquad 4.1$$

$$R = \frac{12^2}{21}$$

$$= 6.86\Omega$$

The constant resistance load used has a resistance value of about 6.86Ω.

The voltmeter in Figure *4.1* measures the supercapacitor terminal voltage at intervals, while the ammeter measures the discharge current. Figure *4.2*, Figure *4.3* and Figure *4.4* give the graphical representations of the discharge behaviour for the three different supercapacitors under constant resistance load.

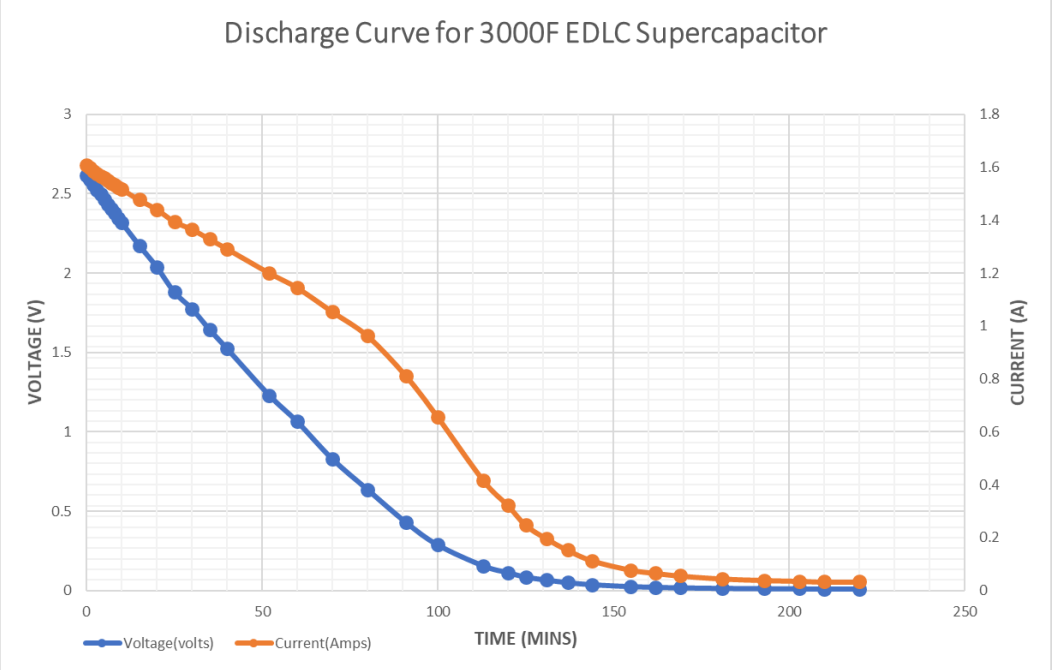

Figure 4.2. Constant resistance discharge curve for an EDLC supercapacitor.

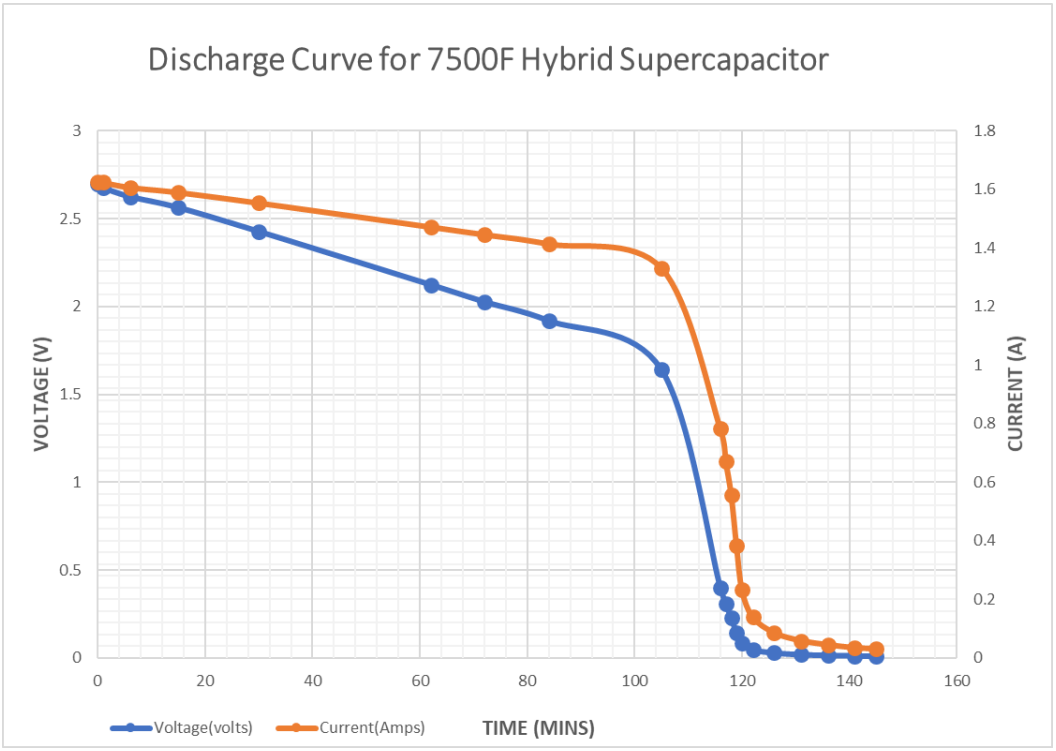

Figure 4.3. Constant resistance discharge curve for a hybrid supercapacitor.

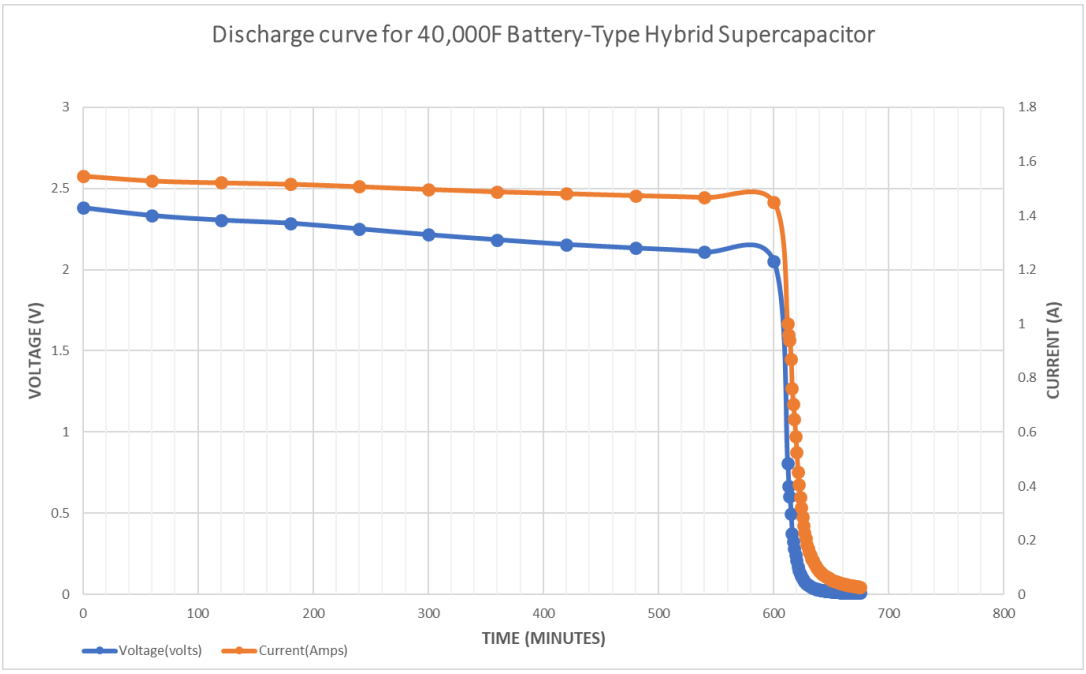

Figure 4.4. Constant resistance discharge for battery-type hybrid supercapacitor.

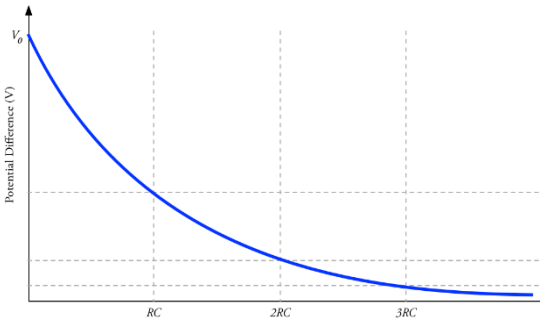

Figure 4.5. Discharge curve of a normal capacitor.

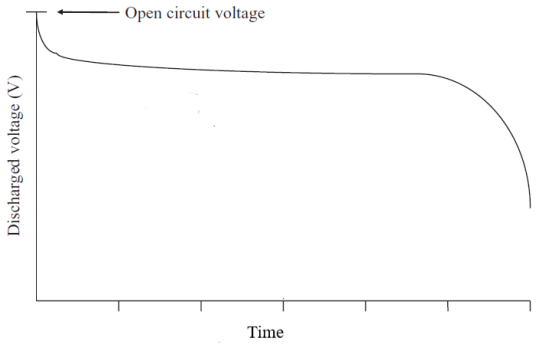

Figure 4.6. Discharge curve of a rechargeable battery.

From the graphs of Figure *4.2*, Figure *4.3* and Figure *4.4* above, the discharge curve of an electrochemical double layer supercapacitor is similar to that of a normal electrolytic capacitor. The voltage and current undergo exponential decay during discharge. *Figure 4.5* and Figure *4.6* show the typical discharge curves of a normal capacitor and a battery respectively under constant resistance load. The discharge curves of the three graphs tend towards the behaviour of the battery energy storage device as the technologies move from the EDLC type to Pseudocapacitive hybrid supercapacitor and to the battery type hybrid supercapacitor. This highlights the improvement in the energy density of supercapacitors technologies. From a voltage value of 2V to the rated 2.7V, the battery-type hybrid supercapacitor can be approximated as a constant voltage source. The same applies to the 7,500F supercapacitor from about 1.6V to the rated 2.8V.

4.2 Constant Current Discharge

A more commercially viable test is carried out, where the supercapacitors are tested at constant current discharge. In this test, the supercapacitor is treated as a battery,

and the C-rate calculated. This test is necessary as the devices are expected to supply constant power to loads in real life application.

4.2.1 C-rate calculation

The C-rate is a measure of the discharge rate of a battery (in this case supercapacitor) in relation to its maximum capacity. 1 C rate means that the discharge current would discharge the battery in one hour. It is expressed in Ampere-hour.

The energy stored in a capacitor is given by the following equation:

$$E = \frac{CV^2}{2} \qquad 4.2$$

The flat part of the curve of Figure ***4.4*** is the useful section for energy back up. This is the part where the voltage of the supercapacitor experiences minor change per unit time during discharge process. The supercapacitor acts as a voltage source at this stage of discharge. This part is used for the C- rate calculation. It is averaged at 2.2V for the battery-type hybrid supercapacitor.

40,000F battery-type supercapacitor:

C = 40,000F V = 2.2V

$$\mathrm{E} = \frac{40{,}000 \text{ X } 2.2^2}{2}$$

E = 96,800 Joules.

From basic knowledge of electricity calculations,

$$Power = \frac{Energy}{Time} \qquad 4.3$$

In terms of their SI units,

$$Watt = \frac{Joule}{Second} \quad (4.4)$$

From equation 4.4, Joules is equivalent to Watt-second. Hence, 96,800 Joules = 96,800 Watt-second

$$\frac{Watt - second}{Volts} = Amp - sec \quad (4.5)$$

$$\frac{96{,}800 \text{ watt} - \text{second}}{2.2 \text{ V}} = 44{,}000 \text{ Amp-sec}$$

1hr = 3600 sec

Therefore,

$$\frac{44{,}000 \text{ amp} - \text{second}}{3600} = 12.2 \text{ Amp-hr}$$

When a single 40,000 Farad battery-type supercapacitor is used as an energy backup device in a power system, a current of approximately 12.2A would discharge the device for one hour. The calculated current may differ from measured values, this may be attributed to the fact that capacitance of a supercapacitor does not stay constant throughout discharge process.

Similar calculation is done for the 7,500F pseudocapacitive hybrid supercapacitor and its current at 1 C rate is obtained.

7,500 F supercapacitor:

C = 7,500 V = 2.3V (from Figure *4.3*)

$$E = \frac{7{,}500 \text{ X } 2.3^2}{2}$$

E = 19,838 Joules.

$$\frac{19{,}838\ \text{Watt}-\text{second}}{2.3\ \text{V}} = 8{,}625\text{Amp-sec}$$

$$\frac{8{,}625\ \text{Amp}-\text{second}}{3600} = 2.4\ \text{Amp-hr}$$

The 3000F EDLC do not have enough flatness on its curve to be treated as a constant voltage source.

C-rate for the 40,000F SC = 12.2 Ahr

C-rate for the 7500F SC = 2.4 Ahr

4.2.2 Discharge comparison at C-rates

To draw constant current out of the devices, a constant current circuit may be designed in the lab. This circuit can be based on MOSFETS or BJTs. At the saturation region of a MOSFET, the drain current stays constant when the drain source voltage changes. In this region, the drain current depends only on the gate-source voltage. Hence, to achieve a constant drain current, the gate-source voltage is kept constant. Similar behaviour is seen in a bipolar junction transistor. This feature is employed in the design of a constant current load circuit. Figure *4.7* is a sample circuit of a constant current load where the gate-source voltage of the MOSFET is kept constant.

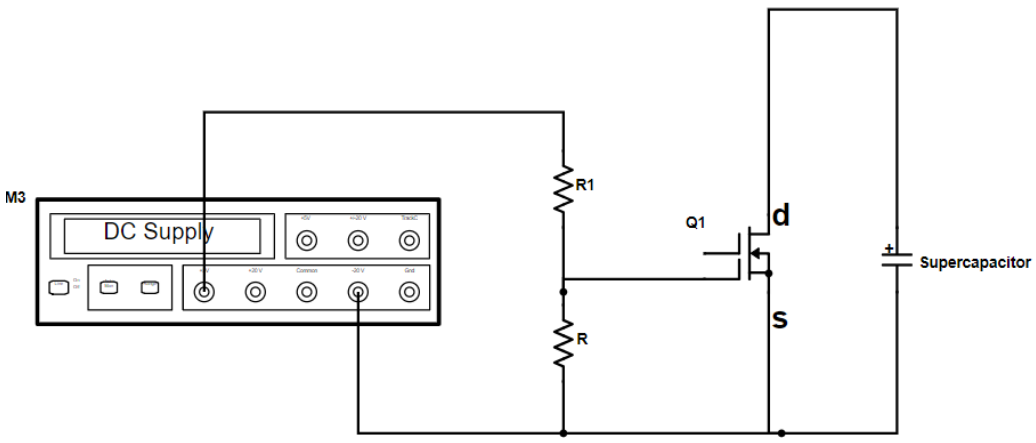

Figure 4.7. Constant current load circuit.

For accurate results, *TEXIO pxl-151A*, a solid-state electronic load device was used. The supercapacitors were discharged at the calculated C-rates and the characteristic curves are obtained.

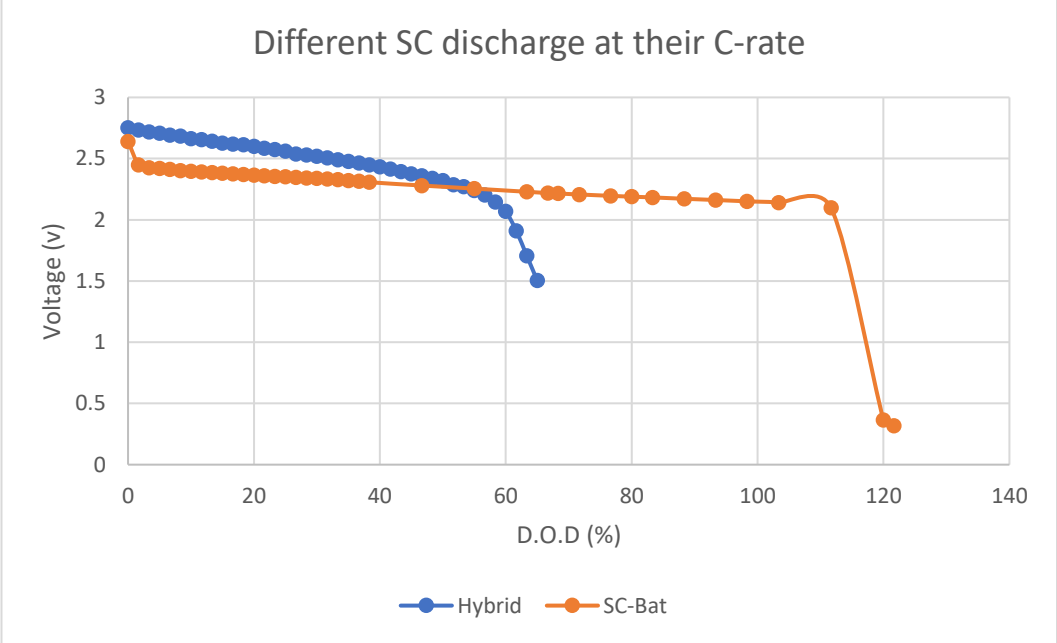

Figure 4.8. Constant current discharge curves.

In the ideal situation, the discharge curve at C-rate extends up to 100% D.O.D. However, as shown in the curves above, this may not always be obtained practically. As seen on the curves above, the battery-type supercapacitor acted as a constant voltage source for more than one hour when a current of 12.2 A was drawn from it. Similar behaviour is seen in the pseudocapacitive hybrid supercapacitor when a lower current of 2.4 A was drawn from it.

4.2.2.1 Battery type supercapacitor performance at different C-rates.

The battery-type supercapacitor was tested at different C-rates. As shown in Figure *4.9*, the device showed behaviour similar to the battery energy storage device. Higher C-rates tend to have less depth of discharge than lower C-rates. Therefore,

just like in the battery, the battery-type supercapacitor makes available more energy when discharged at lower current values.

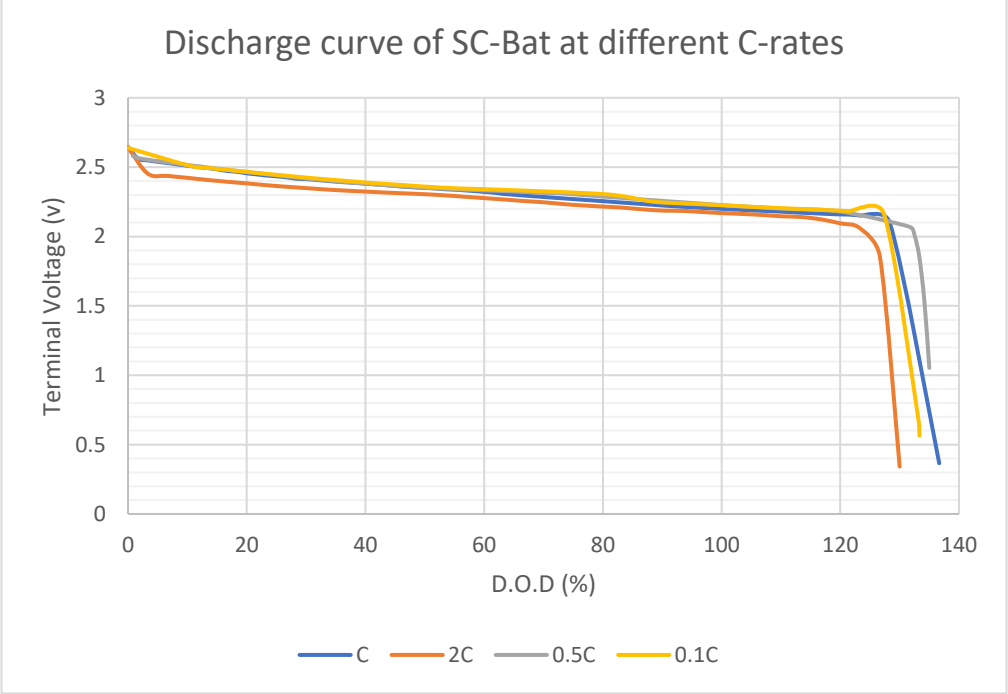

Figure 4.9. Graph showing discharge curves of the SAMWHA 40,000F battery type supercapacitor at different C-rates.

4.3 Equivalent Series Resistance (ESR) Measurement

Supercapacitors generally have lower ESR than battery energy storage devices. However, the ESR of different supercapacitors varies according to the technologies inherent in the devices. The constant current discharge method and the dynamic discharge method are two ways to measure the ESR of a supercapacitor[78]. While the constant current method involves a simple discharge at constant current, the dynamic discharge method involves discharge at different regimes of constant current. Both methods have been proven to provide accurate results. However, the constant current discharge method was adopted for this experiment due to its simplicity. This experiment measures the ESR of the three supercapacitor technologies in study. Figure *4.10* is the circuit set up used in the measurement.

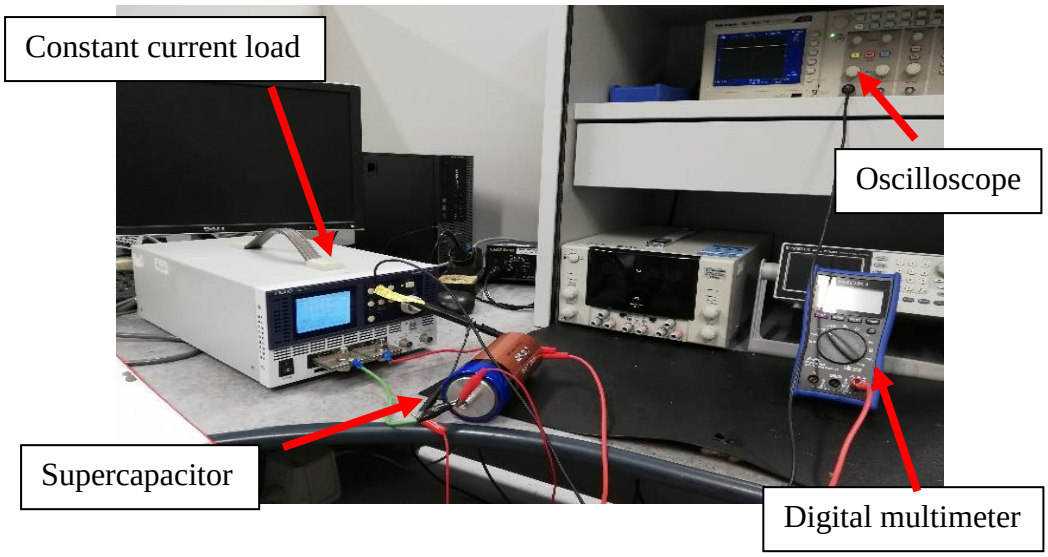

Figure 4.10. ESR measurement circuit set up.

The devices are first charged to rated voltage, a constant current load is connected to discharge the supercapacitors at constant current while the voltage is being monitored using an oscilloscope. The oscilloscope time scale is set to 1 second per division to get a better view of the trace. Figure *4.11* shows the trace for the 40,000F supercapacitor discharged at 10A.

Figure 4.11. ESR measurement trace.

$$ESR = \frac{\Delta V}{I} \quad 4.6$$

Where, I = Constant discharge current.

For the three supercapacitors, different current values were used for the measurement and the ESR at each current is obtained. This was done to increase the accuracy of the final ESR value. Table 4.1 is a summary of the result.

Table 4.1: *Measured Values of Different Supercapacitor ESR*

SC Types	**ΔV_1(V)**	**ΔV_2 (V)**	**ΔV_3 (V)**	**ESR_1 (mΩ)**	**ESR_2 (mΩ)**	**ESR_3 (mΩ)**	**ESR_{AVG} (mΩ)**
3,000F	0.048 , I = 10A	0.06, I = 15A	0.124 , I = 20A	5	4	6	5
7,500F	0.072, I = 5A	0.036, I = 3A	0.022, I= 1.5A	14	12	15	14
40,000F	0.12 , I = 10A	0.2 , I = 20A	0.32 , I = 30A	12	10	11	11

From Table 5.1 it is seen that the equivalent series resistance of the supercapacitors has no definite pattern with the electrode technology, ESR is largely determined by the electrolyte and separator inside the supercapacitor. Table 4.2 compares key features of some commercially available supercapacitor technologies with the prototype 40,000F battery-type hybrid supercapacitor.

Table 4.2: *Different Supercapacitor Technologies and Key Features*

Manufacturer	**Technology**	**Capacitance (F)**	**Rated Voltage (V)**	**Energy density (Wh/L)**	**Power density (W/L)**	**DC ESR (mΩ)**	**cycle life**
Ioxus.Inc	EDLC	3,150	2.7	7.76	12,563	0.26	1,000,000
Varta microbattery	Hybrid (EDLC-pseudo Asymmetric)	90	8.4	9.58	900	270	> 500,000
Nesscap Ultracapacitors (A maxwell Technologies company)	Pseudocapacitor	300	2.3	10.53	1,768	20	100,000
JM Energy	Hybrid (composite)	3,300	3	20	12,000	1	> 500,000
Samwha	Hybrid (battery-type)	40,000	2.7	67.3	3093	0.7	20,000

Chapter Five

Boost Converter Design

5.1 Brief Description

A boost converter was designed for the 12V LED load. A simple non-isolated boost topology was chosen because of the low power level of the load. The power stage consist of an inductor, an electronic switch, a diode and a capacitor connected as shown in Figure *5.1*.

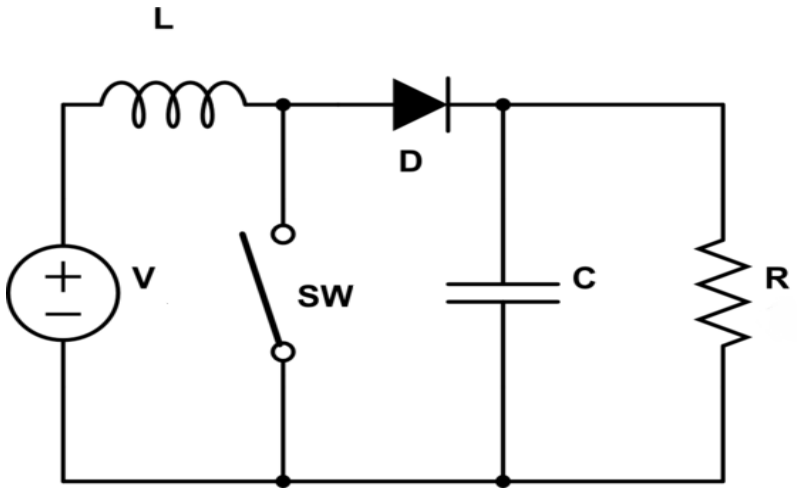

Figure 5.1. Non-isolated boost converter.

When the switch is closed, the diode is reverse biased while the input current rises linearly through the inductor. During this time, the load current is supplied by the output capacitor. When the switch opens, the diode is forward biased, therefore allowing current flow to the output load while the inductor current falls. In this operation, the volt-second balance rule in the inductor applies. Figure *5.2* shows the voltage and current waveforms across the inductor. To obtain a maximum back up time from an energy storage device, the losses in the incorporated power converters must be minimum. Therefore, in the design of the power converter, efficiency consideration is crucial. A simple non-isolated boost converter, by characteristics

is not as efficient as the transformer isolated counterparts. However, a properly designed boost converter circuit can achieve an efficiency of 70% to 75%.

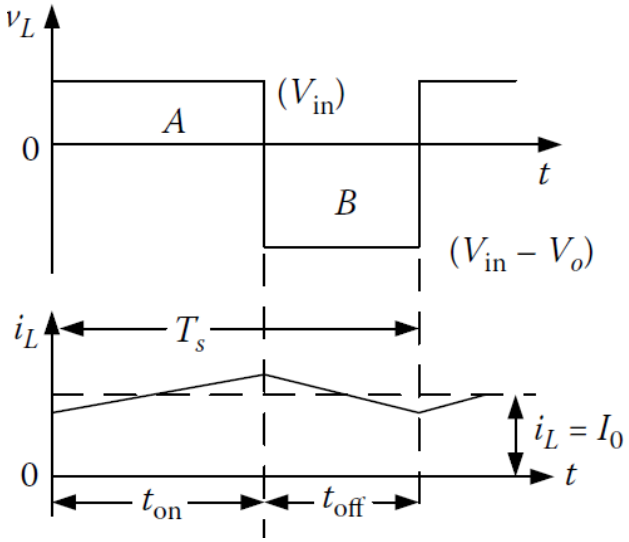

Figure 5.2. Inductor voltage and current waveforms.

5.2 LED Characteristics

LED was used as the load to demonstrate the supercapacitor's energy back up capability. A 5W, 5V Philips LED was used for the boost converter circuit. The LED characteristics is shown below.

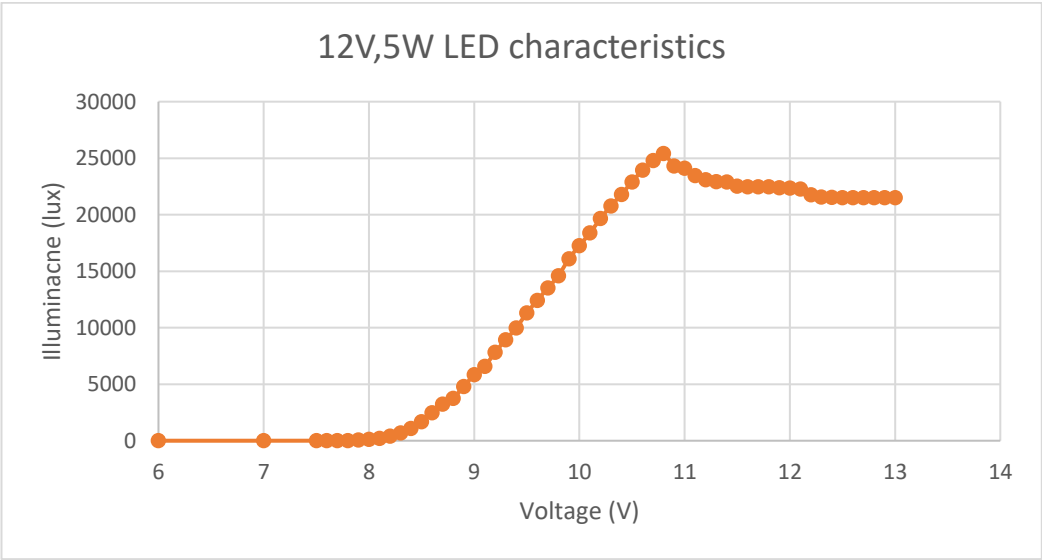

Figure 5.3. Variation of the LED illuminance with voltage.

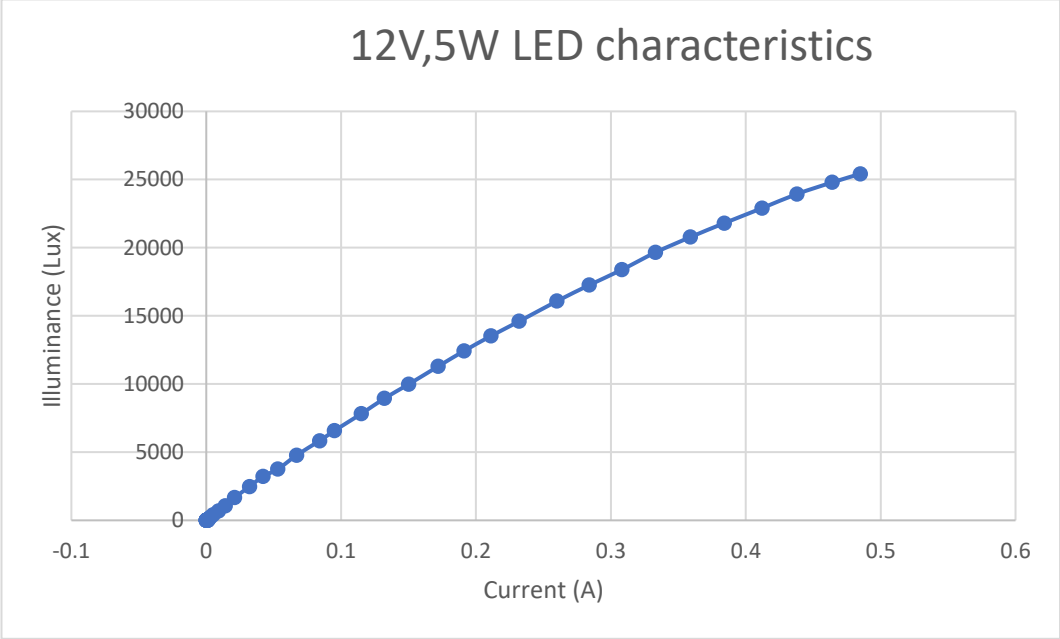

Figure 5.4. Variation of the LED illuminance with current.

At a voltage of 12V, the LED illuminance is about 23,000lux, while the current is 0.45A. This is used as the load specification for the boost converter.

5.3 Power Stage Design

The aim of the converter is to step up the supercapacitor voltage to 12V as required by the LED load. The supercapacitor used for this project is the higher energy-dense 40,000F battery-type hybrid supercapacitor. As discussed in chapter 4, the battery-type supercapacitor acts as a voltage source from 1.8V to 2.7V where a current supply by the supercapacitor only leads to a minimal change in terminal voltage. This is thence the input voltage range of the converter. From Figure *5.3* and Figure *5.4*, the LED current requirement at 12V is 450mA. The converter is designed to withstand two LED loads, hence an operating current of 900mA. To have a safety margin, the maximum output current is designed to be 1A.

The converter specification is summarised in Table 5.1.

Table 5.1: *Boost Converter Specifications*

Minimum Input Voltage	1.8V
Maximum Input Voltage	2.7V
Output Voltage	12V
Maximum Output Current	1A
Efficiency	70%

5.3.1 Frequency selection

Unlike many component parts of a converter, the selection of an operating frequency does not require a standard equation, rather it involves several parameter considerations. It is a trade-off between the size of components to be used and the overall efficiency of the converter. High operating frequency requires smaller sized components for implementation. Meanwhile, high frequency creates additional losses in the circuit. These losses comprise of the RFI/EMI losses and the switching losses. A converter can have one percent loss in efficiency for every 100 kHz rise in frequency of operation [79]. Therefore, a 200 kHz switching regulator with an efficiency of 93 percent, could have an efficiency of about 90 percent when operated at 500 KHz.

On the other hand, at low frequency of operation, the required components are bigger in size while the losses are reduced. In this case, the ohmic conduction losses are dominant. Therefore, the optimum frequency value for a specific converter is a value where expected efficiency is achieved and reasonably sized components are used. A rule of thumb, is to use lower frequencies for applications where load current is higher than 10A, and higher frequencies for applications where load

current is less than 10A [79]. In this context, frequencies below 100 KHz are considered low. The power requirement for this converter is a maximum of 12 watt, with a maximum load current of 1A. Going by the rule of thumb stated above, the operating frequency is chosen as 300 KHz.

5.3.2 Inductor selection

The selection of an inductor as opposed to the frequency selection has a more quantitative approach to it. The chosen inductor should be able to withstand the peak inductor current without saturation. The inductance also limits the ripple current to the desired value. Generally, the inductor should limit the maximum ripple current to about 20% of the average inductor current. The size of inductance is inversely proportional to the peak current flowing through it. Therefore, lower inductance values result to high peak current which may stress the switching transistor. Hence in the selection of the inductor, the inductance value should be high enough to limit the peak current to a considerable level, and low enough to allow enough current at the minimum input voltage. Inductance calculation using the maximum input voltage can yield a figure which may be too high for situations of minimum input voltage, while calculation using the minimum input voltage can yield a figure which may be too low for periods of maximum load current. Because of this, an average value of the input voltage range was used in the calculation of the inductance. The converter is expected to work in continuous conduction mode up to the minimum load current of 450mA, this was also considered in the selection.

During the MOSFET on time (t_{on}) the voltage across the inductor is the input voltage (V_{in}).

The following inductor equation applies,

$$V_L = \frac{dI_L}{dt} L \quad (5.1)$$

Where,

dt is the switch on-time and dI_L is the ripple current.

Therefore, the inductance (L) becomes,

$$L = \frac{dt}{dI_L} V_L \quad (5.2)$$

In non-ideal conditions, the voltage across the inductor is less than V_{in}. This is due to the voltage drop across the MOSFET (V_{ds}) caused by the $R_{ds(on)}$ of the MOSFET. Non-ideal situations are considered in order to improve the accuracy of the calculation.

$$L = \frac{(V_{in} - V_{ds})dt}{dI_L} \quad (5.3)$$

On time, (dt) = DTs (5.4)

D = duty cycle T_s = switching period.

The voltage transfer function of a boost converter is given as follows,

$$\frac{V_o}{V_{in}} = \frac{1}{1 - D} \quad (5.5)$$

Substitute for D and T_s in equation 5.1

$$L = \frac{(V_{in} - V_{ds})}{dI_L} \times \frac{(V_o - V_{in})}{V_o} \times \frac{1}{f} \quad (5.6)$$

V_{ds} is assumed to be 0.2V which is expected to be close to the actual value when a MOSFET with low $R_{ds(on)}$ is used.

The ripple current (dI_L) by rule of thumb is not expected to exceed 20% to 30% of the maximum inductor current $I_{L(max)}$. 15% is assumed for this calculation.

$$I_{L(max)} = \frac{V_o \times I_o}{V_{in(min)} - V_{ds}} \quad 5.7$$

$$I_{L(max)} = \frac{1 \times 12}{1.8 - 0.2}$$

$I_{L(max)} = 7.5A$

$dI_L = 0.15 \times 7.5 = 1.1A$

V_{in} = average input current = 2.25V V_o = 12V f = 300kHz V_{ds} = 0.2V

$$L = \frac{(2.25 - 0.2)}{1.1} \times \frac{(12 - 2.25)}{12} \times \frac{1}{300000}$$

$L = 5\mu H$

For lower ripple current, the inductance value can be increased. The peak inductor current is calculated from Equation 5.8

$$I_{L(peak)} = I_{L(max)} + 0.5(dI_L) \quad 5.8$$

$I_{L\,(peak)} = 7.5 + 0.5(1.1)$

$I_{L\,(peak)} = 8.05A$

For efficiency improvement, an inductor with low series resistance is preferred.

EPCOS B82559A inductor is used for this design. The key specifications are stated in Table 5.2

Table 5.2: *Boost Converter Inductor Specifications*

Part number	B82559A5682A020
Inductance	6.8µH ±10%
Maximum DC Current	19A
Maximum DC resistance	2.9mΩ

The minimum output current is the current requirement of one LED load.

$I_{o(min)} = 0.45A$

The converter is expected to still operate at continuous conduction mode (CCM) when the output current is 0.45A. To check that the selected inductor is suitable for continuous conduction mode operation, consider Figure *5.5*.

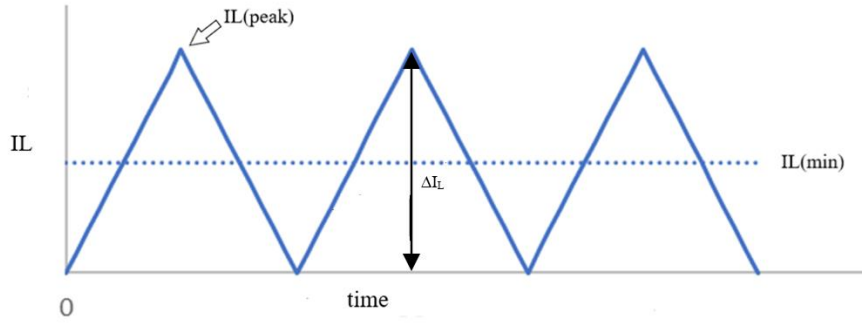

Figure 5.5. Inductor voltage and current waveforms.

For CCM,

$I_{L(min)} > 0.5dI_L$

Where $I_{L(min)}$ = Minimum inductor current

$I_{L(min)}$ occurs at maximum input voltage and minimum output current.

From Equation 5.7,

$$I_{L(min)} = \frac{0.45 \times 12}{2.7 - 0.2}$$

$I_{L(min)}$ = 2.16A

The above value is higher than half of the ripple current (0.55A), hence the converter is expected to remain in continuous conduction mode at the minimum output current.

5.3.3 MOSFET selection

Losses in the switching power MOSFET represent a major part of the total losses in a boost converter. Therefore, to obtain a good efficiency in boost converter design, adequate care is taken in the selection of a power MOSFET. Basically, the chosen MOSFET should be able to withstand the peak inductor current without breakdown. When the switch is off, the voltage across the drain and source is equivalent to the sum of the output voltage and the diode forward voltage. Hence the $V_{ds(max)}$ of the MOSFET should be above the sum (V_o + V_d). Switching losses in a MOSFET are not critical when operating at frequencies below 400KHz, at such frequencies, the conduction loss dominates[80]. Therefore, among other specifications of the MOSFET, the $R_{ds(on)}$ should be as low as possible. The switching losses are proportional to the total gate charge of the MOSFET, hence a lower total gate charge would reduce the losses. For an operating input voltage of 1.8V to 2.7V, the gate threshold voltage of the MOSFET should be low enough to start the converter at the minimum input voltage. With the above factors put into

consideration, IRF7401PBF MOSFET is selected, the key specifications are stated in Table 5.3

Table 5.3: *Boost Converter Power MOSFET Specification*.

$R_{ds(on)\ max}$	22mΩ
Maximum continuous Drain-source current	8.7A
Maximum gate threshold voltage	0.7V
Maximum Drain-source voltage	20V
Typical gate charge	48nC

5.3.4 Diode selection

When the MOSFET switch is open, the inductor current flows through the diode to the output. Therefore, the diode should be able to withstand the inductor peak current. A low voltage drop across the diode improves efficiency. During the MOSFET on time, the voltage across the diode in the reverse direction is equivalent to the output voltage. Therefore, the chosen diode should have a reverse breakdown voltage higher than the output voltage. This is easily obtained as the output voltage has a low value of 12V, however, for high voltage applications, this could be a challenge. A Schottky diode is always preferred in converter applications, due to its fast switching and low forward voltage drop. PDS1040-13 Schottky diode is chosen for this design, the key specifications are shown in Table 5.4

Table 5.4: *Boost Converter Diode Specification*.

Maximum forward voltage drop	0.51V
Maximum reverse voltage	40V
Maximum continuous current	10A

5.3.5 Output capacitor selection. The major function of the output capacitor in a boost converter is to supply the output current when the MOSFET switch is closed. The capacitor voltage drops when the output current is being supplied, it charges back when the MOSFET is open. This repetitive change in the capacitor voltage appears in the output as the output voltage ripple of the converter. To limit the output voltage ripple, the output capacitor should be high enough to supply the maximum output current with minimal voltage drop. The ESR of the capacitor contributes to the voltage ripple as voltage is dropped across the ESR. The output voltage ripple for this design is limited to 100mV and the required capacitance is calculated accordingly. .

Consider the capacitor formula of equation 5.9

$$I_o = C\frac{dV}{dt} \qquad 5.9$$

The capacitance is therefore given as;

$$C = \frac{I_o \times dt}{dV} \qquad 5.10$$

Where, I_o = Output current

dt = MOSFET on-time

dv = Output voltage ripple.

To achieve the desired maximum voltage ripple, the minimum capacitance required becomes,

$$C_{min} = \frac{I_{o(max)} \times D_{(max)}}{dV \times f} \qquad 5.11$$

From equation 5.5,

$$D_{max} = \frac{V_o - V_{in(min)}}{V_o} \quad 5.12$$

Equation 5.11 becomes;

$$C_{out(min)} = \frac{I_{o(max)} \times [V_o - V_{in(min)}]}{dV \times f \times V_o} \quad 5.13$$

$$C_{out(min)} = \frac{1 \times [12 - 1.8]}{0.1 \times 300000 \times 12}$$

$C_{out(min)}$ = 28µF

The above value is the minimum capacitance required, a capacitance value 3 to 4 times larger can be used. The ESR of the capacitor should be as low as possible to reduce the voltage ripple. A common practise is to connect capacitors in parallel. The parallel connection reduces the effective resistance while increasing the total capacitance. A low resistance capacitor like the ceramic capacitor is mostly used in the same way to achieve a lower ESR. Low ESR also improves the system stability. Three 330µF tantalum capacitor were used for this design. Tantalum was preferred due to its low ESR.

5.3.6 Input capacitor selection

The function of the input capacitor in a boost converter is to reduce the current peak drawn from the source. It also helps in noise rejection. For a source with very limited current capability, a well selected input capacitor ensures that the peak input current remains within the limit of the source capability. The source for this design is a supercapacitor. The supercapacitor has very low impedance and can deliver a large amount of current. Therefore, the need for large input capacitor is reduced.

An input capacitor with low ESR improves the efficiency of the converter. The same capacitance as the output capacitor was used for the input capacitor.

5.4 Control Circuit Design

Control system is necessary to ensure stability of the converter output at different circuit conditions. There are different types of control system used in power converters, each of them offers unique advantages. The two most popular control methods include:

- Voltage mode control
- Current mode control

5.4.1 Voltage mode control

This was the first method used in control circuits. It consists of a single feedback path. As shown in Figure *5.6*.

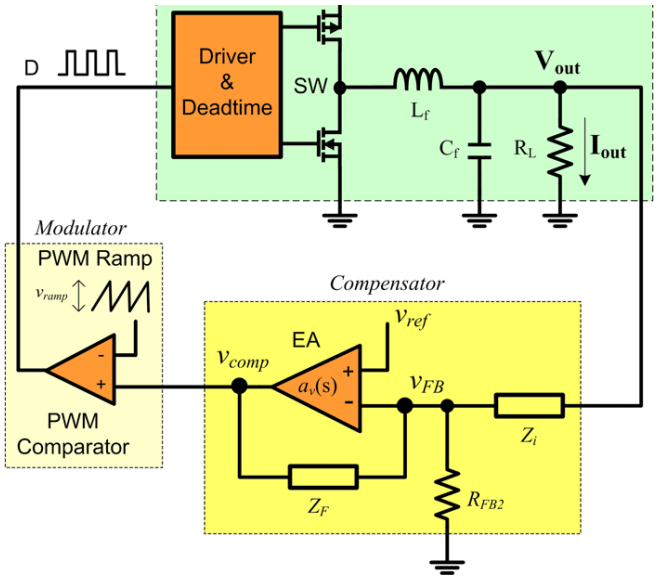

Figure 5.6. Voltage-mode control.

A voltage divider circuit formed by R_{FB2} and Z_i feeds a scaled sample of the output voltage to the compensator circuit. The compensator basically consists of a

comparator which produces on its output, the difference between the sampled output voltage and a reference voltage. The compensator output is called the error signal. It becomes the control voltage fed into the non-inverting input of the Pulse-width modulation (PWM) comparator. A clock circuit provides voltage ramp signal of triangular waveform at the inverting input of the PWM comparator. The output of the PWM comparator is a square wave with the appropriate duty cycle needed to maintain a constant voltage at the converter output. The voltage mode control circuit is easier to design, it is cheaper, and it is less susceptible to noise. However, one of the draw backs of the voltage mode control is its slower response to voltage variations. This problem is taken care of in the more recent method of control, which is the current- mode control.

5.4.2 Current mode control

This method of control was developed after the voltage mode control method. It uses the inductor current as a control parameter to maintain stability in the circuit. The current mode control method is more complex than the voltage mode control. Figure *5.7* illustrates the working principle of the current mode control method.

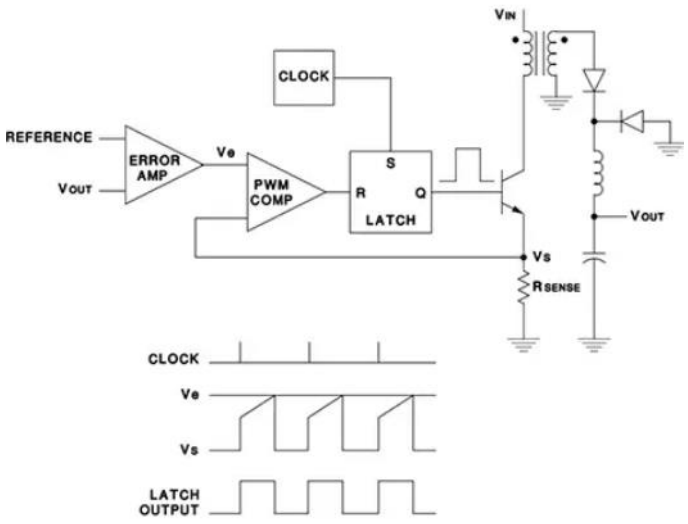

Figure 5.7. Current-mode control.

It consists of the error amplifier and the PWM comparator as used in the voltage mode control. In this case, the ramp voltage signal is provided by the circuit inductor current. A second feedback loop of the inductor current is introduced in the circuit, the current is sensed by a current sensing resistor, where the voltage across the resistor is a measure of the amount of current flowing through it. The measured voltage from the current sensing resistor is fed into the inverting input of the PWM comparator. The error voltage is fed into the non-inverting input of the comparator. The output of the comparator is a square wave whose duty cycle depends on the slope of the ramp voltage and the value of the control voltage. Since the inductor current slope is determined by ($V_{in} - V_o$), the current mode control responds faster to changes in the line voltage[81]. Additionally, it has a higher gain bandwidth than the voltage mode control. One of the major draw backs of the current mode control is its instability at duty cycles above 50%. Noise at the current sense resistor causes signal jitter on the ramp signal. This jitter is made worse when the slope of the ramp is less. A slope compensation mechanism is always used to increase the slope of the ramp and reduce the effect of jitter. .

The supercapacitor voltage, which is the input voltage of the boost converter is expected to continually drop as it discharges. As described above, the current mode control method has a faster response to line voltage changes. Therefore, a current mode control method was preferred for this project. .

5.4.3 Control IC selection

The control circuits for power converters are always available in integrated circuit packages. Many manufacturers embed in the ICs other circuits alongside the control circuits. Some of these circuits include the MOSFET driver circuits and the power

switch itself. Since the power switch for this design has already been selected, a control IC without the power switch is the desired IC for control. The input voltage range of the IC should also be within the input voltage range of the converter. MAX669 current mode controller was used for the control circuit. The key features are stated in Table 5.5

Table 5.5: *Boost Converter Controller Specifications*

Input Voltage range	1.8V to 28V
Control method	Current mode
Frequency range	100Khz to 500Khz
Efficiency	Over 90%

5.4.3.1 Setting the frequency

The frequency of operation is set by connecting the suitable resistor between pin 2 and GND of the controller. The resistor value is found using Equation 5.14

$$R_{(osc)} = \frac{5 \times 10^{10}}{f} \qquad 5.14$$

For a frequency of 300 KHz,

$$R_{(osc)} = \frac{5 \times 10^{10}}{300 \times 10^{3}}$$

$R_{(osc)}$ = 167 kΩ

The closest standard resistor value to 167 kΩ is used.

$R_{(osc)}$ = 165 kΩ (E96 series)

5.4.3.2 Current sense resistor

The voltage between the current sense pin and GND should not exceed 85mV. This is a value set by the manufacturer of the controller. Maximum voltage at the current sense pin occurs at the peak inductor current. Therefore, the sense resistor is chosen to ensure the voltage limit is not exceeded at the peak inductor current.

$I_{L(peak)}$ as calculated from Equation 5.8 is 8.05A.

$$R_{(cs)} = \frac{85 \times 10^{-3}}{8.05}$$

$R_{(cs)}$ = 10mΩ

5.4.3.3 Feedback resistors

The feedback resistors sample a factor of the output voltage to the controller's feedback pin. The resistors were chosen in the kilo-ohm region to reduce the quiescent current of the circuit.

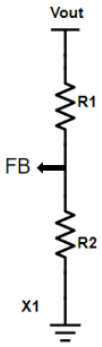

Figure 5.8. Feedback voltage divider circuit.

$$R1 = \frac{R2 \times V_{(out)}}{V_{(ref)}} - R2 \qquad 5.15$$

Where, V(ref) = 1.25V,

Let R2 be 105kΩ,

$$\text{R1} = \frac{105{,}000\ x\ 12}{1.25} - 105{,}000$$

R1 = 909k

5.4.3.4 Bypass capacitors

Bypass capacitors provide low resistance path to ground for noise signal. This is necessary to reduce electrical noise in the IC and circuit in general. They also help to improve the transient response of the system. The power pins of the IC are bypassed with ceramic capacitors. The power pins include; VCC, REF and LDO. VCC pin is bypassed with a 0.1uF capacitor, the REF pin is bypassed with a 0.22uF capacitor while the LDO is bypassed with a 1uF capacitor. The capacitors are connected from the respective pins to ground. The values of the capacitances used were recommended by the IC manufacturer. Bypass capacitors are always connected as close to the pins as possible to avoid further parasitic impedances.

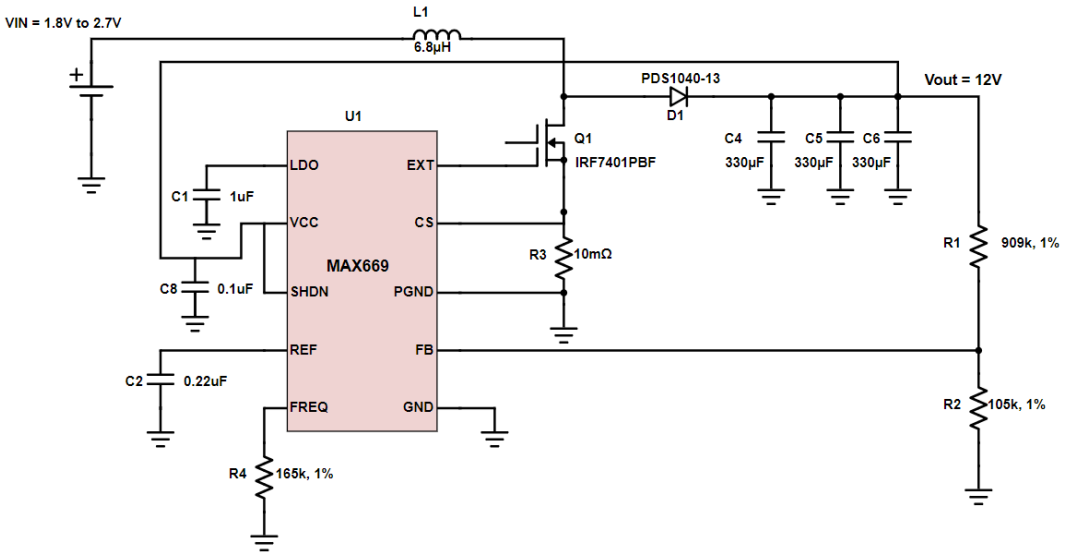

Figure 5.9. The final circuit of the boost converter.

5.5 Printed Circuit Board Layout Design

A printed circuit board was designed to implement the circuit. Some of the chosen components for the converter are surface mount components, hence a PCB design is inevitable. The circuit involves high switching current which are bound to generate noise signals. Therefore, adequate PCB layout design is crucial for a better circuit performance. Some key rules adhered to in PCB layout design include:

- High current traces should be made as short and wide as possible to reduce the parasitic impedances.
- Star ground concept should be used to avoid ground current flowing in the circuit.
- The loops containing the switching currents should be made as small as possible.
- High noise areas should be kept away from sensitive pins of the controller.
- Since all the return current pass through the ground, a ground plane should be used.

Manufacturers always recommend a PCB layout for their controllers. However, due to variations in components sizes and specifications, the recommended layouts are usually not suitable. Figure *5.10* shows the PCB layout used for this design.

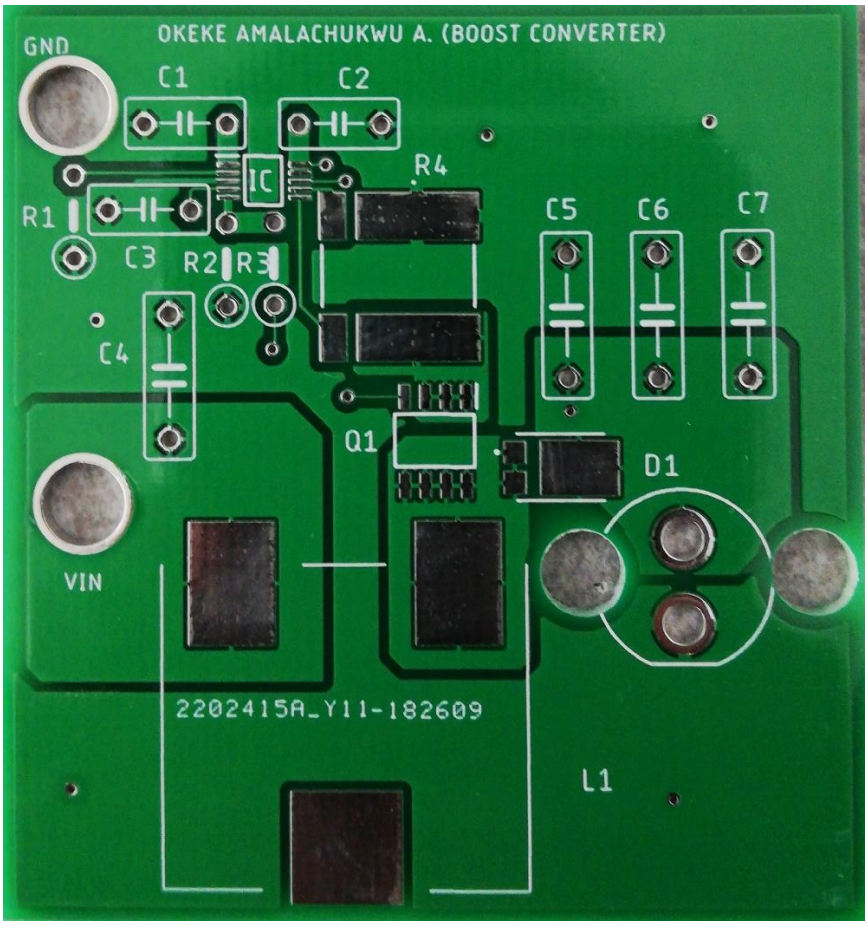

Figure 5.10. Boost converter PCB layout.

5.6 Test and Measurement

The converter was implemented, and several tests and measurements were conducted to ascertain its performance with regards to the supercapacitor application. The following tests and measurements were done:

- Line Regulation
- Load Regulation
- Efficiency Measurement

5.6.1 Line regulation

The converter output was measured at different input voltages. The converter is intended to regulate from 1.8V to 2.7V input voltage, which is the voltage range of

the supercapacitor. Figure *5.11* shows the line regulation of the converter. As seen from the graph, the converter output stayed at approximately 11V as the supercapacitor discharged from 2.66V to around 2.2V. At 1.8V input voltage, the converter output dropped to approximately 10.5V.

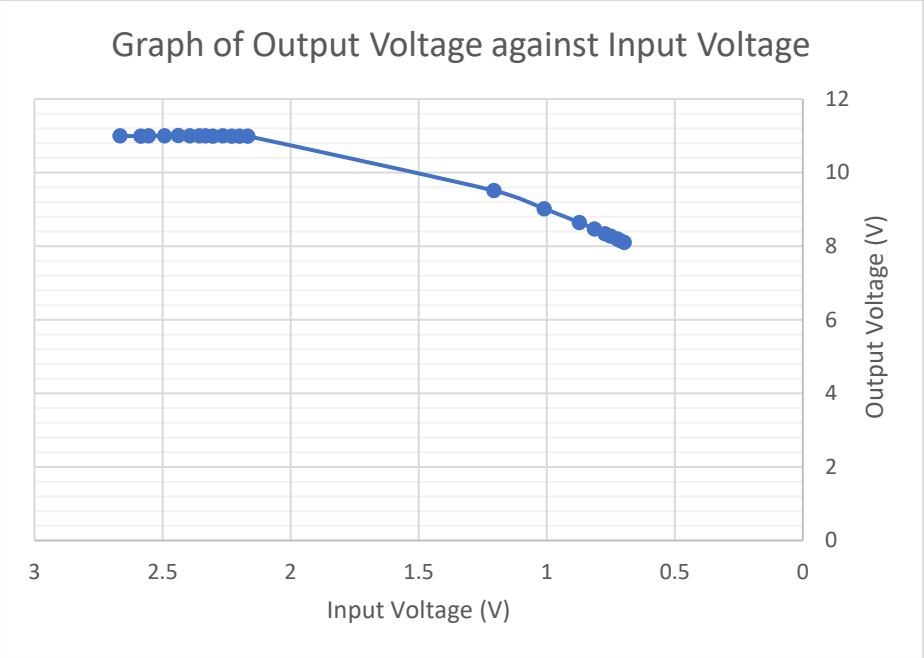

Figure 5.11. Line regulation.

5.6.2 Load regulation

The converter is expected to power two LED loads which would draw a maximum of 1A. Several resistive loads were connected at the output while the output voltage measured. This was done to ascertain the performance of the converter at changing loads current. Figure *5.12* shows the load regulation curve for the converter. The output voltage stayed at approximately 11V from a load of 0.2A to 0.7A, from 0.8A to 1A the output voltage was 10.5V. This is good enough for the intended purpose.

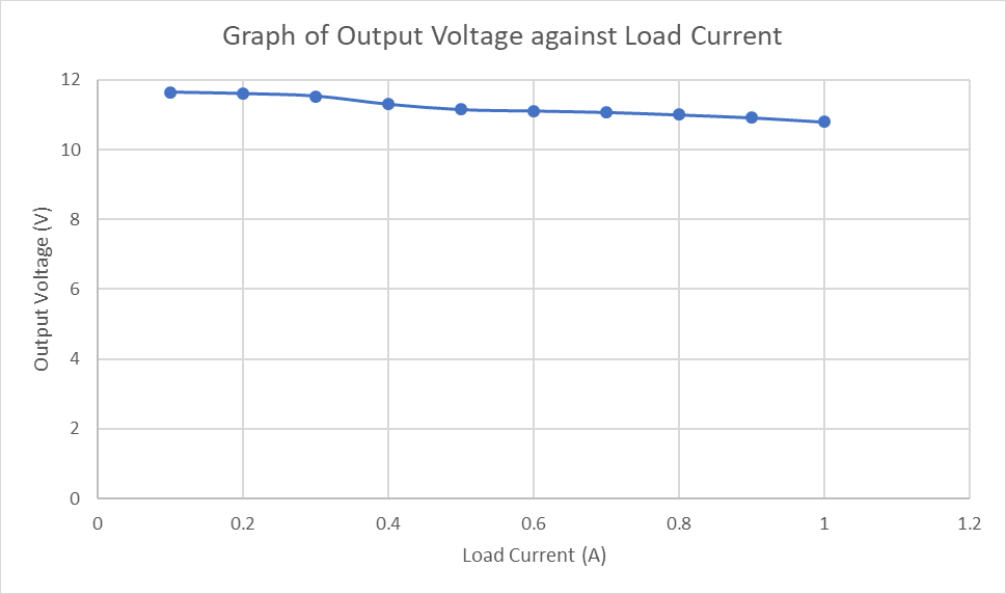

Figure 5.12. Load regulation.

5.6.3 Efficiency

The efficiency of the converter was calculated at different input voltages. The boost converter acts as a constant power load to the source, therefore the input current rises as the supercapacitor voltage decreases. The increase in current leads to more losses and a steady drop in the efficiency. *Figure 5.13* shows a graph of efficiency against the input voltage as obtained from the converter. The measurements were taken while the output voltage stayed constant, this occurs from input voltage of 2.2 to 2.7V. Below 2.2V the output voltage drops, and the brightness of the LED is reduced, this means a reduction in the power output. A maximum efficiency of about 76% and a minimum efficiency of 65% were obtained.

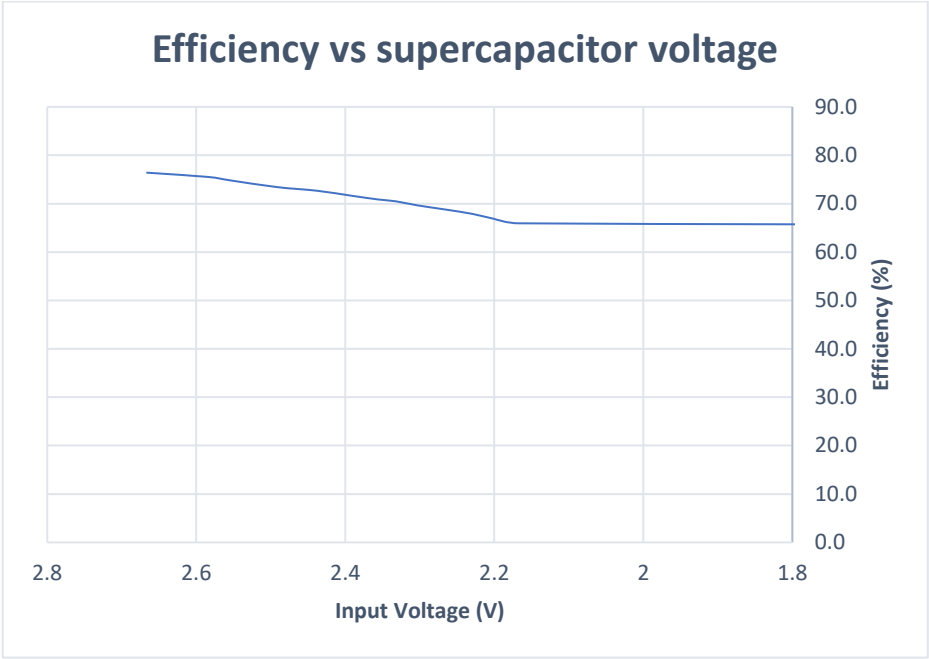

Figure 5.13. Boost converter efficiency performance.

Figure 5.14. Boost converter implemented circuit.

Figure 5.15. Boost Converter - supercapacitor working set up.

5.6.4 Operating waveforms

The waveforms at the diode, MOSFET and converter output are obtained while on load, using an oscilloscope. The different waveforms are shown below.

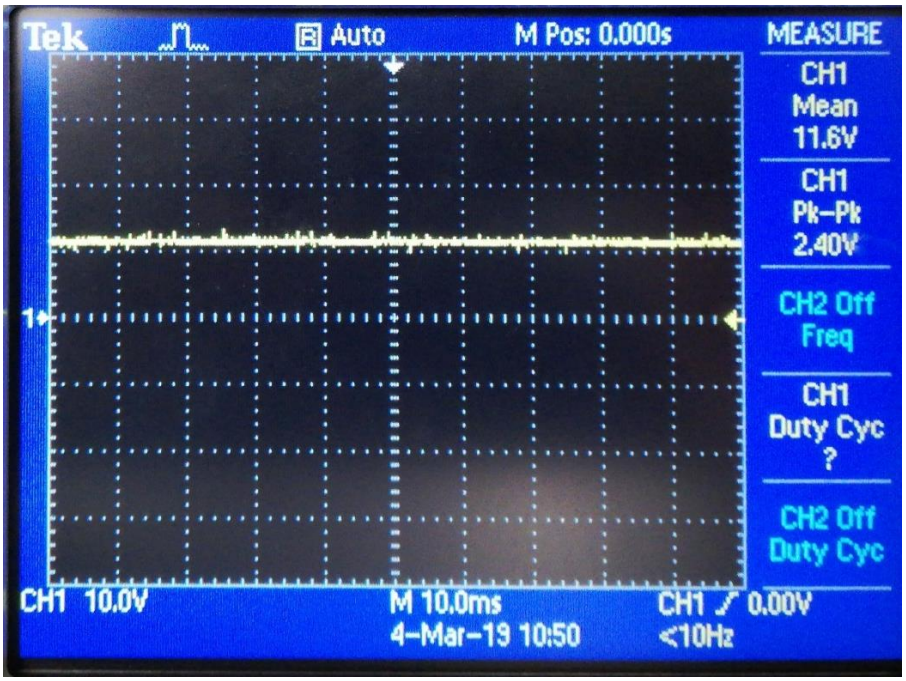

Figure 5.16. Output voltage waveform.

Figure 5.17. MOSFET gate waveform.

Figure 5.18. Diode waveform.

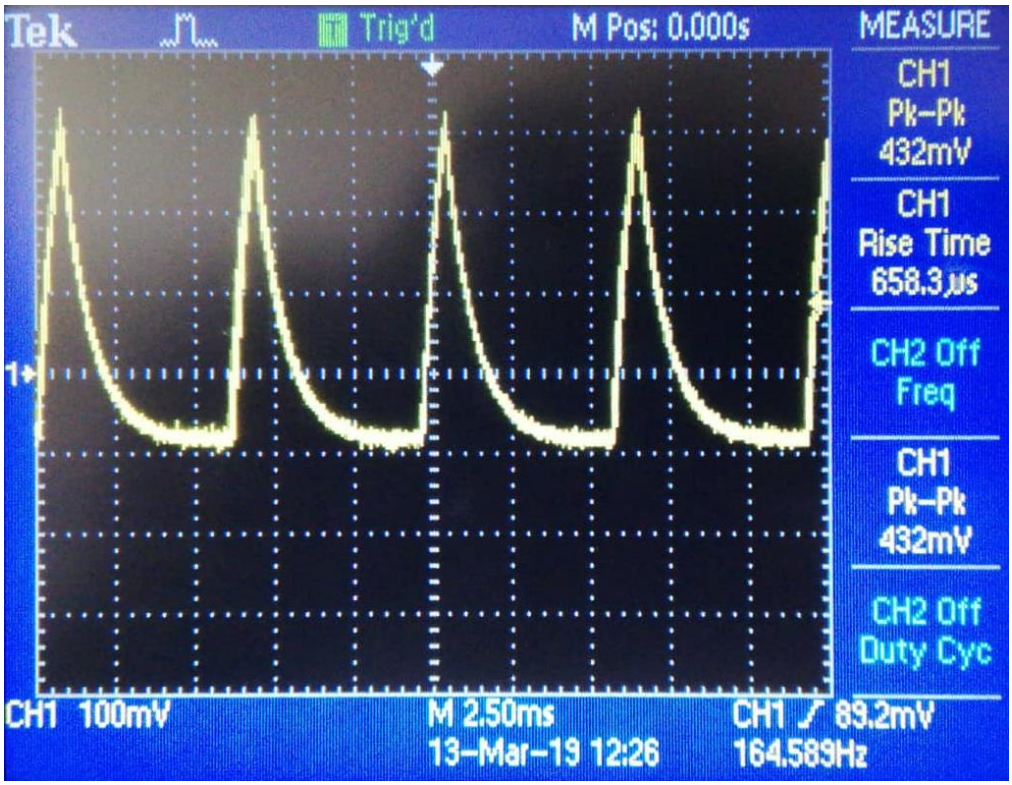

Figure 5.19. Inductor waveform.

Chapter Six

Supercapacitor Application for Street Lighting Systems

6.1 Street Lighting System

The energy storage capability of the battery-type supercapacitor can be harnessed for application in street lighting systems. Street lights are generally designed to illuminate after sunset and go off at sun rise. Therefore, in a 24-hour period, the street lights ideally work for approximately 12hours. This makes the DC microgrid a preferred system of energy supply to the street lights. During the day, the solar panels charge the supercapacitors, while at night, the charged supercapacitors supply the required energy for the streetlights to work. This system also eliminates the need for long power cables as the lighting systems operate as stand-alone. .

Figure 6.1. A stand-alone street lighting system.

To demonstrate this application of the supercapacitor, a prototype system was designed. A 100-Watt LED flood light was used as the load while the prototype was designed to light up the LED for 1 hour. The design is made of two parts:

- Supercapacitor Bank
- Power Converter

6.2 Supercapacitor Bank

This involves the series or parallel connection of different supercapacitor devices to meet the energy requirements of the load. A 100-Watt rated LED load ideally consumes 100 Watt-hr of energy after 1 hour of on-time. However, the LED was tested to ascertain the actual consumption. The illuminance of the LED was monitored against the voltage and current level. Figure *6.2* shows the variation of illuminance with voltage of the flood light.

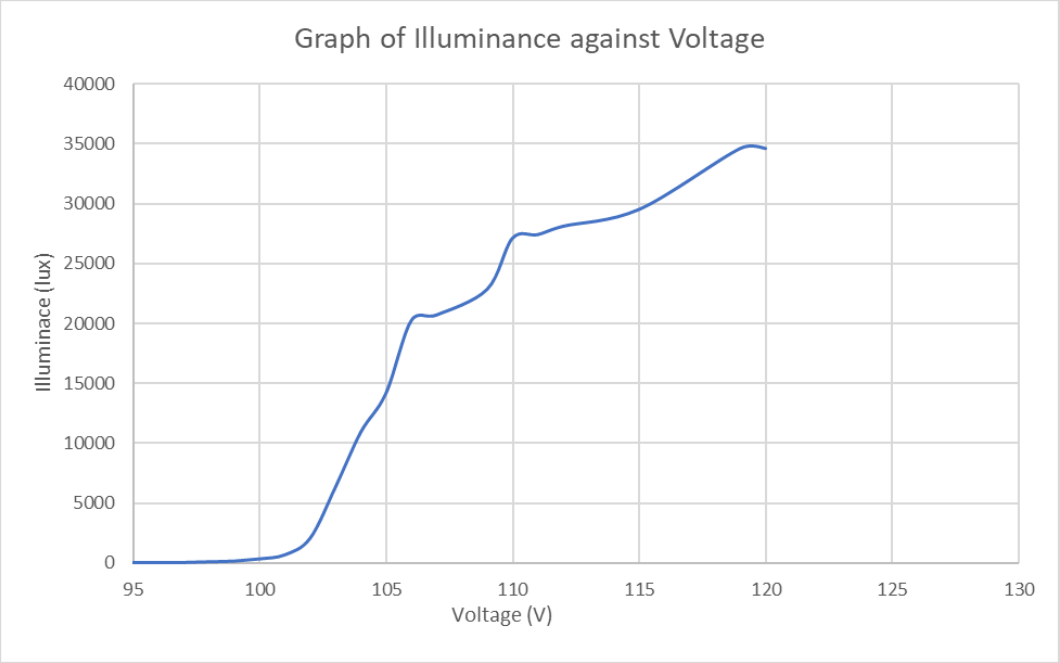

Figure 6.2. Illuminance curve of the sample LED load.

According to the graph above, the LED has maximum illuminance at a voltage level of 119V, 120V. The current at this point was measured to be 1.05A. Hence the supercapacitor bank specifications is calculated thus:

$$\text{Load Consumption} = 120\text{V x } 1.05\text{ A} = 126\text{W}$$

$$\text{On} - \text{time} = 1\text{ hour} = 1\text{ x } 60\text{ x } 60\text{ seconds}$$

$$\text{Energy consumption over 8 hr} = 126\text{ x } 60\text{ x } 60 = 453{,}600\text{ Watt} - \text{seconds}$$

Assuming power converter efficiency of 75%,

$$\text{Energy requirement of SC bank} = \frac{453{,}600}{0.8} = 604{,}800\text{ Watt} - \text{seconds}$$

Watt-second is equivalent to joules, hence 604,800 Watt-seconds = 604,800 J

Therefore, the minimum energy requirement of the supercapacitor bank for a one-hour on-time is 604,800 J (equivalent to 168 Wh). .

As stated in chapter four, from the graph of Figure *4.4*, the flatness of the curve occurs from 1.8V to 2.7V. This region is the desired region of operation as an energy storage device. Therefore, each supercapacitor in the bank is expected to only discharge from about 2.7V to 1.8V. During this time, the energy discharged by the supercapacitor is the difference of the energy stored at 1.8 V from energy stored at 2.7V. The energy stored in a capacitor is given by Equation 6.1

$$E = \frac{CV^2}{2} \qquad 6.1$$

$$\text{Energy suplied by each SC} = \frac{C\text{ x } 2.7^2}{2} - \frac{C\text{ x } 1.8^2}{2} \qquad 6.2$$

For a single 40,000F Supercapacitor,

$$\frac{40{,}000 \text{ x } 2.7^2}{2} - \frac{40{,}000 \text{ x } 1.8^2}{2} = 81{,}000\text{J}$$

Therefore, for an energy of 604,800 J,

$$\text{Number of supercapacitors required} = \frac{604{,}800}{81{,}000} = 7.5$$

The supercapacitor bank consists of 8 units of 40,000F battery-type supercapacitors connected in series. A series connection is preferred, to reduce the input-output voltage differential of the converter for a better efficiency. For longer hours of operation, similar calculation is performed to determine the number of supercapacitors required. In comparison to a battery solution, the 40,000F supercapacitor has an average cycle life of 20,000, while a lithium battery has an average cycle life of 1,200. On the assumption of a full cycle charge of the supercapacitor bank in a day of operation, the bank would theoretically last for 20,000 days (54 years) as against the battery solution of 1,200 days (3 years). Since the 40,000F supercapacitor is a prototype and commercially unavailable as at the time of writing this thesis, its cost cannot be ascertained. However, in terms of longevity of solution, the supercapacitor solution proves to be a superior choice.

6.2 Power Converter Design

A push-pull converter was designed to power the 100-Watt LED flood light. Due to the increased power level of the load, a non-isolated boost converter was not used. Boost converters are characteristically inefficient when compared to other topologies. The push-pull boost topology was chosen as the ideal topology for this application. The decision was based on the consideration of efficiency, cost and power level. While push-pull converter is less efficient than the full bridge and half

bridge, it is less expensive to implement. Table 6.1 compares some isolated switch-mode converter topologies in terms of obtainable efficiency, cost and power level.

Table 6.1: *Power Topologies Compared*[82]

Topology	Power (Watts)	Typical Efficiency	Relative Cost
Flyback	150	75	1.5
Forward	150	75	1.8
Push-Pull	500	80	1.8
Half-Bridge	500	85	2
Resonant LLC	500	90	2

The working principle of a push-pull converter has been described in detail on section 0 of this thesis. Figure *6.3*, Figure *6.4*, and Figure *6.5* show the different stages of operation of the push-pull converter power stage.

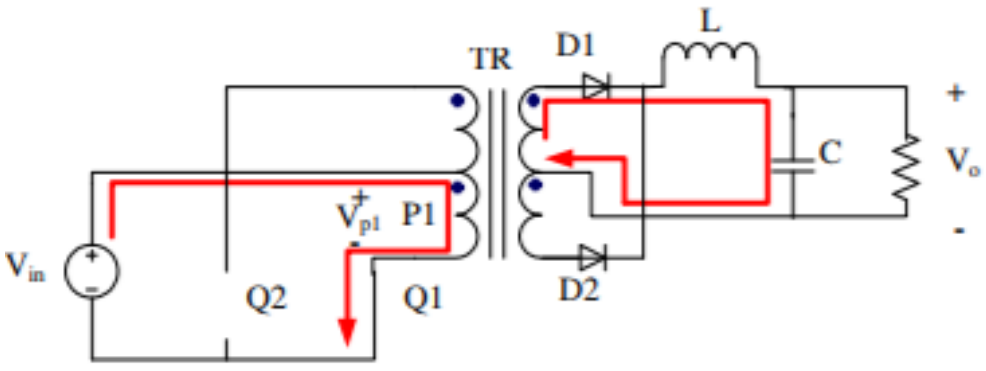

Figure 6.3. Push-pull converter operation stage one (0 < t < DT).

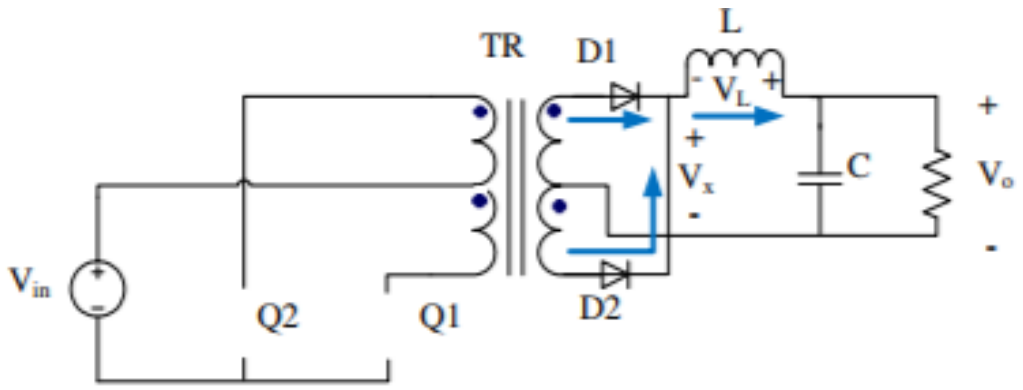

Figure 6.4. Push-pull converter operation stage two (DT < t < T/2).

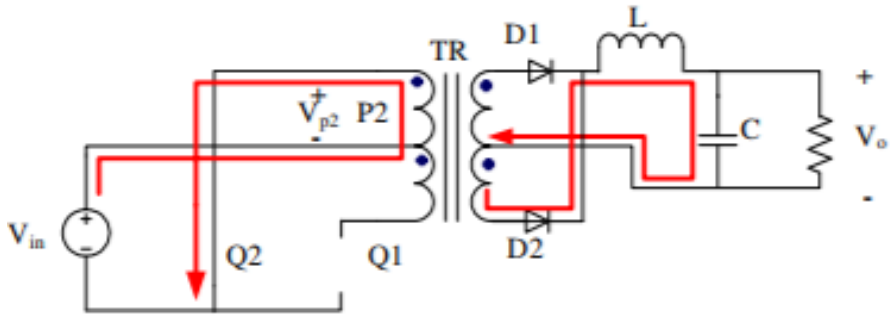

Figure 6.5. Push-Pull converter operation stage three (T/2 < t < T/2 + DT).

The two halves of the primary winding create flux on the core in opposite directions. This helps to reset the core after each half cycle to avoid saturation. However, in practical implementation, when the two primary windings are not accurately matched, making one winding to create higher or lower flux than the second winding, the additional flux gradually walks the transformer core into saturation. Therefore, care is taken in the transformer design and implementation.

The design steps for a push-pull converter are summarised below:

- Define Specification
- Transformer design
- Filter design

- Diode selection
- MOSFET selection
- Control circuit and Feedback design
- Simulation
- Printed Circuit board design.

6.3.1 Specification

The push-pull converter's input is the voltage from the supercapacitor bank, while the output powers the flood light. Each supercapacitor of the bank can discharge only from 2.7V to 1.8V. Therefore, the array of 8 supercapacitors in series has a minimum voltage of (8 x 1.8V) and a maximum voltage of (8 x 2.7V). The flood light displayed maximum illuminance at 120V while drawing a dc current of 1.05A. From the above information, the converter specification is summarized:

Minimum input voltage = 14V

Maximum input voltage = 22V

Output voltage = 120V

Maximum output current = 1.3A

Power output = 156W

Operating frequency = 50 KHz

6.3.2 Transformer design

The transformer is responsible for the change in voltage level of the push-pull converter input. For a boost function, this means a step-up transformer. Therefore, a well-designed transformer is integral in the operation of a push-pull converter. The transformer in push-pull topology is centre tapped; the push-pull operation is already described in section 2.3.7 of this thesis. While the push-pull transformer is centre tapped, only one half of each winding works at a time. In a push-pull

transformer design, care is taken to ensure that the two switches S1 and S2 do not turn on at the same time. While each switch conducts current during one half of the cycle, the transformer core conducts flux during both halves of the switching cycle. For this reason, the transformer core of a push-pull converter operates at twice the switching frequency. Since the halves of both the primary and secondary windings are wound out of phase, the transformer core experiences flux swing in both directions. This phenomenon makes the core of the push-pull transformer more efficiently used than with other transformer isolated topologies. It is a common practice to oversize the push-pull transformer to reduce the tendency of core saturation. .

The following steps are followed in the transformer design:

- Core material selection
- Core size calculation
- Primary turns
- Secondary turns
- Winding topology
- Wire gauge calculation

Loss calculation and expected efficiency.

6.3.2.1 Core material selection

There are different ferromagnetic materials used in the manufacture of transformer core, each with varying properties. The material for a push-pull converter should be specifically designed for transformer operations. Such materials are basically expected to have high saturation flux density, high curie temperature, low residual flux density and low losses at the operating frequency. Curie temperature is the temperature beyond which a material loses its magnetic properties, thus the selected

material should have a high curie temperature rating. For this design, the N87 ferrite core was used. It is highly permeable with base material of manganese and zinc (MnZn), maximum flux density of 390mT at 100 ^{o}C with curie temperature greater than 210 ^{o}C. .

6.3.2.2 Core size

The core size determination in transformer design involves several iterations. Two approaches are possible in the selection of core size. The less popular approach is the use of nomograms. They are core size charts provided by some manufacturers of core materials. For a more optimized transformer design, the Area-product (AP) approach is used. This is the product of the core winding window area and the core cross-sectional area.

In this method, the core size is calculated from the area product equation. It offers a more approximate solution to the choice of core size. Equation 6.3 gives the area-product formula. Majority of the equations used in this design are obtained from Keith Billings book titled: “switch mode power supply handbook”[83].

$$AP = \left(\frac{11.1 \text{ x } Pin}{K \text{ x } \Delta B \text{ x } f}\right)^{1.143} \quad 6.3$$

Where,

P_{in} = input power

f = operating frequency

ΔB = flux density swing

K = Topology constant

Equation 6.3 is based on the following assumptions:

1. Wire current density = 450 A/cm^2
2. Temperature rise = 30 ^{o}C
3. Core loss = 100 Mw/cm^3

The quantities that make up the area product equation are explained in detail:

Input Power (P_{in})

The transformer input is the same as the converter input. With converter output of 156W, and assuming a converter efficiency of 80%, the input power is 195W. However, the push-pull transformer is always designed above the normal rating, hence the transformer is designed for 200W power input.

Flux Density Swing (ΔB)

High flux density swing leads to higher core loss. For maximum efficiency in transformer design, the cores loss is designed to be equal or near equal to the copper loss. Additionally, the selected flux value should not exceed the saturation flux density of the core material, which is 0.4T according to the N87 core material datasheet. Figure *6.6* extracted from the *Magnetics* website, a magnetic component manufacturer, offers a quick guide to flux density selection. According to the curve, the suitable flux density at 100 KHz is 1000gauss, which is equivalent to 0.1 tesla.

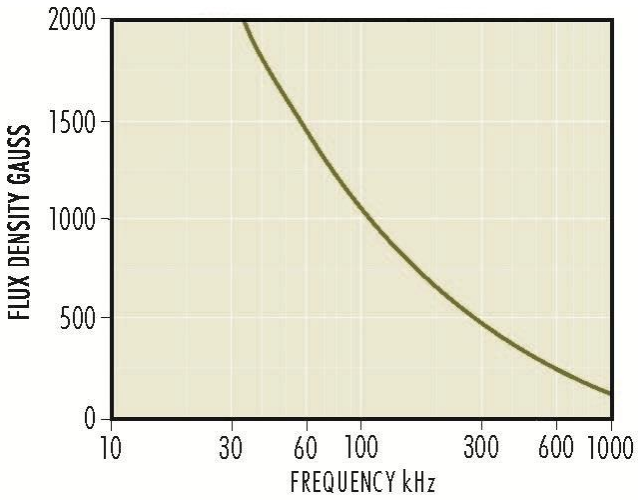

Figure 6.6. Suitable flux density at selected frequency.[84]

For a push-pull operation, the flux density swings in two directions +B and -B. Therefore, the maximum flux density swing is twice the B_{max} value.

Hence, $\Delta B = 0.2T$.

Topology Constant (K)

The topology constant (K) is a product of the Primary area factor (K_p), winding packing factor (K_u) and RMS current factor (K_T)

$K = K_p K_u K_T$

Table 6.2 shows the constant values for different converter topologies.

Table 6.2: *Topology Constants for Transformer Design*[83]

Converter type	Primary form	Secondary form	K_p (A_p/A_{wb})	K_u	K_t (I_{dc}/I_p)	K′ $(K_p \cdot K_u \cdot K_t)$
Forward	SE	CT	0.32	0.4	0.71	0.091
	SE	SE	0.4	0.4	0.71	0.114
Full and half	SE	CT	0.41	0.4	1.0	0.164
bridge	SE	SE	0.5	0.4	1.0	0.2
CT push-pull	CT	CT	0.25	0.4	1.41	0.141
	CT	SE	0.295	0.5	1.41	0.208

For centre tap primary, centre tap secondary push-pull converter K = 0.141. The area product is therefore calculated:

$$AP = \left(\frac{11.1 \text{ x } 200}{0.141 \text{ x } 0.2 \text{ x } 100{,}000}\right)^{1.143} = 0.76\text{cm}^4$$

EPCOS ETD core 34/17/11 with area product of 0.8cm^4 is used.

The core specification is as shown in Table 6.3

Table 6.3: *Transformer Core Specifications*

Material	N87 ferrite
Effective core area	97.1mm^2
Core Volume	7630mm^3
Path length	78.6mm

Since a temperature rise of 30 ^oC is assumed in the Area-product formula, the total power loss of the transformer should not exceed $\frac{30}{\text{Core thermal resistance } (Ø)}$

$$Ø = 53 \text{ x } (\text{Vcore})^{-0.54} \quad 6.4$$

Where,

Ø = core thermal resistance

V_{core} = core volume in cm^3

$$Ø = 53 \text{ x } (7.63)^{-0.54}$$

Ø = 17.7 $^oC/W$

$$\text{Total power loss (P)} = \frac{30}{17.7}$$

P = 1.7 Watts

For optimum efficiency, the core loss is restricted to about 44% of the total loss.

Core loss = 0.44 x 1.7 = 0.748 Watt

Copper loss = 1.7 – 0.748 = 0.952 Watt

Hence, the transformer design is such that the losses are limited to the above values.

6.3.2.3 Secondary turns

The number of secondary turns (Ns) is preferably calculated first since the secondary side of the transformer has a more constant voltage than the primary side. Equation 6.5 gives the number of turns in the secondary side of the transformer.

$$N_s = \frac{V_s \text{ x } t_{on(max)}}{\Delta B \text{ x } A_e} \qquad 6.5$$

Where,

V_s = Voltage across the secondary winding at maximum duty cycle (V_{out} + V_{diode}.) This is approximated to 124V to make up for voltage drops due to PCB trace resistance.

$t_{on\ (max)}$ = maximum on-time expressed in (μs) = 0.5 x DT_s (the 0.5 factor is included since the switching frequency is half of the transformer operating frequency for a push-pull converter) . Assuming a maximum duty cycle of 47% which is typical of a push-pull operation,

$$t_{on(max)} = \frac{0.5 \text{ x } 0.47}{100{,}000}$$

$$t_{on(max)} = 9.4\ \mu s$$

A_e = effective core area = 97.1mm^2

Therefore,

$$N_s = \frac{124 \text{ x } 9.4}{0.2 \text{ x } 97.1}$$

$$N_s = 60 \text{ turns}$$

6.3.2.4 Primary turns

The number of primary turns is similarly calculated at a condition of maximum on-time, which occurs at the minimum input voltage.

The $V_{in(min)}$ is approximated to 12.96V to make up for voltage drops across the switching device and due to the PCB trace resistance.

$$N_p = \frac{12.96 \text{ x } 9.4}{0.2 \text{ x } 97.1}$$

$$N_p = 6 \text{ turns}$$

6.3.2.5 Wire gauge calculation

To calculate the wire size, the following factors are considered:

- Skin effect
- Maximum available area for a turn
- Total copper loss

Skin effect: This is the tendency of high frequency current to flow on the outer layer of a conductor. This reduces the effective cross-sectional area of the conductor thereby increasing losses in the form of heat. To reduce the losses due to skin effect, the chosen wire diameter should not be greater than twice the penetration depth.

$$\text{Penetration depth } (\Delta) = \frac{69.66}{\sqrt{f}} \qquad 6.6$$

$$\text{Penetration depth } (\Delta) = \frac{69.66}{\sqrt{100{,}000}}$$

$$= 0.22\text{mm}.$$

Hence, to avoid skin effect, the wire diameter should not exceed 0.44mm.

Maximum available area for a turn: The cross-sectional area occupied by a single turn is equivalent to the cross-sectional area of the conductor. The bobbin size and the total number of turns determine the maximum area available for a turn. The chosen wire size should be such that it does not exceed this area. .

To calculate the available area, consider the area product of the core,

$AP = A_e \text{ X } A_w = 0.8cm^4$

$0.8cm^4 = (0.8 \text{ X } 10^4)\ mm^4$

$A_e = 97.1mm^2$

$$\text{Window area (Aw)} = \frac{0.8\ x\ 10^4}{97.1} = 82.4mm^2$$

The bobbin takes about 35% of the core window area. The remaining area is used for the winding, RFI screens and winding separators. .

Available winding area = 0.65 X 82.4 = $53.55mm^2$

The layers of RFI screen and winding separators occupy about 50% of the winding area. If equal area is assigned to the primary and secondary winding.

Primary winding area = Secondary winding area = 0.25 X 53.55 = $13.39mm^2$

Therefore,

$$\text{The maximum area available for a single primary turn} = \frac{13.39}{12}$$

= $1.11mm^2$

For a conductor of round cross-sectional area, the maximum allowable diameter is given by Equation 6.7

$$d = \sqrt{\frac{4 \text{ x } A}{\pi}} \qquad 6.7$$

Where,

A = the area available for a single turn.

$$d = \sqrt{\frac{4 \text{ x } 1.11}{\pi}}$$

$= 1.2mm^2$

Total copper loss: For a maximum temperature rise of 30 ^oC, the total copper loss of the conductors should not exceed the 0. 952Watt limit as calculated above. Copper loss is determined by the amount of current flowing through a conductor and the conductor resistance. Since the current flow is determined by the converter specification and load requirement, the copper loss is only controlled by choosing a conductor with low enough resistance.

With all the above factors put into consideration, a litz wire is preferred for the primary winding. The specification of the wire is shown in Table 6.4.

Table 6.4: *Primary Winding Wire Specifications*

Number of strands	137
Diameter of a single strand	0.071mm
Total cross-sectional area	$0.53mm^2$
Resistance	0.0000326 Ω/mm

The diameter of 0.071 is less than the skin depth, thus meeting the requirement for skin effect reduction. The total cross-sectional area of the litz wire also fits in to the available area of $0.9mm^2$.

For the secondary winding,

$$\text{The area occupied by a single secondary turn} = \frac{14.97}{120}$$

$= 0.12mm^2$

$$d = \sqrt{\frac{4 \text{ x } 0.12}{\pi}} = 0.36mm$$

Maximum diameter for a turn = 0.4mm

Copper enamel wire, 26AWG is used for the secondary winding. The key specifications are shown in Table 6.5

Table 6.5: *Secondary Winding Wire Specifications*

Material	Copper
Diameter of conductor	0.4mm
Resistance	0.000134 Ω/mm

The wire diameter is a little higher than the maximum diameter of a turn. However, the deficit of the area occupied by the primary winding makes up for this situation.

6.3.2.6 Loss and efficiency calculation

To calculate the maximum copper loss of the wire, the maximum dc and ac currents are calculated.

$$I_{s(dc)max} = I_{(out)max} \text{ x } D_{max} \quad 6.8$$

$$I_{s(ac)max} = I_{s(dc)max} \text{ x } \sqrt{\frac{1 - D_{max}}{D_{max}}} \quad 6.9$$

$$I_{p(dc)max} = \frac{I_{s(dc)max}}{n} \quad 6.10$$

$$I_{p(ac)max} = \frac{I_{s(ac)max}}{n} \quad 6.11$$

Where,

$I_{s(dc)max}$ = Maximum secondary dc current

$I_{p(dc)max}$ = Maximum primary dc current

$I_{s(ac)max}$ = Maximum secondary ac current

$I_{p(ac)max}$ = Maximum primary ac current

D_{max} = Maximum duty cycle

$I_{(out)max}$ = Maximum output current

n = turns ratio $\left(\frac{N_p}{N_s}\right)$

$$I_{(out)max} = 1.3A$$

$$I_{s(dc)max} = 1.3 \text{ x } 0.47 = 0.6A$$

$$I_{s(ac)max} = I_{s(dc)max} \text{ x } \sqrt{\frac{1-0.47}{0.47}} = 0.64A$$

$$I_{p(dc)max} = \frac{0.6}{0.102} = 5.85A$$

$$I_{p(ac)max} = \frac{0.64}{0.102} = 6.27A$$

The dc resistance of the winding is given by equation 6.12

$$R_{dc} = \text{MLT x number of turns x R/mm} \qquad 6.12$$

Where,

R/mm = Resistance of conductor per millimetre length

MLT = Mean length per turn (mm). This is equivalent to the circumference of the bobbin,(πd) where d is the bobbin diameter (11.8mm according to the datasheet).

For the primary winding,

$$R_{dc} = 11.8 \text{ x } \pi \text{ x } 8 \text{ x } 0.0000326$$

= 0.0096 Ω

Dc primary copper loss = 5.85^2 X 0.0096 = 0.32W.

Since the skin depth requirement is met, R_{dc} is assumed to be approximately equal to R_{ac}

Therefore, AC Primary copper loss = 6.27^2 X 0.0096 = 0.38W

Total primary copper loss = 0.38 + 0.32 = 0.7Watt

For the secondary winding,

MLT = πd (d = bobbin diameter + (2 x diameter of primary wire))

MLT = π(11.8 + 1.64) = 42.23mm

$R_{dc} = 42.23 \text{ x } 77 \text{ x } 0.000134$

= 0.44 Ω

Dc secondary power loss = 0.6^2 X 0.44 = 0.16W

Ac secondary power loss = 0.64^2 X 0.44 = 0.18W

Total secondary copper loss = 0.16 + 0.18 = 0.34W

Total copper loss = 0.34 + 0.7 = 1.04W

This is slightly higher than the maximum copper loss of 0.952W required for optimum efficiency. However, the difference in practical implementation of the transformer is negligible and can be ignored.

For a load of 156W, the expected efficiency can be calculated.

$$\text{Efficiency} = \frac{100 \text{ x } (156 - (1.04 + 0.66)}{156} = 98.9\%$$

However, the above figure is ideal, but it serves as a good guide. The winding architecture and the overall practical implementation of the transformer plays a key role in the efficiency.

6.3.3 Inductor selection

When either of the switches is on, the inductor current rises, during the dead time period when both switches are off, the inductor current discharges to the load. The Volt-second product during this time must be equal to avoid inductor saturation. The inductance value can be determined by considering either the on-period or the off-period.

At t_{on} ,

$$V_L = (nV_{in} - V_d) - V_o \quad 6.13$$

Where,

n = turns ratio $\left(\frac{N_p}{N_s}\right)$

V_d = Voltage drop across the diode

Vo = Output Voltage.

From the voltage-current relationship of an inductor,

$$V_L = L\left(\frac{dI_L}{dt_{on}}\right) \quad 6.14$$

Substituting equation 6.13 into 6.14, while replacing t_{on} with DT_s,

$$L = \frac{(nV_{in} - V_d - V_o) \text{ x } DT_s}{dI_L} \quad 6.15$$

dI_L = Inductor ripple current

Ripple current should be limited to about 20-30% of the maximum current. The inductor ripple current for this design is chosen to be 0.2 of 1.3A.

D = maximum duty cycle = 0.47

$T_s = \frac{1}{f_s}$ (f_s is the switching frequency of the MOSFET)

From the push-pull converter power transfer function, nV_{in} is deducted thus:

$$nV_{in} = \frac{V_o}{2D} \quad 6.16$$

$$L = \frac{(\frac{120}{2 \text{ x } 0.47}) \quad - \ 0.7 \ - \ 120) \text{ x } 0.47 \text{ x } 1}{0.2 \text{ x } 50{,}000}$$

L = 327µH

In addition to the above inductance value, the selected inductor should be able to withstand the inductor peak current. The peak current is given as follows,

$$I_{L(peak)} = I_{o(max)} + \left(\frac{\Delta I_L}{2}\right) \quad 6.17$$

$$I_{L(peak)} = 1.3 + \left(\frac{0.2}{2}\right)$$

= 1.4A

6.3.4 Capacitor selection

The function of the output capacitor is to limit the output voltage ripple of the converter, and to improve the transient response of the converter. Unlike in the boost converter, there is a continuous flow of current through the capacitor from the inductor. During the dead time, when the two switches S1 and S2 are off, the inductor ripple current flows through the capacitor. The voltage across the capacitor drops due to the ESR of the capacitor. The voltage drop is given by the following equation.

$$V_{C(ESR)} = \Delta I_L \text{ X ESR} \quad 6.18$$

The inductor limits the slew rate of the output current. Therefore, periods when there is a transient demand for more current by the load, the output capacitor supplies the current. A voltage drop due to this action is also experienced by the

capacitor. This voltage drop can be quantified by considering the capacitor voltage current relationship of Equation 6.19,

$$I_C = C\left(\frac{\Delta V_C}{dt}\right) \quad 6.19$$

$$C = \frac{\Delta I \text{ x } t_{on}}{\Delta V}$$

The ESR voltage drop constitutes for about 75% of the total voltage drop across the capacitor. Hence the voltage drop caused by a change in the output current is approximately 0.25 of the total voltage drop. .

The voltage ripple is chosen to be 0.5V

Hence,

$$C = \frac{0.2 \text{ x } 0.47}{0.25 \text{ x } 0.5 \text{ x } 50{,}000}$$

C = 15 µF

The maximum ESR required to limit the output voltage ripple to 0.5V is given as,

$$ESR = \frac{0.75 \text{ x } 0.5}{0.2}$$

= 1.875Ω

Hence, the capacitor should have ESR not greater than 1.875Ω while the voltage rating should be higher than the output voltage of 120V. .

6.3.5 Diode selection

The diodes conduct current alternatively in similar pattern to the primary side MOSFET switches. When any of the diodes is switched off, twice the secondary side voltage of the transformer is applied across it. Therefore, the selected diode

should be able to withstand a reverse voltage higher than twice the voltage of the transformer secondary.

$$2V_s = 2 \text{ x } V_{in(max)} \text{ x } \left(\frac{N_s}{N_p}\right) \qquad 6.20$$

Where,

Vs = secondary side voltage

$$2\ x\ 21\ x\ \left(\frac{60}{6}\right) = 420V$$

Hence, the diode reverse voltage should be above 420V. The selected diode should withstand both the expected maximum forward current and the peak current.

The maximum forward current through the diode is equivalent to the maximum output current which is 1.3A, while the peak current is equivalent to the inductor peak current which is 1.4A. .

6.3.6 MOSFET selection

One of the draw backs of the push-pull converter topology is the voltage stress exerted on the MOSFET switches during t_{off}. At this time, the voltage across the drain and source is ideally equivalent to twice the input voltage. However, in practical application this voltage includes the spikes due to the circuit leakage inductances. Therefore, the selected MOSFET should be able to withstand a drain-source voltage of ($2V_{in(max)}$ + V_{spikes}) where V_{spikes} is estimated as 30% of the voltage.

MOSFET $V_{DS(max)}$ > (2 x 22) + (0.3 x 2 x 22)

MOSFET $V_{DS(max)}$ > 57.2V.

The MOSFET should be able to withstand the maximum primary current.

Assuming a worst transformer efficiency of 90%.

$$I_{pri(max)} = \frac{V_s \text{ x } I_s}{0.9 \text{ x } V_{pri(min)}} \quad 6.21$$

$$I_{pri(max)} = \frac{124 \text{ x } 1.3}{0.9 \text{ x } 12.96} = 13.8A$$

This current is not continuous through the MOSFETs. It is pulsed at a duty cycle less than 50%, with a ramp-on-a-step waveform. For simplicity of analysis, the pulses are approximated to a flat top rectangular wave pulse. The flat top current (I_{pft}) can be found. The average current is approximately 0.8 I_{pft} [85]

$$P_{in} = V_{in} \text{x } I_{pft} \text{ x } 0.8 \quad 6.22$$

Maximum current occurs at minimum input voltage, hence;

$$I_{pft} = \frac{P_{in}}{V_{in(min)} \text{ x } 0.8} \quad 6.23$$

Assume a converter efficiency of 75%.

$$I_{pft} = \frac{156}{12.96 \text{ x } 0.8 \text{ x } 0.75} = 20.06A$$

$I_{avg(max)}$ = 0.8 X 20.06 = 16.04A

Therefore, the $I_{DS(max)}$ of the selected MOSFET should be higher than the expected 16A. At a switching frequency of 50 KHz, conduction losses in the MOSFET dominates. Hence, the selected MOSFET should have a low R_{DSon} to reduce conduction losses. A lower total gate charge reduces the switching losses.

6.3.7 Control circuit and feedback design

Current mode control method is chosen for the control circuit. The push-pull topology is prone to flux imbalances on the primary side. This can be a result of power switches that are not exactly matched, the additional flux if not taken care of would drive the core into saturation. Current mode control method takes care of this situation by using the primary winding current to generate the ramp signal. A dead time after each switch turns off is also necessary to ensure that the two switches are not turned on at the same time. LTC3723-1 current mode push-pull controller is suitable for this application. It incorporates a programmable dead time between the switching of the two gate drivers.

6.3.7.1 Setting the frequency

The switching frequency is set by connecting a timing capacitor to the "CT" pin of the controller. The capacitor value is calculated using Equation 6.24 as specified by the manufacturer.

$$C_T = \frac{1}{14.8k \text{ x } f_{osc}} \qquad 6.24$$

Where f_{osc} = oscillator frequency, which is twice the switching frequency of each MOSFET.

For a switching frequency of 50kHz, f_{osc} = 100kHz

$$C_T = \frac{1}{14.8 \text{ x } 100 \text{ x } 10^6} = 680pF$$

6.3.7.2 Current sense resistor

LTC3723-1 controller uses a current sense resistor to create a ramp voltage signal for the control circuit. The current sense pin also incorporates voltage comparators to detect over current situations. The maximum voltage on the current sense pin for safe operation is 0.3V, this occurs at the peak primary current. I_{pft} was calculated from equation 6.23. This calculation assumed a flat-topped waveform with the middle point of the ramp chosen as the $I_{pft.}$ To make margin for the actual peak current, say 30% of $I_{pft.}$

$$I_{peak} = I_{pft} + 0.3\ I_{pft} \qquad 6.25$$

$I_{peak} = 14.78 + (0.3 \times 14.78) = 19.214A$

$$R_{sense} = \frac{0.3}{19.214} = 0.0156\Omega$$

A ceramic bypass capacitor is also connected close to this pin to ensure that voltage spikes do not get into the current sense amplifier.

The controller has a provision for an optional slope compensation. A resistor connected from the current sense resistor to the CS pin helps to improve the slope compensation. .

6.3.7.3 Feedback circuit

To maintain isolation between the primary and the secondary side of the transformer, an optocoupler is used for the feedback circuit. The output of the optocoupler is connected directly to the COMP pin of the controller, thereby bypassing the feedback (FB) pin. A voltage reference is also used at the output of the converter to drive the LED which is the input of the optocoupler. LT1431 Programmable voltage reference and MOC207 optocoupler are preferred for the

feedback circuit. Figure *6.7* shows the pin-out configuration and circuit of the voltage reference. The feedback resistors (R1 and R2) are used to set the output voltage of the converter while V+ is the bias input voltage of the voltage reference. The allowable maximum voltage on V+ is 36V, therefore a Zener diode is used to power the IC from the converter output of 120V. Coll pin provides the voltage reference for the LED of the optocoupler, while R_L controls the current through the LED.

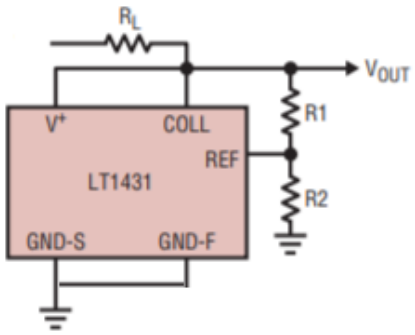

Figure 6.7 LT141 Programmable voltage reference.

According to the datasheet, the REF pin has a voltage reference of 2.5V and requires a typical bias current of 0.2µA. This is considered in choosing R1 and R2.

$$R2 = \frac{Vref}{I_{R2}} \qquad 6.26$$

If 2µA is allowed through R2,

$$R2 = \frac{2.5}{2 \text{ x } 10^{-6}} = 1.25M\Omega$$

$$Vo = \left(1 + \frac{R1}{R2}\right) Vref \qquad 6.27$$

$$R1 = \left(\frac{120}{2.5} - 1\right) 1.25 \text{ x } 10^{6} = 59M\Omega$$

BZX84C8V2L Zener diode is used to power the IC from the 120V output of the converter. It has a minimum Zener voltage of 7.7V and a minimum bias current of 5mA. The maximum power dissipation is 250mW. For a zener bias current of 10mA, the resistor value is calculated thus:

$$\mathrm{R(zener)} = \frac{120 - 7.7}{10 \times 10^{-3}} = 12\mathrm{k\Omega}$$

Optocoupler:

Selecting the right resistor values is crucial to the safety and effectiveness of the optocoupler. The optocoupler circuit is shown in Figure *6.8* R_P is the pull-up resistor, while R_L is the LED current limiting resistor. The pull-up resistor pulls the COMP pin of the PWM controller to 5V when maximum duty cycle is desired. Vref is the 5V reference voltage of the PWM controller.

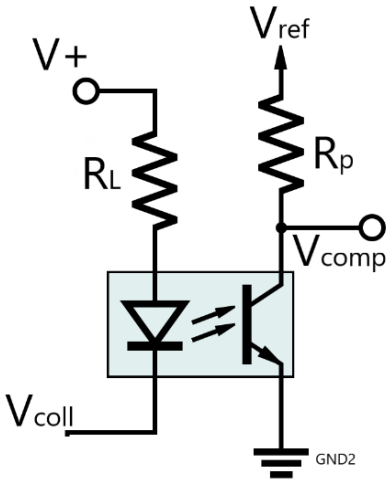

Figure 6.8. Optocoupler circuit.

The following are the key specification of the optocoupler:

LED Maximum forward current = 60mA

Current transfer ratio (CTR) = 100% – 200% (typical =150%)

LED forward voltage = 1.15V - 1.5V

Photo-transistor maximum dark current = 50nA

The maximum current to be passed through the LED is chosen to be 70% of $I_{F(max)}$

I_{LED} = 0.7 x 60 = 42mA

The minimum R_P is calculated such that the 5V of Vref is dropped across it when a zero duty cycle is desired at the worst case CTR.

$$R_{P(min)} = \frac{V_{ref(min)} - 0}{I_F \text{ x worst case CTR}} \quad 6.28$$

$$R_{P(min)} = \frac{4.925 - 0}{0.042 \text{ x } 1}$$

$R_{P(min)} = 117.2\Omega$

The maximum R_P is also calculated such that minimal voltage is dropped across it when the phototransistor is open and only the leakage current flows through the collector. This is to maintain the maximum duty cycle voltage of 4.5V.

$$R_{P(max)} = \frac{V_{ref(min)} - 4.5}{I_{leakage(max)}} \quad 6.29$$

Maximum leakage current = 50nA (from the datasheet),

$$R_{P(max)} = \frac{4.925 - 4.5}{50 \text{ x } 10^{-9}}$$

$R_{P(max)} = 8.5M\Omega$

The pull-up resistor range is 117.2Ω – 8.5MΩ. Therefore, any resistor value chosen within this range is suitable for the optocoupler circuit. A 270Ω resistor is used for this design. .

With the chosen pull-up resistor value, the new maximum and minimum collector currents are calculated.

$$I_{C(min)} = \frac{V_{ref(min)} - 4.5}{R_{pull-up}} \quad 6.30$$

$$I_{C(min)} = \frac{4.925 - 4.5}{270} = 0.0016A$$

$$I_{C(max)} = \frac{V_{ref(max)} - 0}{R_{pull-up}} \quad 6.31$$

$$I_{C(max)} = \frac{5.075 - 0}{270} = 0.0188A$$

Using the worst case CTR of 100% to decide the corresponding LED minimum and maximum forward current, the LED current is equal to the collector current.

$I_{F(min)}$ = 1.6mA

$I_{F(max)}$ = 18.8mA.

The current limiting resistor R_L should be able to allow a current range of $I_{F(min)}$ to $I_{F(max)}$.

$$R_{L(max)} = \frac{V_{+(min)} - V_F - V_{coll(max)}}{I_{F(min)}} \quad 6.32$$

$$R_{L(max)} = \frac{7.7 - 1.5 - 2.51}{0.0016}$$

$$R_{L(max)} = 2306.25\Omega$$

The minimum resistance should be such that the maximum current of the LED is not exceeded. This maximum current is chosen to be 70% of the datasheet maximum.

$$R_{L(min)} = \frac{V_{+(max)} - V_{F(min)} - V_{coll(min)}}{0.7\ I_{F(max)}} \quad 6.33$$

$$R_{L(min)} = \frac{8.7 - 1.15 - 2.49}{0.7 \text{ x } 0.06}$$

$$R_{L(min)} = 120.48\Omega$$

RL is chosen to be 1kΩ resistor

6.3.8 Design simulation

Time limited the lab implementation of this circuit. However, to confirm the design component values and workability of the circuit, a simulation is performed. A spice model of the LTC3723-1 controller is made available by the manufacturer, this is used to create a schematic of the circuit. The transformer turns ratio is represented in spice by coupled inductors where the turns ratio is proportional to square of the inductance ratio. While a software simulation assumes perfect coupling of the transformers, in practical implementation, this is not achieved. Therefore, for practical implementation, snubber circuits are optimally designed and connected across the drain and sources of the MOSFETs to reduce the ringing and clamp the voltage. Figure *6.9*, Figure *6.10*, and Figure *6.11* show the design layout, the MOSFET gate signals and the input/output voltage signals respectively.

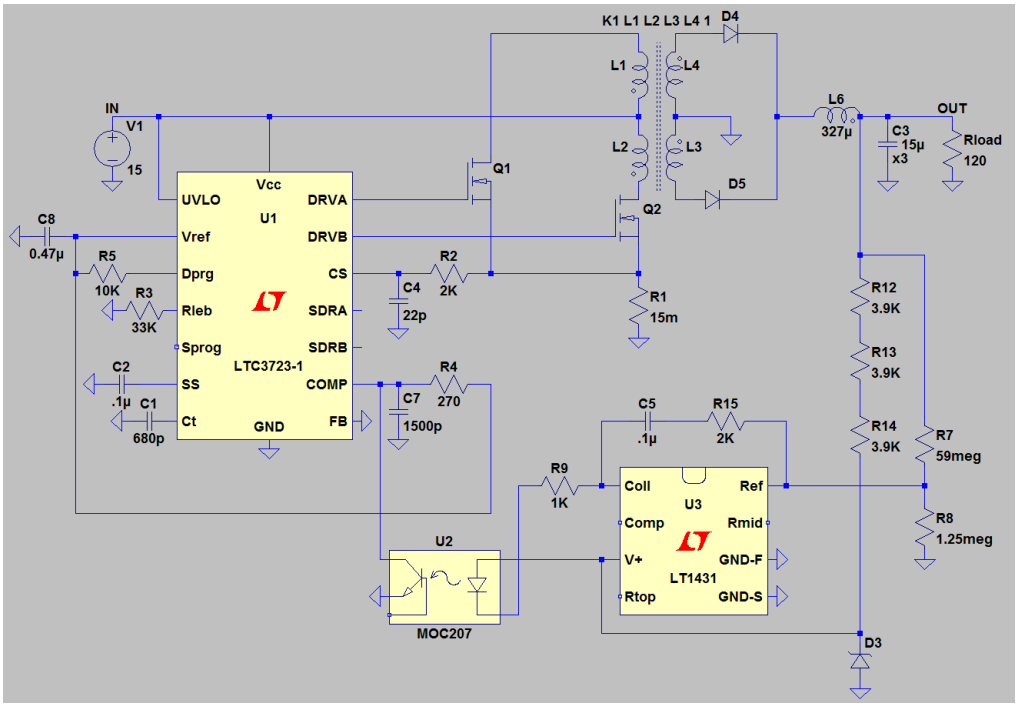

Figure 6.9. Final circuit layout of the push-pull converter.

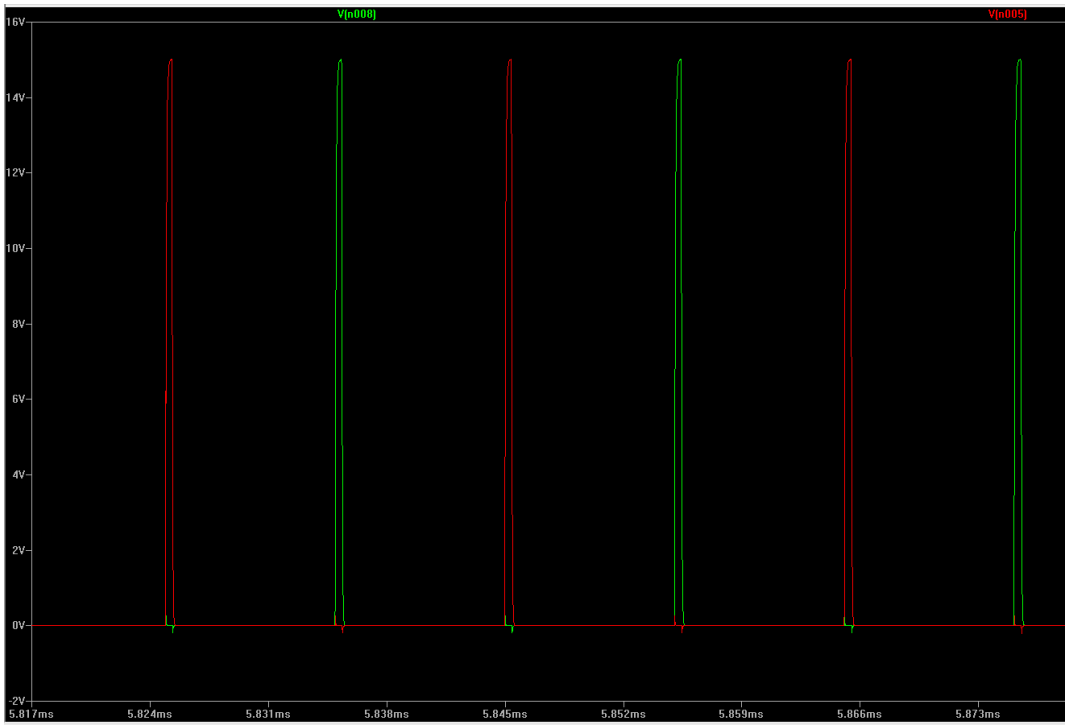

Figure 6.10. MOSFET gate signals for push-pull converter.

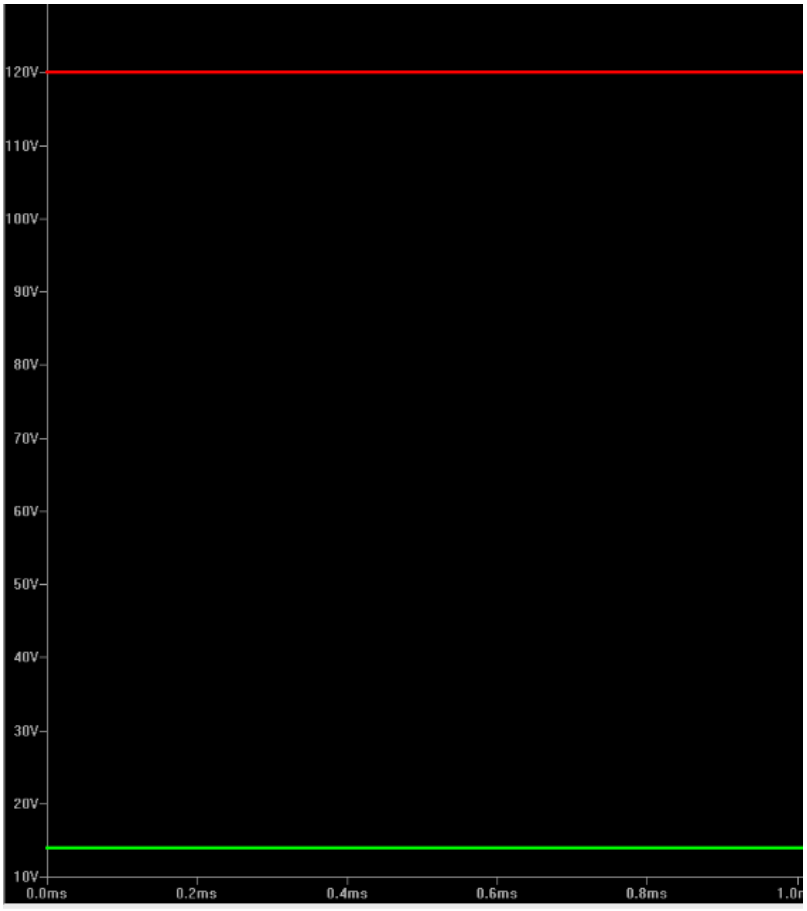

Figure 6.11. Input/output voltage signals.

Chapter Seven

Conclusion and Future Development

7.1 Conclusion

Energy storage in renewable energy systems have proven to be inevitable as the energy sources are erratic. The battery energy storage system has been the most popularly used. In this work, the potentials of the supercapacitor energy storage device in renewable energy systems has been accessed. Various technologies of supercapacitors available in the industry today was explored in chapter three, the objects of technology investigated in this chapter comprise of the electrode materials and the electrolytes. Some commercially available supercapacitor types were subjected to various laboratory tests and their performance at different conditions compared. The battery-type hybrid supercapacitor has so far proved to be the best available supercapacitor technology in terms of energy density. The 40,000 Farad battery-type hybrid supercapacitor manufactured by SAMWHA capacitor group is one of the highest capacities of such technology successfully produced.

Chapter five presented a detailed design description of a low input voltage boost converter used to demonstrate the supercapacitor's energy back up capabilities. The highly optimised design showed a maximum efficiency of 76% which occurred at the maximum input voltage.

Street lighting system based on DC micro grid was shown in chapter six. Supercapacitor array was used as the energy storage device, and a suitable power

converter was designed. The necessary design calculations were done, and the final circuit was simulated.

The battery energy storage system is undoubtedly the most popular energy storage system for renewable energy applications. With the development of the battery-type hybrid supercapacitor, and the continuous research work in the supercapacitor topics, energy storage in renewable energy system may take a new dimension.

7.2 Future Development

The energy storage capability of the battery-type hybrid supercapacitor has been demonstrated using the boost converter circuit for a 12V LED load. Attempt was made to implement a push-pull converter which would enable the supercapacitor to illuminate a street lighting system. In the future, the designed circuit can be practically implemented in the lab, analysed and optimised for best performance. Synchronous rectification may be adopted in the circuit to further improve its efficiency. To reduce the size of the converter, a planar transformer may be used instead. More efficient converter topologies like the half bridge and full bridge converters may also be designed for the supercapacitors when higher power loads are used.

In the testing and comparison of different supercapacitor technologies, the surge resistant properties can also be investigated. This would also educate the scientist on the more suitable supercapacitor technologies for surge resistant purposes. The self-discharge rates of the different technologies of supercapacitors can also be ascertained and compared.

References

1. Administration, E.I. and G.P. Office (2016). *International Energy Outlook 2016: With Projections to 2040*. Government Printing Office.
2. Tol, R.S. 2018. The economic impacts of climate change. *Review of Environmental Economics and Policy*, *12*(1), 4-25.
3. Gielen, D., et al. (2018). *Global energy transformation: a roadmap to 2050.* International Renewable Energy Agency: Abu Dhabi, Vereinigte Arabische Emirate, p. 76.
4. Divya, K., & Østergaard, J. (2009). Battery energy storage technology for power systems—An overview. *Electric Power Systems Research 79*(4), 511-520.
5. Wind energy today (January 9, 2019). Available from: https://windeurope.org/about-wind/wind-energy-today/.
6. *New Zealand wind industry.* (January 9, 2019) Available from: http://www.windenergy.org.nz/wind-energy/nz-windfarms.
7. *Offshore wind energy*. (January 9, 2019) [cited Available from: https://www.boem.gov/Offshore-Wind-Energy/.
8. Hosenuzzaman, M., et al. (2015). Global prospects, progress, policies, and environmental impact of solar photovoltaic power generation. *Renewable and Sustainable Energy Reviews, 41*, 284-297.
9. Dimroth, F., et al. (2016) Four-junction wafer-bonded concentrator solar cells. *IEEE Journal of Photovoltaics, 6*(1), 343-349.
10. *China Installs 24.3 Gigawatts Of Solar In First Half Of 2018* (January 9, 2019. Available from: https://cleantechnica.com/2018/08/06/china-installs-24-3-gigawatts-in-first-half-of-2018/.
11. Zarfl, C., et al. (2015). A global boom in hydropower dam construction. *Aquatic Sciences, 77*(1), 161-170.

12. *Energy in New Zealand*. (January 11, 2019) Available from: www.mbie.govt.nz/assets/d7c93162b8/energy-in-nz-18.pdf.

13. Donatini, F. (2018). Geothermal Power. Power Engineering: Advances and Challenges, Part A: Thermal, Hydro and Nuclear Power: p. 179.

14. Glassley, W.E. (2018). *Geology and Hydrology of Geothermal Energy.* Power Stations Using Locally Available Energy Sources: A Volume in the Encyclopedia of Sustainability Science and Technology Series, Second Edition: p. 23-34.

15. *Geothermal Energy.* New Zealand geothermal energy. Available from: https://nzgeothermal.org.nz/elec_geo/.

16. Fernando, J., et al. (2014). *Implementation of the supercapacitor-assisted surge absorber (SCASA) technique in a practical surge protector*. In *Industrial Electronics Society, IECON 2014-40th Annual Conference of the IEEE*. IEEE.

17. Östergård, R. (2011). *Flywheel energy storage: a conceptual study*.

18. Faraji, F., Majazi, A., & Al-Haddad, K. (2017). A comprehensive review of flywheel energy storage system technology. *Renewable and Sustainable Energy Reviews,* 67, 477-490.

19. Luo, X., et al. (2015). Overview of current development in electrical energy storage technologies and the application potential in power system operation. *Applied Energy*, 137, 511-536.

20. Sutanto, D., & Cheng, K. (2009). *Superconducting magnetic energy storage systems for power system applications*. in *Applied Superconductivity and Electromagnetic Devices. ASEMD 2009. International Conference on*. 2009. IEEE.

21. Vulusala, G., V.S., & Madichetty, S. (2018). Application of superconducting magnetic energy storage in electrical power and energy systems: a review. *International Journal of Energy Research, 42*(2), 358-368.

22. Zhang, G., et al. (2011). The construction progress of a high-Tc superconducting power substation in China. *IEEE Transactions on Applied Superconductivity, 21*(3), 2824-2827.

23. Biswas, M.M., et al. (2013). Towards implementation of smart grid: an updated review on electrical energy storage systems. *Smart Grid and Renewable Energy, 4*(01), 122.

24. Winter, M., & Brodd, R.J. (2004) *What are batteries, fuel cells, and supercapacitors?* ACS Publications.

25. Kularatna, N. (2016). *DC Power Supplies: Power management and surge protection for power electronic systems.* CRC Press.

26. Drummer, G. (1997). *Electronic inventions and discoveries: electronics from its earliest beginnings to the present day*. CRC Press.

27. Middlebrook, R.D., & Cuk, S. (1976). *A general unified approach to modelling switching-converter power stages*. in *1976 IEEE Power Electronics Specialists Conference*. IEEE.

28. Conway, B.E. (2013). *Electrochemical supercapacitors: scientific fundamentals and technological applications.* Springer Science & Business Media.

29. Viswanathan, B. (2017). *Chapter 13 - Supercapacitors*, in *Energy Sources*, B. Viswanathan, Editor. Elsevier: Amsterdam. p. 315-328.

30. Conway, B., Birss V., & Wojtowicz, J. (1997). The role and utilization of pseudocapacitance for energy storage by supercapacitors. J*ournal of Power Sources, 66*(1-2), 1-14.

31. Muzaffar, A., et al. (2019). A review on recent advances in hybrid supercapacitors: Design, fabrication and applications. *Renewable and Sustainable Energy Reviews, 101*, 123-145.

32. Yang, K.-L., et al. (2001). Electrosorption of ions from aqueous solutions by carbon aerogel: an electrical double-layer model. *Langmuir, 17*(6), 1961-1969.

33. Grevillot, G. (1989). *Separation processes based on electrosorption phenomena, in Adsorption: Science and Technology*. Springer. p. 193-221.

34. Javed, M.S., et al. (2016). A high-performance flexible solid-state supercapacitor based on Li-ion intercalation into tunnel-structure iron sulfide. *Electrochimica Acta, 219*, 742-750.

35. Yan, J., et al. (2014). Recent advances in design and fabrication of electrochemical supercapacitors with high energy densities. *Advanced Energy Materials, 4*(4).

36. Iro, Z.S., Subramani C., & Dash, S. (2016). A brief review on electrode materials for supercapacitor. *International Journal of Electrochemical Science, 11*(12), 10628-10643.

37. Pandolfo, A., & Hollenkamp, A. (2006). Carbon properties and their role in supercapacitors. *Journal of Power Sources, 157*(1), 11-27.

38. Ahmadpour, A., & Do, D. (1996) The preparation of active carbons from coal by chemical and physical activation. *Carbon, 34*(4), 471-479.

39. Lota, K., Sierczynska, A., & Acznik, I. (2013) Effect of aqueous electrolytes on electrochemical capacitor capacitance. *Chemik, 67*(11), 1138-1145.

40. Halper, M.S., & Ellenbogen, J.C. (2006). *Supercapacitors: A brief overview.* MITRE Nanosystems Group.

41. Frackowiak, E., et al. (2002). Nanotubular materials as electrodes for supercapacitors. *Fuel Processing Technology, 77*, 213-219.

42. Kim, T., et al. (2018). Cutting-processed single-wall carbon nanotubes with additional edge sites for supercapacitor electrodes. *Nanomaterials, 8*(7), 464.

43. Chang, Z.-H., et al. (2018). Electrochemical deposition of highly loaded polypyrrole on individual carbon nanotubes in carbon nanotube film for supercapacitor. *Chemical Engineering Journal, 337*, 552-559.

44. Sun, P., et al. (2017). Ultrathin MnO2 nanoflakes deposited on carbon nanotube networks for symmetrical supercapacitors with enhanced performance. *Journal of Power Sources, 341*, 27-35.

45. Pröbstle, H., Saliger, R., & Fricke, J. (2000). *Electrochemical Investigation of Carbon Aerogels and their Activated.* Characterisation of Porous Solids V, 2000. 128,. 371.

46. Stoller, M.D., et al. (2008). Graphene-based ultracapacitors*. Nano Letters, 8*(10), 3498-3502.

47. Liu, C., et al. (2010). Graphene-based supercapacitor with an ultrahigh energy density. *Nano Letters, 10*(12), 4863-4868.

48. Kakaei, K. (2019). Graphene-based electrochemical supercapacitors. In Kakaei, K., Esrafili, M.D., & Ehsani, A. (Eds.) *Interface Science and Technology*. Elsevier. p. 339-386.

49. Li, Q., et al., (2018). Ruthenium based materials as electrode materials for supercapacitors. *Chemical Engineering Journal, 333*, 505-518.

50. Frackowiak, E., et al., (2006). Supercapacitors based on conducting polymers/nanotubes composites. *Journal of Power Sources, 153*(2), 413-418.

51. Frackowiak, E., & Beguin, F. (2001). Carbon materials for the electrochemical storage of energy in capacitors. *Carbon, 39*(6), 937-950.

52. Prakash, J., et al. (1998). *Pseudo-capacitor device for aqueous electrolytes*. Google Patents.

53. Largeot, C., et al. (2008). Relation between the ion size and pore size for an electric double-layer capacitor. *Journal of the American Chemical Society, 130*(9), 2730-2731.

54. Sato, T., Masuda, G., & Takagi, K. (2004). Electrochemical properties of novel ionic liquids for electric double layer capacitor applications. *Electrochimica Acta, 49*(21), 3603-3611.

55. Simon, P., & Burke, A. (2008). Nanostructured carbons: double-layer capacitance and more. *The Electrochemical Society Interface, 17*(1), 38.

56. Fletcher, S., Black, V.J., & Kirkpatrick, I. (2014). A universal equivalent circuit for carbon-based supercapacitors. *Journal of Solid State Electrochemistry, 18*(5), 1377-1387.

57. Fletcher, S., et al. (2017). The modelling of carbon-based supercapacitors: Distributions of time constants and Pascal Equivalent Circuits. *Journal of Power Sources, 345*, 247-253.

58. Hart, B.E., & Peekema, R.M. (1972). *Electrochemical double layer capacitor*. Google Patents.

59. Qu, D., & Shi, H. (1998). Studies of activated carbons used in double-layer capacitors. *Journal of Power Sources, 74*(1), 99-107.

60. Kularatna, N. (2014). *Energy Storage devices for electronic systems: rechargeable batteries and supercapacitors*. Academic Press.

61. Conway, B.E. (1991). Transition from “supercapacitor” to “battery” behavior in electrochemical energy storage. *Journal of the Electrochemical Society, 138*(6), 1539-1548.

62. Iro, Z.S., Subramani, C., & Dash, S. (2016). A brief review on electrode materials for supercapacitor. *International Journal of Electrochemical Science, 11*, 10628-10643.

63. Brousse, T., Bélanger, D., & Long, J.W. (2015). To be or not to be pseudocapacitive? *Journal of The Electrochemical Society, 162*(5), A5185-A5189.

64. *Commercially available Pesudocapacitor*. Retrived from: http://www.nesscap.com/ultracapacitor/EDLC/Supercapacitor/pseudocapacitor_family.jsp.

65. Shi, S., et al. (2019). Ultrathin manganese oxide nanosheets uniformly coating on carbon nanocoils as high-performance asymmetric supercapacitor electrodes. *Journal of Colloid and Interface Science, 537*, 142-150.

66. Afzal, A., et al. (2017). Polypyrrole/carbon nanotube supercapacitors: Technological advances and challenges. *Journal of Power Sources, 352*, 174-186.

67. Cao, W., & Zheng, J. (2012), Li-ion capacitors with carbon cathode and hard carbon/stabilized lithium metal powder anode electrodes. *Journal of Power Sources, 213*, 180-185.

68. Jeong, K.H., et al. (2016). Electrochemical synthesis of graphene/MnO2 nano-composite for application to supercapacitor electrode. *Journal of Nanoscience and Nanotechnology, 16*(5), 4620-4625.

69. Sheng, L., et al. (2016). High volumetric energy density asymmetric supercapacitors based on well‐balanced graphene and graphene‐MnO2 electrodes with densely stacked architectures. *Small, 12*(37), 5217-5227.

70. Gueon, D., & Moon, J.H. (2017). MnO2 nanoflake-shelled carbon nanotube particles for high-performance supercapacitors. *ACS Sustainable Chemistry & Engineering, 5*(3), 2445-2453.

71. Choi, C., et al. (2016). Elastomeric and dynamic MnO2/CNT core–shell structure coiled yarn supercapacitor. *Advanced Energy Materials, 6*(5), 1502119.

72. Sun, J., et al. (2017). Recent progresses in high-energy-density all pseudocapacitive-electrode-materials-based asymmetric supercapacitors. *Journal of Materials Chemistry A, 5*(20), 9443-9464.

73. Jiang, Q., et al. (2018). All pseudocapacitive MXene‐RuO2 asymmetric supercapacitors. *Advanced Energy Materials, 8*(13), 1703043.

74. Shao, H., et al. (2018). Cobalt phosphate-based supercapattery as alternative power source for implantable medical devices. ACS Applied Energy Materials.

75. Fernando, J., et al. (2014). *Implementation of the supercapacitor-assisted surge absorber (SCASA) technique in a practical surge protector*. in *IECON 2014-40th Annual Conference of the IEEE Industrial Electronics Society*. IEEE.

76. Ariyarathna, T., et al. (2017). *Potential of supercapacitors in novel power converters as semi-ideal lossless voltage droppers*. in *IECON 2017-43rd Annual Conference of the IEEE Industrial Electronics Society*. IEEE.

77. Grama, A., et al. (2009). *Experimental determination of equivalent series resistance of a supercapacitor*. in *Electronics Technology, 2009. ISSE 2009. 32nd International Spring Seminar on*. IEEE.

78. Keeping, S., (2015). *Design trade-offs when selecting a high-frequency switching regulator.* DigiKey TechZone article.

79. Madsen, M., Knott, A., & Andersen, M.A. (2014). Low power very high frequency switch-mode power supply with 50 V input and 5 V output*. IEEE Transactions on Power Electronics, 29*(12), 6569-6580.

80. Mammano, R. (2001). Switching power supply topology voltage mode vs. current mode*. Elektron Journal-South African Institute of Electrical Engineers, 18*(6), 25-27.

81. *Switchmode Power topologies compared*. Available from: https://www.we-online.com/web/en/index.php/show/media/06_passive_components_-_custom_magnetics/pictures_and_graphics_1/midcom_blog_photos/SMPSChart.pdf.

82. Billings, K.H., Morey, T. (2011) *Switchmode power supply handbook*. McGraw-Hill.

83. *Flux density selection*. Available from: https://www.mag-inc.com/Design/Design-Guides/Transformer-Design-with-Magnetics-Ferrite-Cores.

84. Pressman, A. (1997). *Switching power supply design*. McGraw-Hill, Inc.

Appendix A.1

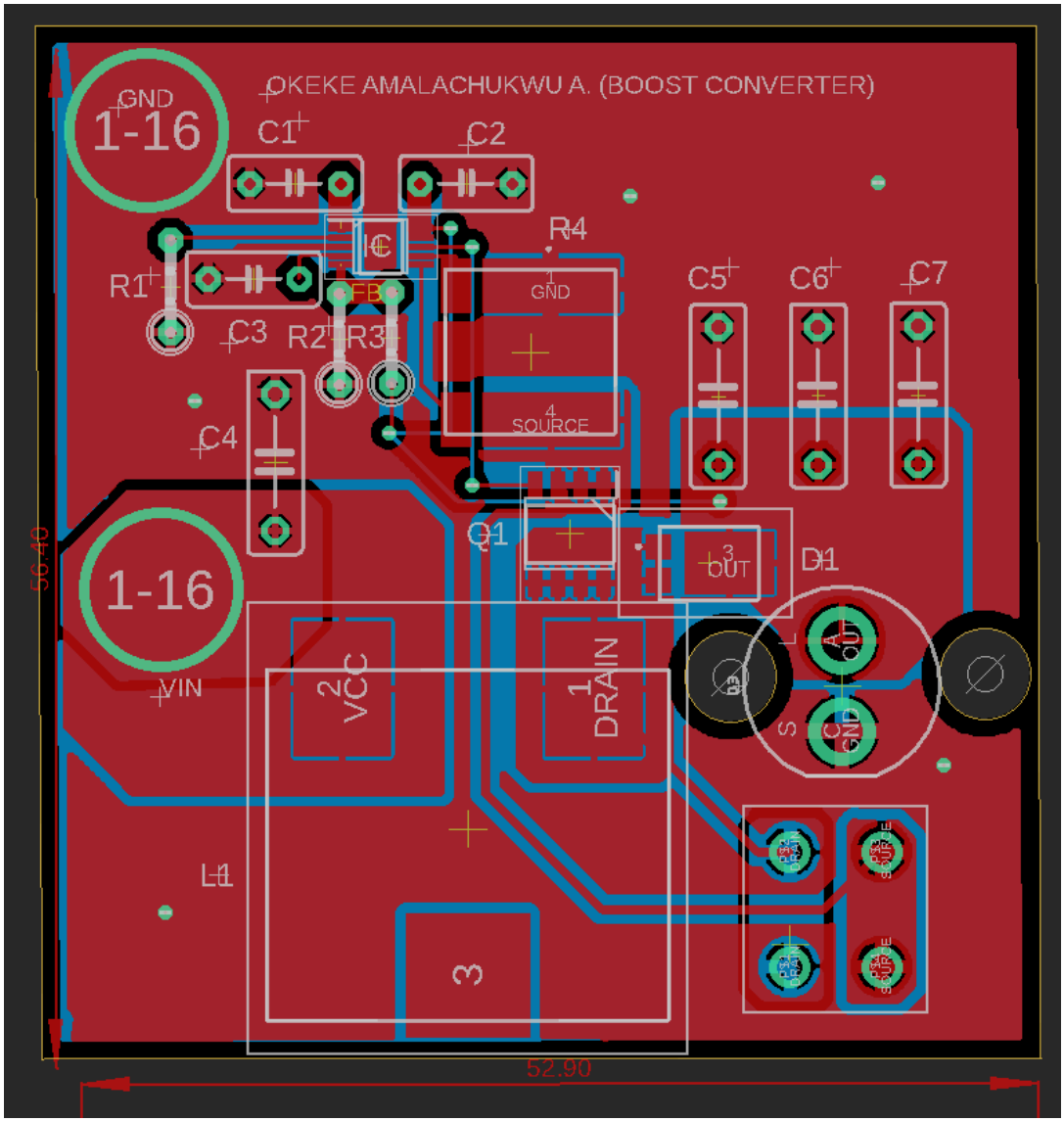

PCB layout for Boost Converter Circuit (Top Layer)

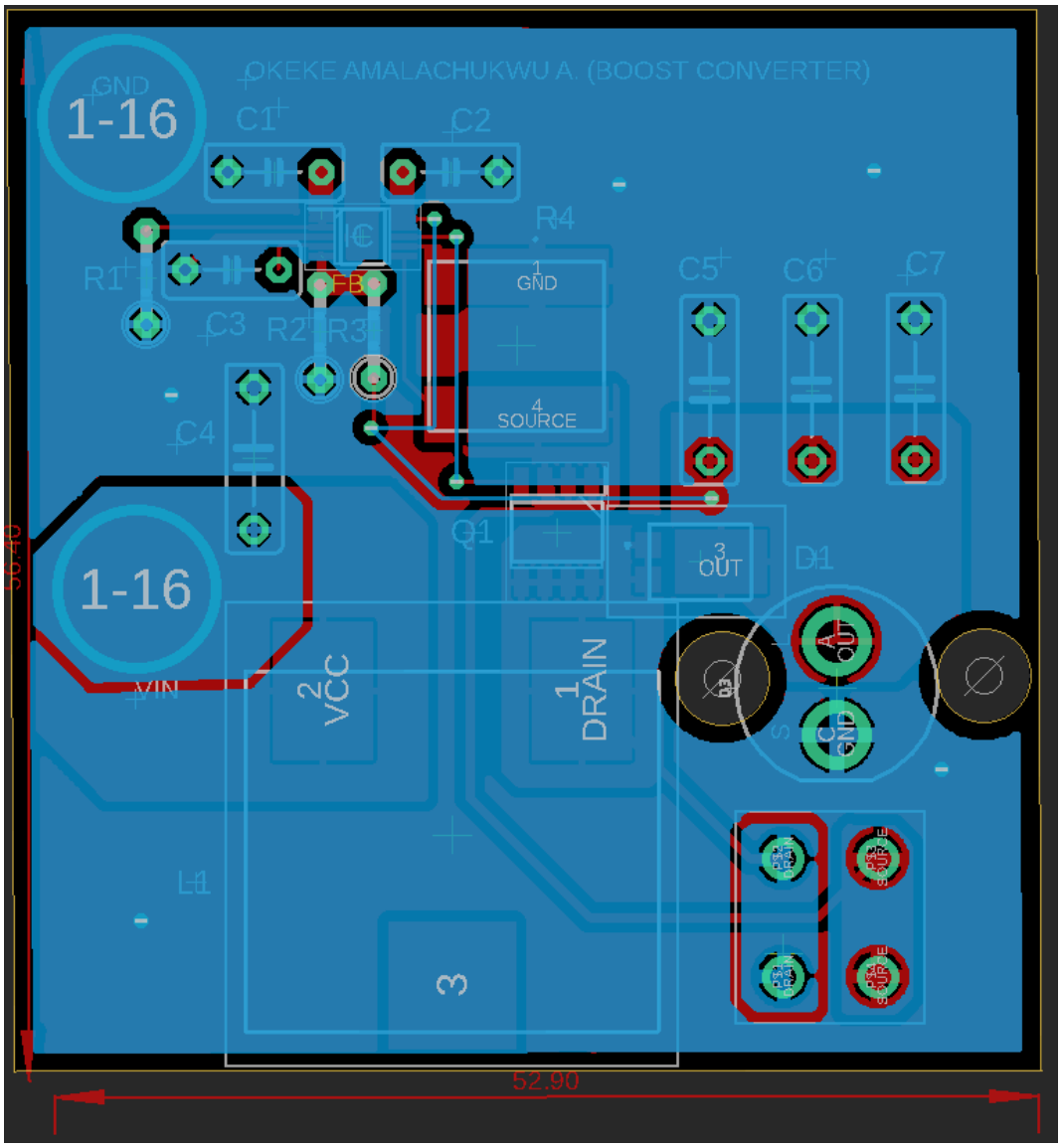

PCB layout for Boost Converter Circuit (Bottom Layer)

Appendix A.2

International
IOR Rectifier

PD - 95724

IRF7401PbF

HEXFET® Power MOSFET

- Generation V Technology
- Ultra Low On-Resistance
- N-Channel Mosfet
- Surface Mount
- Available in Tape & Reel
- Dynamic dv/dt Rating
- Fast Switching
- Lead-Free

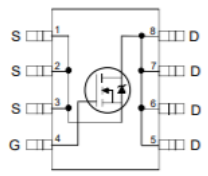

Top View

V_{DSS} = 20V

$R_{DS(on)}$ = 0.022Ω

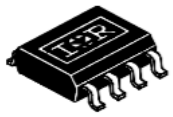
SO-8

Description

Fifth Generation HEXFETs from International Rectifier utilize advanced processing techniques to achieve the lowest possible on-resistance per silicon area. This benefit, combined with the fast switching speed and ruggedized device design that HEXFET Power MOSFETs are well known for, provides the designer with an extremely efficient device for use in a wide variety of applications.

The SO-8 has been modified through a customized leadframe for enhanced thermal characteristics and multiple-die capability making it ideal in a variety of power applications. With these improvements, multiple devices can be used in an application with dramatically reduced board space. The package is designed for vapor phase, infra red, or wave soldering techniques. Power dissipation of greater than 0.8W is possible in a typical PCB mount application.

Absolute Maximum Ratings

	Parameter	Max.	Units
I_D @ T_A = 25°C	10 Sec. Pulsed Drain Current, V_{GS} @ 4.5V	10	A
I_D @ T_A = 25°C	Continuous Drain Current, V_{GS} @ 4.5V	8.7	
I_D @ T_A = 70°C	Continuous Drain Current, V_{GS} @ 4.5V	7.0	
I_{DM}	Pulsed Drain Current ①	35	
P_D @T_A = 25°C	Power Dissipation	2.5	W
	Linear Derating Factor	0.02	W/°C
V_{GS}	Gate-to-Source Voltage	± 12	V
dv/dt	Peak Diode Recovery dv/dt ②	5.0	V/ns
T_J, T_{STG}	Junction and Storage Temperature Range	-55 to + 150	°C

MOSFET datasheet for Boost Converter Circuit

IRF7401PbF

International
IOR Rectifier

Electrical Characteristics @ T_J = 25°C (unless otherwise specified)

	Parameter	Min.	Typ.	Max.	Units	Conditions
$V_{(BR)DSS}$	Drain-to-Source Breakdown Voltage	20	—	—	V	V_{GS} = 0V, I_D = 250µA
$\Delta V_{(BR)DSS}/\Delta T_J$	Breakdown Voltage Temp. Coefficient	—	0.044	—	V/°C	Reference to 25°C, I_D = 1mA
$R_{DS(ON)}$	Static Drain-to-Source On-Resistance	—	—	0.022	Ω	V_{GS} = 4.5V, I_D = 4.1A ③
		—	—	0.030		V_{GS} = 2.7V, I_D = 3.5A ③
$V_{GS(th)}$	Gate Threshold Voltage	0.70	—	—	V	V_{DS} = V_{GS}, I_D = 250µA
g_{fs}	Forward Transconductance	11	—	—	S	V_{DS} = 15V, I_D = 4.1A
I_{DSS}	Drain-to-Source Leakage Current	—	—	1.0	µA	V_{DS} = 16V, V_{GS} = 0V
		—	—	25		V_{DS} = 16V, V_{GS} = 0V, T_J = 125 °C
I_{GSS}	Gate-to-Source Forward Leakage	—	—	100	nA	V_{GS} = 12V
	Gate-to-Source Reverse Leakage	—	—	-100		V_{GS} = -12V
Q_g	Total Gate Charge	—	—	48	nC	I_D = 4.1A
Q_{gs}	Gate-to-Source Charge	—	—	5.1		V_{DS} = 16V
Q_{gd}	Gate-to-Drain ("Miller") Charge	—	—	20		V_{GS} = 4.5V, See Fig. 6 and 12 ③
$t_{d(on)}$	Turn-On Delay Time	—	13	—	ns	V_{DD} = 10V
t_r	Rise Time	—	72	—		I_D = 4.1A
$t_{d(off)}$	Turn-Off Delay Time	—	65	—		R_G = 6.0Ω
t_f	Fall Time	—	92	—		R_D = 2.4Ω, See Fig. 10 ③
L_D	Internal Drain Inductance	—	2.5	—	nH	Between lead tip and center of die contact 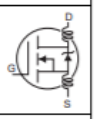
L_S	Internal Source Inductance	—	4.0	—		
C_{iss}	Input Capacitance	—	1600	—	pF	V_{GS} = 0V
C_{oss}	Output Capacitance	—	690	—		V_{DS} = 15V
C_{rss}	Reverse Transfer Capacitance	—	310	—		f = 1.0MHz, See Fig. 5

Source-Drain Ratings and Characteristics

	Parameter	Min.	Typ.	Max.	Units	Conditions
I_S	Continuous Source Current (Body Diode)	—	—	3.1	A	MOSFET symbol showing the integral reverse p-n junction diode. 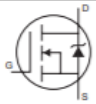
I_{SM}	Pulsed Source Current (Body Diode) ①	—	—	35		
V_{SD}	Diode Forward Voltage	—	—	1.0	V	T_J = 25°C, I_S = 2.0A, V_{GS} = 0V ③
t_{rr}	Reverse Recovery Time	—	39	59	ns	T_J = 25°C, I_F = 4.1A
Q_{rr}	Reverse RecoveryCharge	—	42	63	nC	di/dt = 100A/µs ③
t_{on}	Forward Turn-On Time	Intrinsic turn-on time is negligible (turn-on is dominated by L_S+L_D)				

MOSFET datasheet for Boost Converter Circuit (contd...)

Appendix A.3

TDK

SIFERRIT materials

N87

Material properties

Preferred application			Power transformers
Material			N87
Base material			MnZn
	Symbol	Unit	
Initial permeability (T = 25 °C)	μ_i		2200 ±25%
Flux density (H = 1200 A/m, f = 10 kHz)	B_S (25 °C) B_S (100 °C)	mT mT	490 390
Coercive field strength (f = 10 kHz)	H_c (25 °C) H_c (100 °C)	A/m A/m	21 13
Optimum frequency range	f_{min} f_{max}	kHz kHz	25 500
Hysteresis material constant	η_B	10^{-6}/mT	<1.0
Curie temperature	T_C	°C	>210
Mean value of α_F at 25 … 55 °C		10^{-6}/K	4
Density (typical values)		kg/m³	4850
Relative core losses (typical values)	P_V		
25 kHz, 200 mT, 100 °C		kW/m³	57
100 kHz, 200 mT, 100 °C		kW/m³	375
300 kHz, 100 mT, 100 °C		kW/m³	390
500 kHz, 50 mT, 100 °C		kW/m³	215
Resistivity	ρ	Ωm	10
Core shapes			RM, P, PM, ETD, EFD, E, ER, EP, EQ, ELP, U, Toroid

N87 ferrite core material datasheet

Appendix A.4

Item	Part number	Description	Value
L1	B82559A5682A020	Inductor, Epcos	6.8uH
D1	PDS1040-13	Diode, DIODESZETEX	
Q1	IRF7401PBF	FET, n-channel, Infineon	
C4	PLG0J821MCO1	Capacitor, Electrolytic, Nichicon	820uF
IC	MAX669EUB+	PWM controller, Maxim	
R4	WSL36375L000FEA	Current sense Resistor, Vishay	5mohm
C5, C6, C7	EEUFM1C331	Capacitor, Electrolytic, Panasonic	330uF
R1		Resistor, E96	165k
R3		Resistor, E96	909k
R2		Resistor, E96	105k
C1		Capacitor, Ceramic	1uF
C2		Capacitor, Ceramic	0.1uF
C3		Capacitor, Ceramic	0.22uF

Boost Converter design, Bill of Materials